ΕΘΝΙΚΟ ΜΕΤΣΟΒΙΟ ΠΟΛΥΤΕΧΝΕΙΟ
ΣΧΟΛΗ ΕΦΑΡΜΟΣΜΕΝΩΝ ΜΑΘΗΜΑΤΙΚΩΝ ΚΑΙ ΦΥΣΙΚΩΝ ΕΠΙΣΤΗΜΩΝ

ΔΙΑΤΜΗΜΑΤΙΚΟ ΠΡΟΓΡΑΜΜΑ ΜΕΤΑΠΤΥΧΙΑΚΩΝ ΣΠΟΥΔΩΝ
«ΜΙΚΡΟΣΥΣΤΗΜΑΤΑ ΚΑΙ ΝΑΝΟΔΙΑΤΑΞΕΙΣ»

ΝΕΑ ΦΑΣΜΑΤΟΣΚΟΠΙΚΗ ΠΡΟΣΕΓΓΙΣΗ ΤΩΝ ΦΑΙΝΟΜΕΝΩΝ ΠΑΡΕΜΒΟΛΗΣ ΣΤΟΝ ΚΑΟΛΙΝΙΤΗ

INTERCALATION PHENOMENA IN KAOLINITE: NEW INSIGHTS BY VIBRATIONAL SPECTROSOPY

ΜΕΤΑΠΤΥΧΙΑΚΗ ΕΡΓΑΣΙΑ

της
ΑΝΔΡΕΟΥ ΦΕΒΡΩΝΙΑΣ

Επιβλέπων: Χρυσικός Γεώργιος

Αθήνα
2020

ΕΘΝΙΚΟ ΜΕΤΣΟΒΙΟ ΠΟΛΥΤΕΧΝΕΙΟ
ΣΧΟΛΗ ΕΦΑΡΜΟΣΜΕΝΩΝ ΜΑΘΗΜΑΤΙΚΩΝ ΚΑΙ ΦΥΣΙΚΩΝ ΕΠΙΣΤΗΜΩΝ

ΔΙΑΤΜΗΜΑΤΙΚΟ ΠΡΟΓΡΑΜΜΑ ΜΕΤΑΠΤΥΧΙΑΚΩΝ ΣΠΟΥΔΩΝ
«ΜΙΚΡΟΣΥΣΤΗΜΑΤΑ ΚΑΙ ΝΑΝΟΔΙΑΤΑΞΕΙΣ»

ΝΕΑ ΦΑΣΜΑΤΟΣΚΟΠΙΚΗ ΠΡΟΣΕΓΓΙΣΗ ΤΩΝ ΦΑΙΝΟΜΕΝΩΝ ΠΑΡΕΜΒΟΛΗΣ ΣΤΟΝ ΚΑΟΛΙΝΙΤΗ

INTERCALATION PHENOMENA IN KAOLINITE: NEW INSIGHTS BY VIBRATIONAL SPECTROSOPY

ΜΕΤΑΠΤΥΧΙΑΚΗ ΕΡΓΑΣΙΑ

της
ΑΝΔΡΕΟΥ ΦΕΒΡΩΝΙΑΣ

Επιβλέπων: Χρυσικός Γεώργιος

Εγκρίθηκε από την τριμελή εξεταστική επιτροπή την 21/10/2020

Χρυσικός Γεώργιος	Ράπτης Ιωάννης	Κυρίτσης Απόστολος

Αθήνα
2020

Ανδρέου Φεβρωνία

Acknowledgements

The present thesis was accomplished at the Theoretical and Physical Chemistry Institute of the National Hellenic Research Foundation for the Interdepartmental Postgraduate Program "Microsystems and Nanodevices" of the National Technical University of Athens.

I would like to express my deep and sincere gratitude to my research supervisor, Georgios Chryssikos, Director of Research of the Theoretical and Physical Chemistry Institute of the National Hellenic Research Foundation, for giving me the opportunity to study under his guidance and for the continued support he offered me. His patience, enthusiasm and knowledge always inspire and motivate me to improve my skills and reach my goals.

I am very grateful to my professors Yannis Raptis and Apostolos Kyritsis, members of the committee, for providing me with their help when needed.

I would also like to express my special thanks to Dr. Vassilis Gionis, Senior Researcher of the Theoretical and Physical Chemistry Institute of the National Hellenic Research Foundation, for his encouragement and helpful advice throughout his work.

During the course of my studies I was supported financially by the project “Advanced Materials and Devices” (MIS 5002409) which was implemented at TPCI/NHRF under the “Action for the Strategic Development on the Research and Technological Sector”, funded by the Operational Programme "Competitiveness, Entrepreneurship and Innovation" (NSRF 2014-2020) and co-financed by Greece and the European Union (European Regional Development Fund. The Applied Spectroscopy Lab at TPCI/NHRF covered additional research expenses and travelling costs.

I couldn't express enough thanks to Dr. Eirini Siranidi, Research Associate of the Theoretical and Physical Chemistry Institute of the National Hellenic Research Foundation, for her valuable contribution to this thesis and her friendship.

Special thanks to Dr. Arkadiusz Derkowski as well as Dr. Marek Szczerba and Dr. Barbara Bożek from the Clay Minerals Laboratory of the Institute of Geological

Sciences/Polish Academy of Sciences for the collaboration, discussions and services for the purposes of this study.

The completion of this project could not have been accomplished without the continuous love and support from my parents, my caring sister Nena and my friends Giannis and Rena that are always by my side and encourage me to fulfill my dreams.

Contents

Abstract

Kaolinite is a layered aluminosilicate mineral undergoing spontaneous self-assembly of specific chemical compounds in its interlayer space (intercalation). *Ex-situ* XRD has been exclusively used until now for the study of the sigmoidal intercalation kinetics of kaolinite by monitoring the fraction of expanded material. Although XRD provides a straightforward assessment of the degree of intercalation, changes in the chemical bonding induced by the progressive insertion of the molecules in the interlayer space cannot be observed.

The present thesis aims at monitoring the kinetics of intercalation at the level of chemical bonds. For this, NIR spectroscopy was employed for the first time to study in real-time the intercalation of two reference kaolinites, KGa-1b and KGa-2, with excess N-methyl formamide (NMF) in closed reactors and with controlled conditions. The 2nd derivative of the sharp 2ν(NH) band at 6700 cm^{-1} attributed to the dangling N-H bond of intercalated NMF was selected for monitoring the reaction progress.

Opposite to expectations, the filling of the interlayers by diffusion was too fast to be observed. At any time the system exhibited a two-mode behavior and could be described as a linear combination of two spectra (pristine and fully intercalated kaolinite). NIR-based kinetics exhibited the sigmoidal shape known from XRD, implying that both techniques probe the same aspect of intercalation, which corresponds to the increasing concentration of fully intercalated interlayers.

Both kaolinites presented the same interlayer environment to NMF and did intercalate with the same activation energy (~60 kJ/mol) in the 20-80 °C range. Both demonstrated time-temperature superimposed sigmoidals, which differed in shape. In addition, ~20-30% of KGa-1b and ~60-70% of KGa-2 remained unreacted even after ~1y in contact with NMF at room temperature. Considering the above, it was concluded that intercalation in both kaolinites obeys a common single-step mechanism. It is assumed that this step is the instantaneous expansion of the interlayer which results from the establishment of a critical concentration of NMF chemisorbed on the edges of the particles. The differences between the two systems

were attributed to different morphological or external structural characteristics of the two samples and not to the interlayer.

Various models described in literature (diffusion, Avrami-Erofeev, consecutive-reactions) as well as common solid state reaction equations failed to fit the data. Instead, the sigmoidals were satisfactorily fitted by log-normal functions, representing the temporal distribution of interlayers switching from the pristine to the intercalated state. The sigmoidal shape characterizing each kaolinite must represent a distribution related to particle size, aspect ratio or stacking defects that are intrinsic to this sample. This hypothesis is supported by the study of particle size fractions derived from the bulk material by sedimentation, each of which displayed its own sigmoidal shape and final NMF uptake. Yet the shape of the sigmoidal is not a simple representation of the particle size distributions: small particles produced by milling displayed an entirely different sigmoidal than their naturally separated counterparts.

The shape of the sigmoidals was maintained in the presence of H_2O in the liquid NMF and no interlayer water was observed. A non-monotonic effect on intercalation appeared when increasing H_2O content, in agreement with the literature. High-temperature intercalation at high H_2O content in a closed system resulted surprisingly in low NMF uptake, that could be recovered irreversibly by decreasing the reaction temperature. It was therefore supposed that the equilibrium between dissolved and chemisorbed (on the external surface of the kaolinite) NMF is both, H_2O- and temperature-dependent. On the contrary, once intercalated, NMF is no longer part of the equilibrium.

The present NIR-based investigation may open the way for revisiting the fundamentals of intercalation, also by more sophisticated analysis of XRD data. It may also facilitate the development of applications based on hybrid kaolinitic materials.

Keywords: kaolinite, N-methylformamide, intercalation, kinetics, infrared spectroscopy, Near-infrared spectroscopy (NIR), Attenuated total reflectance (ATR), thermogravimetric analysis (TGA), log-normal distribution.

Περίληψη

Ο καολινίτης είναι ένα φυλλόμορφο αργιλοπυριτικό ορυκτό, στον διαφυλλικό χώρο του οποίου μπορούν να παρεμβληθούν μικρά μόρια συγκεκριμένων χημικών ενώσεων και να αυτο-οργανωθούν. Μέχρι τώρα η μελέτη της σιγμοειδούς κινητικής της παρεμβολής έχει στηριχθεί αποκλειστικά στη περίθλαση ακτίνων Χ (XRD), μέσω της καταγραφής της αύξησης του διεσταλμένου καολινιτικού υλικού. Η τεχνική αυτή προσφέρει άμεση εκτίμηση του βαθμού της παρεμβολής, αλλά οι αλλαγές στους χημικούς δεσμούς που επιφέρει η σταδιακή είσοδος των μορίων στον διαφυλλικό χώρο δεν μπορούν να παρατηρηθούν.

Σκοπός της παρούσας εργασίας είναι η μελέτη της παρεμβολής σε επίπεδο χημικών δεσμών. Για πρώτη φορά μελετήθηκε μέσω της φασματοσκοπίας εγγύς υπερύθρου (NIR) σε πραγματικό χρόνο η αντίδραση παρεμβολής σε δύο πρότυπους τύπους καολινίτη, KGa-1b και KGa-2, που έλαβε χώρα με περίσσεια N-μεθυλοφορμαμίδιου (NMF) κάτω από ελεγχόμενες συνθήκες σε κλειστό σύστημα.

Αντίθετα με ό,τι αναμενόταν, δεν παρατηρήθηκαν φαινόμενα διάχυσης κατά την πλήρωση του διαφυλλικού χώρου. Το σύστημα σε οποιαδήποτε χρονική στιγμή παρουσίαζε συμπεριφορά δύο καταστάσεων και η χρονοσειρά των δεδομένων μπορούσε να αναπαραχθεί ως γραμμικός συνδυασμός των φασμάτων του παρθένου και του πλήρως παρεμβλημένου καολινίτη. Οι κινητικές όπως εξήχθησαν από την φασματοσκοπία υπερύθρου εμφάνισαν σιγμοειδή συμπεριφορά, παρόμοια με την τεχνική XRD, υποδηλώνοντας ότι και οι δύο τεχνικές εξετάζουν το φαινόμενο στην ίδια κλίμακα, η οποία πρέπει να αντιστοιχεί στην αυξανόμενη συγκέντρωση του πλήρως παρεμβλημένου υλικού και όχι στην πρόοδο της πλήρωσης του διαφυλλικού χώρου.

Η οργάνωση του NMF στον διαφυλλικό χώρο και οι διαμοριακές αλληλεπιδράσεις που την χαρακτηρίζουν είναι κοινές στους δύο τύπους καολινίτη και η παρεμβολή στα δύο συστήματα χαρακτηρίζεται από την ίδια ενέργεια ενεργοποίησης (~60 kJ/mol) στην περιοχή θερμοκρασιών 20-80 °C. Επίσης, και οι δύο παρουσίασαν σιγμοειδή υπέρθεση χρόνου-θερμοκρασίας, που όμως διέφερε στο σχήμα για τον καθένα. Επιπλέον, αποδείχτηκε ότι ~20-30% του KGa-1b και ~60-

70% του KGa-2 παραμένει αδρανές σε παρεμβολή ακόμη και μετά από ~1 χρόνο έκθεσης στο NMF σε θερμοκρασία περιβάλλοντος. Λαμβάνοντας υπόψη τα παραπάνω, η παρεμβολή στους δύο καολινίτες βρέθηκε ότι υπακούει σε έναν κοινό μηχανισμό ενός μόνο σταδίου, το οποίο αντιστοιχεί στο ακαριαίο διάνοιγμα του διαφυλλικού χώρου και λαμβάνει χώρα μετά την προσρόφηση ενός κρίσιμου αριθμού μορίων NMF στην εξωτερική πλευρική επιφάνεια των σωματιδίων. Οι διαφορές μεταξύ των δύο συστημάτων θα μπορούσαν να αποδοθούν σε διαφορετικά μορφολογικά ή εξωτερικά δομικά χαρακτηριστικά των δύο τύπων καολινίτη και όχι σε διαφορές του διαφυλλικού χώρου.

Διάφορα μοντέλα που αναφέρονται στην βιβλιογραφία (διάχυση, Avrami-Erofeev, διαδοχικές αντιδράσεις), καθώς και εξισώσεις αντιδράσεων στερεάς κατάστασης απέτυχαν να περιγράψουν τα κινητικά δεδομένα. Αντιθέτως, οι σιγμοειδείς περιγράφηκαν ικανοποιητικά με λογαριθμικές κανονικές (log-normal) κατανομές, που αντιπροσωπεύουν την κατανομή του χρονικού διαστήματος που απαιτείται για την στιγμιαία εναλλαγή από παρθένο σε παρεμβλημένο υλικό. Συνεπώς, το σιγμοειδές σχήμα που χαρακτηρίζει κάθε καολινίτη πρέπει να αντιπροσωπεύει την κατανομή μιας ιδιότητα που σχετίζεται με το μέγεθος των σωματιδίων, τον λόγο επιφάνειας/πάχους και τα ελαττώματα στοίβαξης που είναι εγγενή στο κάθε δείγμα. Αυτή η υπόθεση υποστηρίζεται από τη μελέτη κλασμάτων σωματιδίων διαφορετικού μεγέθους που προήλθαν από το αρχικό υλικό με καθίζηση, καθένα από τα οποία εμφάνισε το δικό του σιγμοειδές σχήμα και διαφορετικό τελικό ποσοστό προσρόφησης NMF. Ωστόσο, το σχήμα των κινητικών δεν συσχετίζεται απλώς με την κατανομή μεγέθους των σωματιδίων: μικρά σωματίδια που παρήχθησαν με άλεση εμφάνισαν μία εντελώς διαφορετική συμπεριφορά από τα αντίστοιχα φυσικώς διαχωρισμένα.

Οι σιγμοειδείς κινητικές διατήρησαν το σχήμα τους παρουσία H_2O στο υγρό NMF χωρίς να παρατηρείται η διείσδυση του νερού στον διαφυλλικό χώρο. Σε συμφωνία με τη βιβλιογραφία, παρατηρήθηκε μη μονοτονική επίδραση στην παρεμβολή κατά την αύξηση του ποσοστού H_2O. Υψηλή θερμοκρασία και υψηλή περιεκτικότητα H_2O σε κλειστό σύστημα οδήγησαν σε μικρή προσρόφηση NMF, η οποία ανακτάται με μη αντιστρεπτό τρόπο μειώνοντας τη θερμοκρασία της αντίδρασης. Συνεπώς, η ισορροπία μεταξύ υγρού και χημιρροφημένου (στην

εξωτερική επιφάνεια του καολινίτη) NMF εξαρτάται τόσο από το H_2O όσο και από τη θερμοκρασία. Αντιθέτως, το NMF που έχει ήδη παρεμβληθεί παύει να αποτελεί μέρος της ισορροπίας.

Η παρούσα φασματοσκοπική μελέτη που βασίστηκε στο NIR ανοίγει τον δρόμο για την επανεξέταση θεμελιωδών θεμάτων της παρεμβολής, με ταυτόχρονη πιο εξειδικευμένη ανάλυση δεδομένων XRD. Επιπλέον, μπορεί να διευκολύνει την ανάπτυξη εφαρμογών βασισμένα σε υβριδικά καολινιτικά υλικά.

Λέξεις κλειδιά: καολινίτης, N-μεθυλοφορμαμίδιο, παρεμβολή, κινητική, φασματοσκοπία υπερύθρου, φασματοσκοπία εγγύς υπερύθρου, αποσβεννύμενη ολική ανάκλαση, θερμοβαρυτική ανάλυση, λογαριθμική κανονική κατανομή.

Chapter 1

Introduction

The present study is the first vibrational spectroscopic real-time investigation of the self-assembly of small organic molecules on kaolinite. Kaolinite is a phyllosilicate mineral and the process of interest involves the spontaneous penetration of the guest molecules (here N-methylformamide, NMF) in the interlayer space, known as intercalation. Understanding the systematics of intercalation is important both fundamentally and applications-wise. This chapter presents the aims of this thesis and introduces the reader to the structure of kaolinite and the vast literature on intercalation.

1.1 Structure of clay minerals. Kaolinite

Clay minerals are hydrous aluminium phyllosilicates, consisting of layers arranged parallel to each other. Each layer is formed by alternating tetrahedral and octahedral sheets.

The structural elements of the tetrahedral sheets are silica tetrahedra (Fig. 1.1). A silicon cation (Si^{4+}) is located in the center of the tetrahedron, the vertex corners of which are occupied by oxygen atoms. Each of the tetrahedra shares three of its vertex oxygen atoms with three adjacent tetrahedra, so that the tetrahedral bases (basal plane), form a hexagonal array in 2-dimensions. The fourth oxygen atom (apical) connects the tetrahedral with the octahedral sheet and points in the same direction for all tetrahedra.

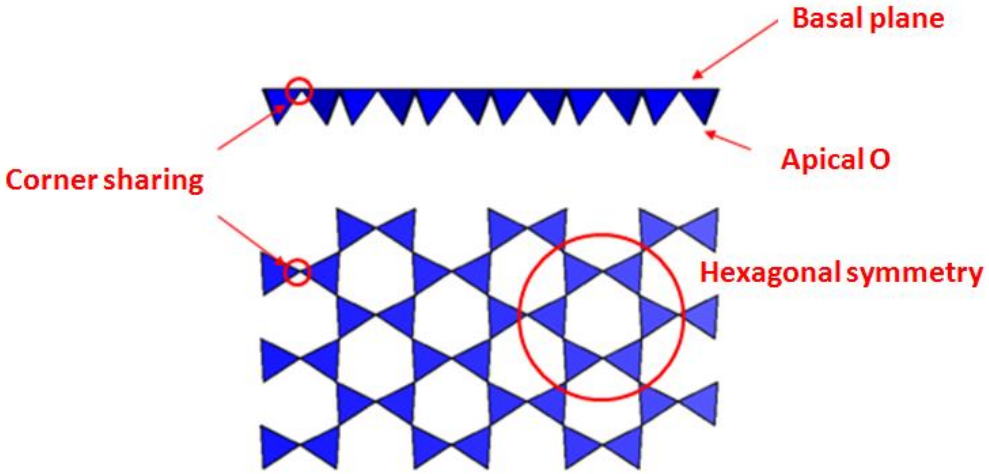

Figure 1.1. Structure of a tetrahedral sheet.

The structural elements of octahedral sheets are octahedra of divalent or trivalent cations (Fig. 1.2). The cation is placed in the center of the octahedron and its vertex corners are occupied either by oxygen atoms of the tetrahedral sheet or by hydroxyl groups. The vertices are shared between adjacent octahedra, creating the octahedral sheet. There are two types of octahedral sheets in clay minerals: the dioctahedral, in which two octahedral positions are occupied by trivalent cations (e.g. Al^{3+}, Fe^{3+}) and one remains vacant, and the trioctahedral, where all three octahedral positions are occupied by divalent cations (e.g. Mg^{2+}, Fe^{2+}).

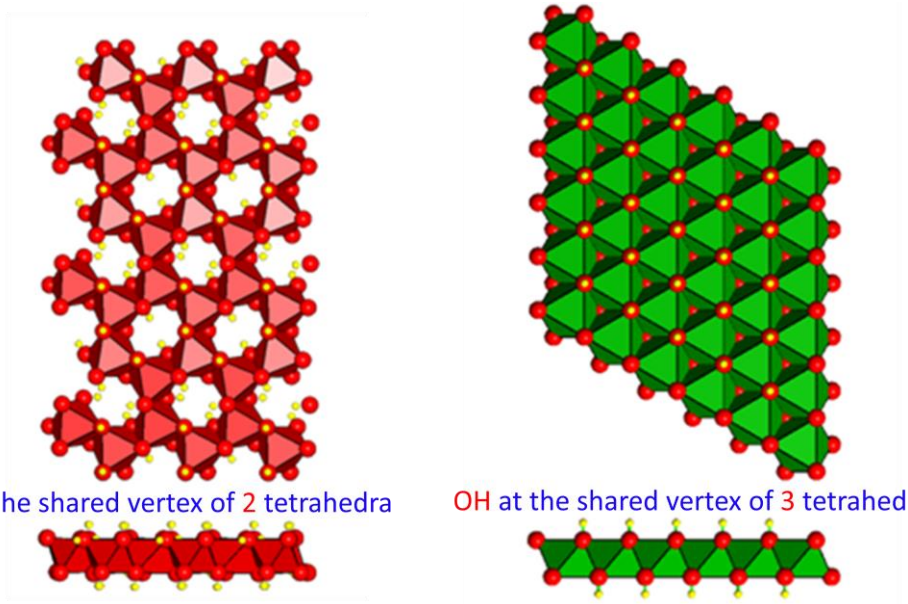

Figure 1.2. Structure of a dioctahedral (left) and a trioctahedral sheet (right), where ● and ● represent hydrogen and oxygen atoms, respectively.

Kaolinite is a clay mineral with widespread abundance and many industrial applications, including ceramics, paper, paint plastic, etc. [Mur88, Mur00]. It is the most common mineral among other polytypes of the kaolin group and can be found in nature as particles, usually hexagonal with a diameter of several hundred nm to several μm and a thickness of less than 100 nm (Fig. 1.3). It displays a triclinic crystal shape (with unit cells parameters *a*=5.15 Å, *b*=8.94 Å, *c*=7.39 Å, α=91,9°, β=105,0°, γ=89,8°) with the chemical formula $Al_2Si_2O_5(OH)_4$ and belongs to C1 group [Bis93]. As a dioctahedral 1:1 mineral it consists of layers formed by the assembling of one tetrahedral silica sheet and one octahedral alumina sheet (Fig. 1.4). Except of the shared oxygen atoms between the sheets there are also alumina hydroxyl groups, called inner OH, which are buried inside the di-trigonal silicate rings. Kaolinite layers are asymmetric and bifunctional, due to hydrophobic behavior of the basal plane of the silica sheet and hydrophilic behavior of the hydroxyls on the surface of the alumina sheet (inner surface OH). The ratio of the inner OH to the inner surface OH is 1: 3. Long hydrogen bonds are developed between the oxygen atoms of the silica's basal plane and the inner surface OH groups of the adjacent alumina sheet, resulting in the stacking of the layers with a d-spacing of ~7.1-7.2 Å [Det14] (Fig. 1.4). The interlayer space is dominated by the H-bonding network (Fig. 1.5). A detailed description of kaolinite's structure which determines the position of the H-atoms is available by Bish [Bis93] and Neder et al. [Ned99].

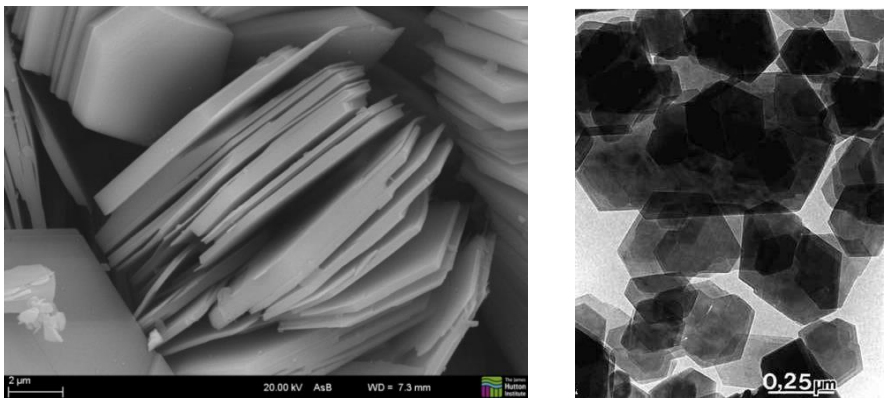

Figure 1.3. (left) Close up of kaolinite in Jurassic sandstone, UK North Sea, (polytype confirmed by XRD). Field of view ≈ 20 μm. Evelyne Delbos, The James Hutton Institute. (right) TEM image of CADAM kaolinite, Brazil. Field of view ≈ 1.2 μm wide. Photo courtesy of Ian Wilson. Images reproduced from the 'Images of Clay Archive' of the Mineralogical Society of Great Britain & Ireland and The Clay Minerals Society (https://www.minersoc.org/images-of-clay.html)

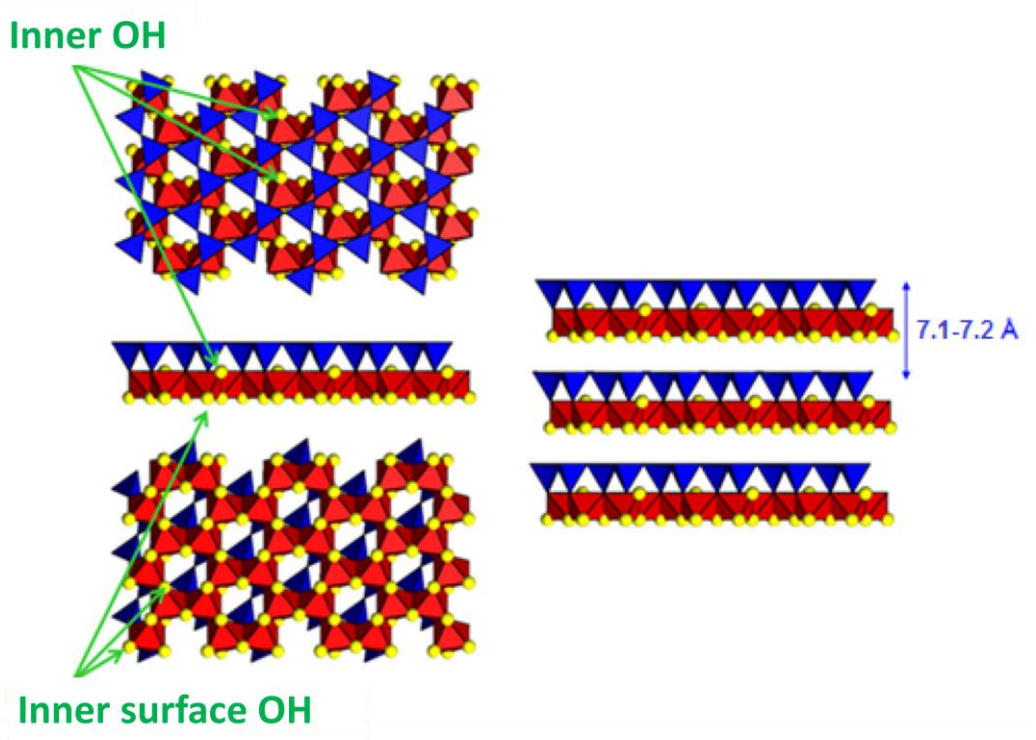

Figure 1.4. Structure of a single kaolinite layer (left) shown from the tetrahedral sheet side (top), from the octahedral sheet side (bottom) and perpendicular to the plane of the layers (middle) and a 3-layered kaolinite structure (right) shown perpendicular to the plane of the layers. The octahedral sheet is in red, the tetrahedral in blue and the hydroxyls in yellow.

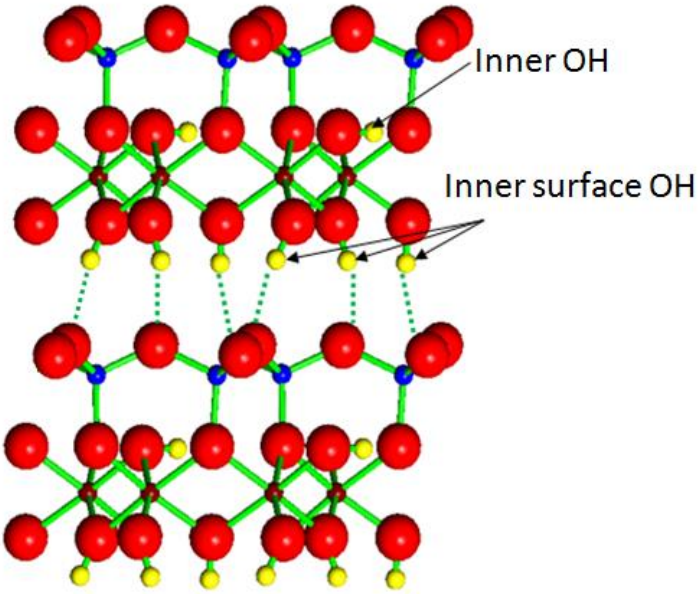

Figure 1.5. Schematic of interactions in kaolinite structure. The silicon, aluminium, oxygen and hydrogen atoms are in blue, brown, red and yellow, respectively. The bonds between the atoms are depicted as green lines and the H-bonds in the interlayer space as dashed lines.

Kaolinite exhibits structural defects which are mostly due to faults in the stacking of the layers [Bri86, Pla89, Kog05]. These are widespread and have a pronounced effect on the XRD pattern. The stacking faults can be related either to the displacement of the adjacent layers or to the vacancy type.

The dioctahedral sheet includes three possible octahedral cation sites, regarding the position of the vacancy, A, B or C, thus there are layers of type A, B or C, respectively. Layers B and C which display chirality (Fig. 1.6) are the most common. Kaolinite particles consist of a single type of layer (B- or C-).

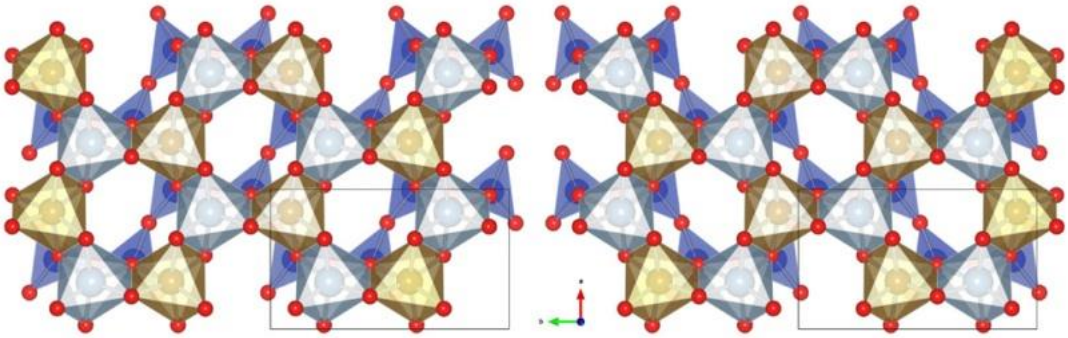

Figure 1.6. B- (left) and C-type (right) layer. Reproduced from Ufer et al. [Ufe15] by permission.

Stacking faults between layers of the same vacancy-type are common. Their identification has been the subject of very detailed research based on the simulation of XRD patterns [Pla77, Bri86, Pla88, Pla89, Art95, Zvy96, Kog05, Kog10]. The most recent refinements involve three energetically favoured layer displacement vectors [Ufe15, Dri16, Sak16]:

$$\boldsymbol{t_1} \approx -\frac{1}{3}\boldsymbol{a}$$

$$\boldsymbol{t_2} \approx -\frac{1}{3}\boldsymbol{a} + \frac{1}{3}\boldsymbol{b}$$

$$\boldsymbol{t_0} \approx -\frac{1}{3}\boldsymbol{a} - \frac{1}{3}\boldsymbol{b} \qquad \textit{Equations } 1.1$$

where $\boldsymbol{a}$ and $\boldsymbol{b}$ are parameters of the unit cell. An ideal ordered kaolinite exhibits solely $\boldsymbol{t_1}$ translation. Disorder can be produced either by interstratification of single layers of different translation vector or by interstratification of packets of a different

ordered stacking. Such interstratification phenomena lead to the formation of high- and low-order kaolinite (HOK and LOK, respectively) (Fig. 1.7).

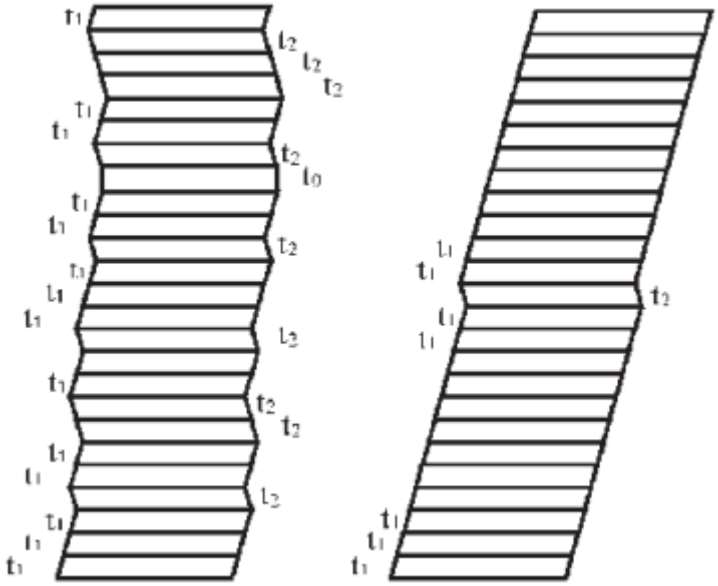

Figure 1.7. Schematic illustration of layer stacking in LOK (left) and HOK (right) phases. Reproduced from Sakharov et al. [Sak16] by permission.

Additionally, a disordered kaolinite may include the occasional stacking of different vacancy type layers, e.g. B in a particle consisting of C-layers [Ufe15, Sak16]. A regular B-C-B-C layering is characterizing dickite, another polytype of the kaolinite family [Bri86].

The effect of the presence and concentration of the aforementioned defects on the XRD pattern of kaolinite has been parametrized by a number of empirical indicators [Bri06], the most common among them is the so-called Hinckley index (HI) [Pla88]. It is calculated by the ratio of the sum of the heights of the reflections $(1\bar{1}0)$ and $(11\bar{1})$ from the inter-peak background and the height of the $(1\bar{1}0)$ peak from the general background. The HI varies between ~0.2 and ~1.5, increasing with higher ordering.

1.2 Intercalation in kaolinite

Opposite to other clay minerals, e.g. smectites or vermiculites, intercalation in kaolinite was untraceable until the late 1950s. In 1961, Wada [Wad61] was the first to achieve intercalation in kaolinite using potassium acetate and observed the expanding of the original ~7.2 Å lattice d-spacing to 14.2 Å. Later, in 1963, Weiss [Wei63] intercalated urea in the clay by increasing the d-spacing to 10.7 Å and proved that the extremely thin-walled porcelain made in China in the 9th century was the result of the "fermentation" of kaolinite with urine.

The relatively late recognition of kaolinite intercalation is attributed to the very limited number of compounds that cleave spontaneously the dense grid of interlayer H-bonds [Det14]. The chemical compounds that can selectively access and directly intercalate kaolinite are divided into 3 groups [Lag06, Klo19]. The first group includes molecules with combined H-bond donor/acceptor properties such as urea, hydrazine, formamide and other small amides, the second dimethyl sulfoxide and other high dipole moment compounds and the third potassium acetate and other short-chain organic acid salts. The insertion of such small molecules leads to an expansion in the *c*-axis direction and a change of the d-spacing from ~7.2 to ~10-14 Å, depending on the guest.

Modern interest in kaolinite intercalation appears to be stimulated by the development of new hybrid materials based on kaolinite. Intercalation of the aforementioned compounds has been found to operate as a preliminary step for the subsequent insertion of many other species that cannot intercalate directly. By the so-called displacement method, the initially intercalated species (preintercalated) are replaced by new ones [Set78, Sug86, Gar00], resulting in the synthesis of nanocomposites with improved properties [Kal11, Ded14, Kot15, Ngn16, Str17, Tch18]. The applications of these new materials concern a wide range of industrial areas, such as health, environmental and material sciences and have revived the interest in understanding the fundamentals of primary intercalation reactions [Zha16, Zha18, Kri18, Mak19].

1.3 Characterization of kaolinite and hybrid kaolinitic materials

1.3.1 X-Ray Diffraction (XRD)

Due to the expansion of the c-axis, kaolinite intercalation has been studied extensively by *ex-situ* X-Ray diffraction (XRD). During intercalation, the intensity of the initial diffraction peak at 2θ≈12.4° corresponding to a d-spacing of ~7.2 Å is progressively decreasing, while the appearance and growth of a new peak at a lower 2θ angle indicates the formation of the expanded state of the mineral lattice. The degree of the reaction, is traditionally determined by the ratio of the integrated intensity of the *001* diffraction peak of intercalated kaolinite divided by the sum of the integrated intensities of the *001* diffraction peaks of intercalated and pristine kaolinite [Ole68, Wie69].

Hach-Ali and Weiss [Hac69] noted that this approach is based on the assumption that the structure and Lorentz polarization factors of the two reflections are identical. They showed that this is contradicted by experiment and can be leading to the overestimation of the final degree of intercalation. Layer deformation and interstratification effects are also not considered [Lag06].

Regardless of these uncertainties, the aforementioned XRD-based monitoring of the reaction progress is very widely used. Intercalation kinetics determined by XRD display almost invariably a sigmoidal time dependence [e.g. Wei63, Ole68, Hac69, Ole70, Cas15, Mak19]. Different models have been proposed to fit the sigmoidals, such as Avrami-Erofeev nucleation and growth models [Hac69, Mak19]. The initial "incubation" step has been associated with the interaction of a small number of guest molecules with the edges of kaolinite, causing a local deformation of the layers on the perimeter of the crystallites [Lag06]. As a result of this deformation, the guest molecules can diffuse cooperatively in the interlayer space, until the saturation of the interlayer. In a different approach, Castrillo et al., [Cas15] considered the intercalation as a sequence of reactions, in which initially guests enter flat in the interlayer and then rearrange cooperatively expanding the lattice structure.

XRD-based investigations have revealed several other interesting aspects of intercalation. One of them concerns the effect of H_2O on intercalation. Specifically, the presence of increasing concentrations of H_2O was reported to induce a non-monotonic effect on the intercalation rate [e.g. Ole68, Ole70, Mak19]. The dependence of intercalation on particle size has been also reported in the literature, with the counterintuitive conclusion that intercalation is reduced in smaller (along *ab*) particles, despite their higher edge-surface [Uwi93, Den02]. Pure kaolinite samples often contain sizable fractions that do not intercalate for unknown reasons [Fro02, Lag06]. The role of kaolinite defect structures [Pla89, Sak16] on intercalation is far from being understood. Finally, de-intercalation seems to alter the structure and properties of the original kaolinite [Bar77, Pla93] and is sometimes accompanied by exfoliation and the formation of nano-scrolls which are relevant to the mineral halloysite [Sin96, Det14, Li15, Li19].

1.3.2 Infrared spectroscopy

Kinetic studies of intercalation are exclusively based on XRD, to the best of our knowledge. Vibrational and primarily mid-infrared spectroscopy (MIR), has assumed a complementary role in the static structural study of the intercalate. Vibrational spectroscopy is sensitive to the changes in chemical bonding which accompany the penetration of the guest species in the interlayer space, such as those involving the inner surface OH groups, or the new bonding arrangement of the intercalated molecule in the interlayer [e.g. Led66, Ole71a, Ole71b, Joh84, Fro98]. The careful study of the latter can reveal information about the orientation of the guests in kaolinite.

Intercalated N-methylformamide (NMF) was thoroughly studied. It exhibits a sharp, high-frequency N-H stretch which suggests that it is ordered and in weak H-bonding interaction with the tetrahedral sheet of kaolinite. On the contrary, the C=O moiety of the amide bond is in strong interaction with the inner surface OH of the mineral, thereby perturbing their vibrational signature [Wei66, Ole71a, Ada79, Cag13]. The arrangement is illustrated in Fig. 1.8.

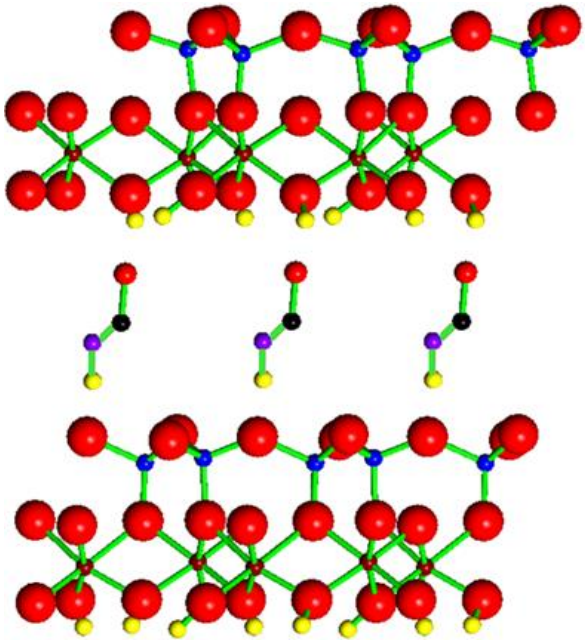

Figure 1.8. Structure of the bonding arrangement of N-H-C-O of NMF in the interlayer space. The silicon, aluminium, oxygen, hydrogen, carbon and nitrogen atoms are in blue, brown, red, yellow, black and purple, respectively.

In a preliminary vibrational investigation of the intercalation of NMF in kaolinite, Andreou [And18] tested the use of non-invasive Attenuated Total Reflection (ATR) mid-infrared technique in the study of the intercalate. This study demonstrated that a thin kaolinite film casted on the diamond ATR element can be subjected to drying, H/D exchange, or exposure to NMF vapors by means of a suitable environmental chamber. The setup was stable enough to allow for monitoring these processes in real time over several hours. Additionally, it was demonstrated that near-infrared (NIR) with diffuse reflectance optics was advantageous for monitoring the sigmoidal time-dependence of intercalation including the non-monotonic effect of H_2O at ambient temperature.

1.4 Aim of the thesis

The kinetics of intercalation are traditionally studied by XRD. A new approach based on infrared spectroscopy, and more specifically on diffuse reflectance in the near-infrared, is proposed in this study. The advantages of this approach are listed below:

First, infrared spectroscopy is complementary to XRD. XRD probes the evolution of coherently expanded interlayers along *001*, whereas vibrational spectroscopy displays specifically the increasing concentration of the intercalated species. It can therefore be anticipated that the two techniques will probe different aspects of intercalation.

Second, infrared spectroscopy is characterized by high chemical specificity. It is therefore more suitable than XRD for examining the dependence of guest-host interactions on the degree of intercalation or the type of the host.

Third, the use of optical fibers enables the coupling of the NIR spectrometer to a close reactor, thereby allowing for the convenient control of experimental conditions (i.e. concentration of NMF and water, temperature).

Finally, modern FTIR spectrometers offer excellent long-term stability, accuracy and reproducibility and can record kinetics with high temporal resolution (≥1min).

The aim of this thesis is to bring forward NIR spectroscopy as a fundamental tool box for the systematic monitoring of kaolinite/NMF intercalation with unprecedented detail.

Chapter 2

Materials and Methods

The characterization of the materials in this work was performed by using Attenuated Total Reflection mid-infrared spectroscopy, diffuse reflectance near-infrared spectroscopy and thermogravimetric analysis (TGA). The materials, methods as well as the experimental details are presented below.

2.1 Materials

Two kaolinite reference samples were used in this study, KGa-1b and KGa-2, source clays of the American Clay Minerals Society. The low-defect KGa-1b sample has identical XRD pattern and a very similar composition to the previously available but recently exhausted KGa-1 and was collected from the Buffalo China Mine located in Washington Country, Georgia [Pru93, Sak16]. KGa-2, also from Georgia (Warren County) is known to have a high-defect structure [Sak16]. Both samples contain small quantities of impurities. Based on the mass loss observed in thermogravimetric analysis diagrams the purity of KGa-1b and KGa-2 was calculated ~96.5% and >99%, respectively, compared to ~96% for both kaolinites in literature [Gug01, Chi01, Dri15].

Sakharov et al. [Sak16] XRD simulations showed that both kaolinites are biphasic and consist of the same two phases, described as high-order (HOK) and low-order kaolinite (LOK), already mentioned in Section 1.1 (Fig. 1.7), albeit in different ratio. The calculated proportions, 71.6% HOK and 28.4% LOK for KGa-1b versus 4%

HOK and 96% LOK for KGa-2, as well as the parameters related to particle size (diameter of the crystallites, D, and mean number of layers, N) are given in Table 2.1. The amounts of t_1, t_2 and t_0 layer displacement (Eq. 1.1), W(t_1), W(t_2) and W(t_0), respectively, contained in HOK and LOK fractions of KGa-1b and KGa-2 were determined for a log-normal distribution of the coherent scattering domain (CSD) thickness along *c*-axis. It is shown that the HOK phase is almost defect-free, in which 97% of the layers demonstrate layer displacement attributed to t_1 translation and 3% to t_2 translation. The LOK phase contains abundant t_2 and some t_0 translations in (35-38% and 5%, respectively), as well as an additional 2-5% of arbitrary stacking faults, Wa.

Table 2.1. Structural parameters of HOK and LOK fractions in KGa-1b and KGa-2. Adapted from Sakharov et al. [Sak16].

Sample phase	**KGa-1b**		**KGa-2**	
	HOK	LOK	HOK	LOK
W(t_1)	0.97	0.55	0.97	0.55
W(t_2)	0.03	0.38	0.03	0.35
W(t_0)	-	0.05	-	0.05
Wa	-	0.02	-	0.05
N	45	45	25	25
D(Å)	200-800	200-800	200-800	200-500
C(%)	28.4	71.6	4.0	96.0

The particle size of KGa-1 and KGa-2 which is set by the dimensions of the *ab*-plane is distributed log-normally according to Uwins et al. [Uwi93] and Drits and Derkowski [Dri15]. The particle size distribution (PSD) analysis for KGa-1 displayed a bimodal PSD with maxima at 3 and 22 μm and a unimodal PSD for KGa-2 with mean size of 10 μm and an asymmetry toward finer particles (Fig. 2.1) [Dri15]. Bimodal particle size distributions in kaolinite are not uncommon [Uwi93]. The XRD patterns indicated that the smaller particle fraction in KGa-1 (<4 μm) is thinner along *c*-axis and more ordered than the >4 μm fraction. Nevertheless, the direct matching of the

discrete populations of the bimodal PSD with the two phases present (HOK and LOK) is not straightforward. Opposite to KGa-1b, all the particles of KGa-2 display the same structural disorder, which is independent of the particle size fraction [Sak16].

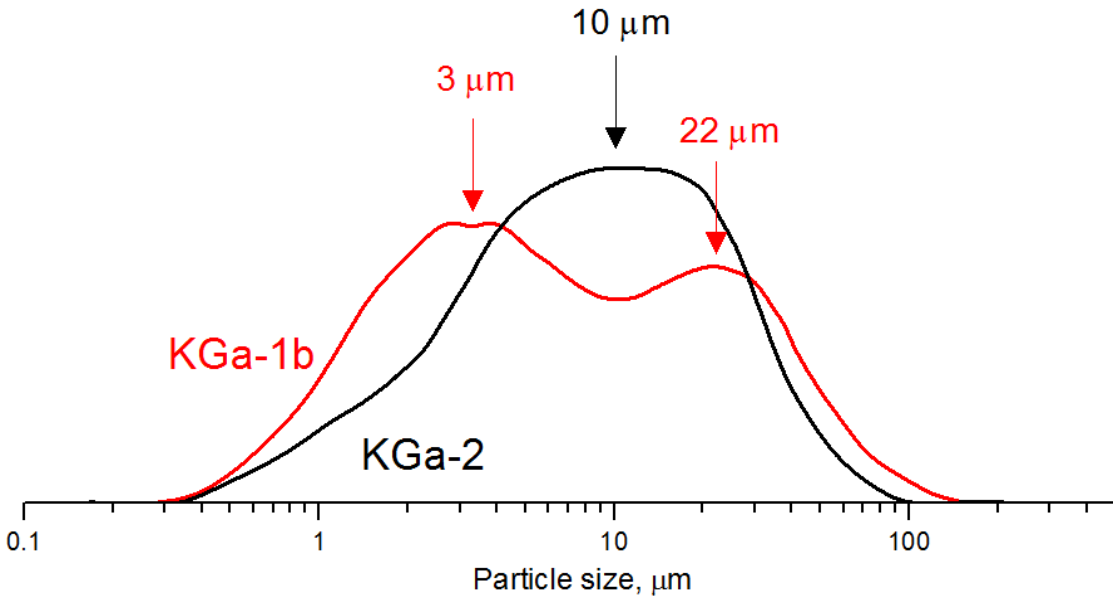

Figure 2.1. Particle size distribution of bulk KGa-1 and KGa-2 samples. Adapted from Drits and Derkowski [Dri15].

In agreement with the above, the Hinckley index (HI) of bulk KGa-1 and KGa-2 samples was ~1 and ~0.2-0.3, respectively [Uwi93, Sor03, Sak16] and was found to increase as the particle size fraction decreases in KGa-1, whereas in KGa-2 is not affected by the particle size [Uwi93].

Bulk, as-received, material was employed throughout this thesis. Selected separations of particle size fractions were performed by sedimentation for the needs of Chapter 7, by our partner laboratory (Clay Minerals Laboratory of the Institute of Geological Sciences/Polish Academy of Sciences) with or without using a Calgon dispersant. Additionally, artificially comminuted samples were prepared by wet McCrone milling. 5 ml of methanol were added to 4 g of kaolinite and milled in a McCrone mill with corundum beads for 2, 10, 20, 30 min. The increase in the milling time results in a reduction of the particle size, presumably by decreasing dimensions along *ab*, but the resulting particle size distributions were not measured.

For intercalation N-methylformamide (NMF) >99% (Aldrich) was used. NMF is a colorless, organic compound with chemical formula CH_3NHCHO (Fig. 2.2), m.p. -4 °C, b.p. 182.5 °C and a density of 1.01 g/ml (i.e. essentially identical to H_2O at room temperature). NMF is hygroscopic, thus, it was dried by the addition of 4Å molecular sieves and stored sealed.

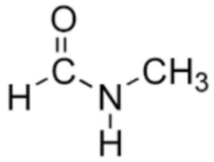

Figure 2.2. The chemical formula of NMF.

The kaolinite/NMF hybrid materials were prepared by mixing and grinding the components, in the absence or presence of water, in an agate mortar. Immediately after mixing, they were transferred in a closed vial in the desired temperature for hours or days to self-organize. Typical mixtures included mixing at ambient conditions of 1 g of kaolinite pre-dried at 100 °C for 2 h with 1 g of NMF/H_2O solution. In these proportions the mixture is in the form of a paste.

To remove excess NMF from the final reaction mixtures, these were washed with dioxane, an organic heterocyclic compound of formula $C_4H_8O_2$ which is a good solvent for NMF, accompanied by drying at ambient temperature for one day [Tun96].

2.2 Methods

2.2.1 Attenuated total reflection (ATR)

The Attenuated total reflection (ATR) technique is typically applied to the mid-infrared region (4000-400 cm^{-1}), where the resonance of the fundamental vibrational modes of the molecules occurs.

The ATR technique is based on the total internal reflection phenomenon. A crystal with high refractive index (n_1) transparent to infrared radiation is used as the

internal reflection element. The less optically dense sample (refractive index=n_2) is placed on the crystal, in such way to achieve very good contact. When the incident beam reaches the crystal-sample interface at an angle θ greater than the critical angle $\theta_c=\arcsin(n_2/n_1)$ it becomes totally internally reflected.

An evanescent wave is created within the sample, the amplitude of which decreases exponentially with the distance from the interface. The spectrum is collected from the penetration depth, d_p, of the radiation in the sample and is determined by the following relationship [Chr17]:

$$d_p = \frac{\lambda}{2\pi n_1 \sqrt{sin^2\theta - (\frac{n_2}{n_1})^2}} \qquad Equation\ 2.1$$

where λ is the wavelength. Typical penetration depths are of the order of a few μm (usually up to 10 μm). As it is expressed by the Equation 2.1, the penetration depth is dependent on the wavelength, meaning that for thick samples (>few d_p) weaker bands would appear at lower λ and stronger bands at higher λ. Consequently, the spectrum would be deformed. To avoid this effect, the spectra are corrected for the effect of the wavelength on the penetration depth.

Attenuated total reflectance (ATR) spectra in the mid infrared were measured on two Fourier transform instruments (Equinox 55 or Tensor II by Bruker), both equipped with single reflection diamond ATR accessories (Miracle by PIKE Technologies) and DLATGS detectors. ATR data acquisition was synchronized with NIR acquisition (Section 2.2.2) by means of a coupling environmental chamber as described by Bukas et al. [Buk13] (Fig. 2.3).

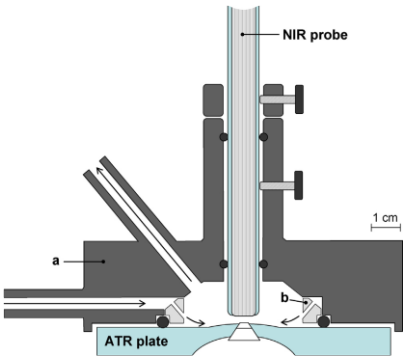

Figure 2.3. Cross section of the environmental chamber designed to couple the single reflection diamond ATR cell with the NIR fiber optic probe. Reproduced from Bukas et al. [Buk13] by permission.

2.2.2 Near-infrared spectroscopy (NIR)

The Near Infrared (NIR) technique uses radiation in the 12500-4000 cm^{-1} range to observe the higher-order vibrational modes (overtones and combinations), specifically involving light atoms, such as hydrogen. Consequently vibrations involving C-H, N-H and O-H bonds are strongly active in the NIR, whereas those involving Si-O, Al-O are not.

NIR data collection on powders or pastes is usually based on diffuse reflection optics and can be performed by various accessories, such as optical fibers or integration sphere.

A Fourier transform instrument (Vector 22N by Bruker) operating in diffuse reflectance by means of a 1.5m long fiber optic bundle probe was used for the NIR data acquisition. Thick, opaque slurries of KGa-1b/NMF (2g, 1:1 by weight) were introduced into a small glass reactor (~5ml), which was hermetically attached to the tip of the optical fiber probe. The closed system was then immersed in a thermostatic bath (20-80 ^{o}C). For smaller quantities, 50 mg of kaolinite were mixed with 50 mg of NMF in a miniature version of the reactor. High quality spectra of 100 scans at a resolution of 4 cm^{-1} and a temporal resolution varying between 5 and 30 min depending on temperature, were recorded. Fourier transform was computed using a Blackman-Harris 3-term apodization and a zero filling factor of 2 (digital resolution 2 cm^{-1}).

In another experiment, an integrating sphere arrangement was used on the same Fourier transform instrument. The quartz window of the integrating sphere has a diameter of ~2 cm. All measurements were performed by placing the sample straight on the integration sphere window and using an environmental cup to isolate the sample. The collection of these spectra was done with a resolution of 4 cm^{-1} and a zero filling factor of 2 (digital resolution 2 cm^{-1}) by averaging 300 scans.

The 2^{nd} derivatives of the mid and near-IR absorption spectra were computed via the Savitzky-Golay subroutine of the Opus software (Bruker Optics) with 9-point smoothing, unless otherwise indicated.

2.2.3 Thermogravimetric analysis (TGA)

Thermogravimetric analysis (TGA) is a technique of thermal analysis in which the change in mass of a sample is measured as a function of temperature in a heating experiment or as a function of time during isothermal analysis.

Pure kaolinite is anhydrous, so it does not display mass loss below 300 °C. In a TGA diagram the only mass loss of kaolinite appears between 400 °C and 600 °C due to the removal of hydroxyls (dehydroxylation) as water [Dri15] and corresponds to 14% mass loss. Intercalated NMF is removed at lower temperatures, thus the portion of the NMF uptake in kaolinite can be well defined. In the case of pastes (1:1 wt) both liquid and intercalated NMF are present in the sample displaying overlapping loss events in the TGA diagram. For that reason, it was found convenient to remove the excess of liquid NMF before TGA analysis, by washing with dioxane and drying at ambient temperature for ~1d [Tun96], but this method leads to the removal of some portion of intercalated NMF [Lag06].

Thermogravimetric traces were recorded on a TGA Q500 analyzer (TA Instruments). The 10±1 mg samples were equilibrated at 40 ^{o}C and then scanned to 800 ^{o}C with rate 10 ^{o}C/min, under dry N_2 purging (60mL/min). A hypothetical stoichiometric intercalation (2 NMF molecules per unit cell) would be manifested by a low temperature mass loss equal to 22.9% of the mass of the pristine kaolinite [And18].

Chapter 3

Intercalation Kinetics: Temperature-dependence

NIR and ATR spectroscopic techniques are evaluated for monitoring intercalation reactions in real time and suitable proxies are defined in this chapter. For the first time, kinetics based on NIR spectroscopy are reported for two kaolinite samples, KGa-1b and KGa-2, and their temperature-dependence is examined over a wide temperature range (25-75 °C).

3.1 ATR vs. NIR monitoring techniques

Preliminary studies [And18] have indicated that both, ambient temperature ATR and NIR techniques record spectral changes of KGa-1b/NMF samples due to intercalation. In order to compare the two techniques in terms of their suitability for the kinetic monitoring of intercalation, a synchronous ATR-NIR experiment was performed following Bukas et al. [Buk13]. The KGa-1b/NMF paste (1:1 wt) is deposited on the ATR crystal and above it, in a very close distance, the NIR probe is stabilized. In this way, the synchronized ATR and NIR spectrometers probe the same sample from opposite sides. The area is sealed with a special cell in order to preserve the NMF-saturated environment and prevent the sample from drying. The experiments are not temperature adjusted, but they can be useful for investigating long-time processes at ambient temperature over the broadest frequency possible range.

The 49h-long time series of the absorbance spectra in the 2ν(OH) and 2ν(NH) as well as in the ν(OH) and ν(NH) ranges are shown in Fig. 3.1 (upper and lower, respectively). The relative intensity of the signature of intercalated (6700, 3420 cm^{-1}) vs. liquid (~6620, ~3300 cm^{-1}) NMF is clearly stronger in the NIR than in the ATR spectra. This is because H-bonding in liquid NMF suppresses the anharmonicity of the N-H dipole and results in a "forbidden" weak and broad stretching overtone band. In the intercalated state, the intermolecular H-bonding network of NMF is broken and the N-H bond of the intercalated species becomes dangling. The dangling N-H of intercalated NMF is highly anharmonic and yields overtones that are stronger and sharper than those of liquid NMF [Fol71, Sie02]. This is the main reason why NIR is more suitable for the real time investigation of the NMF intercalation.

Similar anharmonicity differences between reactants and products were explored for the kinetic monitoring of indigo intercalation in palygorskite, a spontaneous reaction occurring when crystalline indigo and the mineral are heated moderate temperatures [Tsi12]. The N-H functionalities of indigo are in strong H-bonding interaction with C=O in the crystalline state and produce a weak overtone signal. On the contrary, intercalated indigo molecules bear a dangling N-H bond with a strong overtone signature. Besides anharmonicity changes, achieving fast data acquisition under environmentally controlled conditions is straightforward in NIR, especially in the diffuse reflectance mode by optical fibers or integrating spheres, but not in the mid-infrared [Chr17].

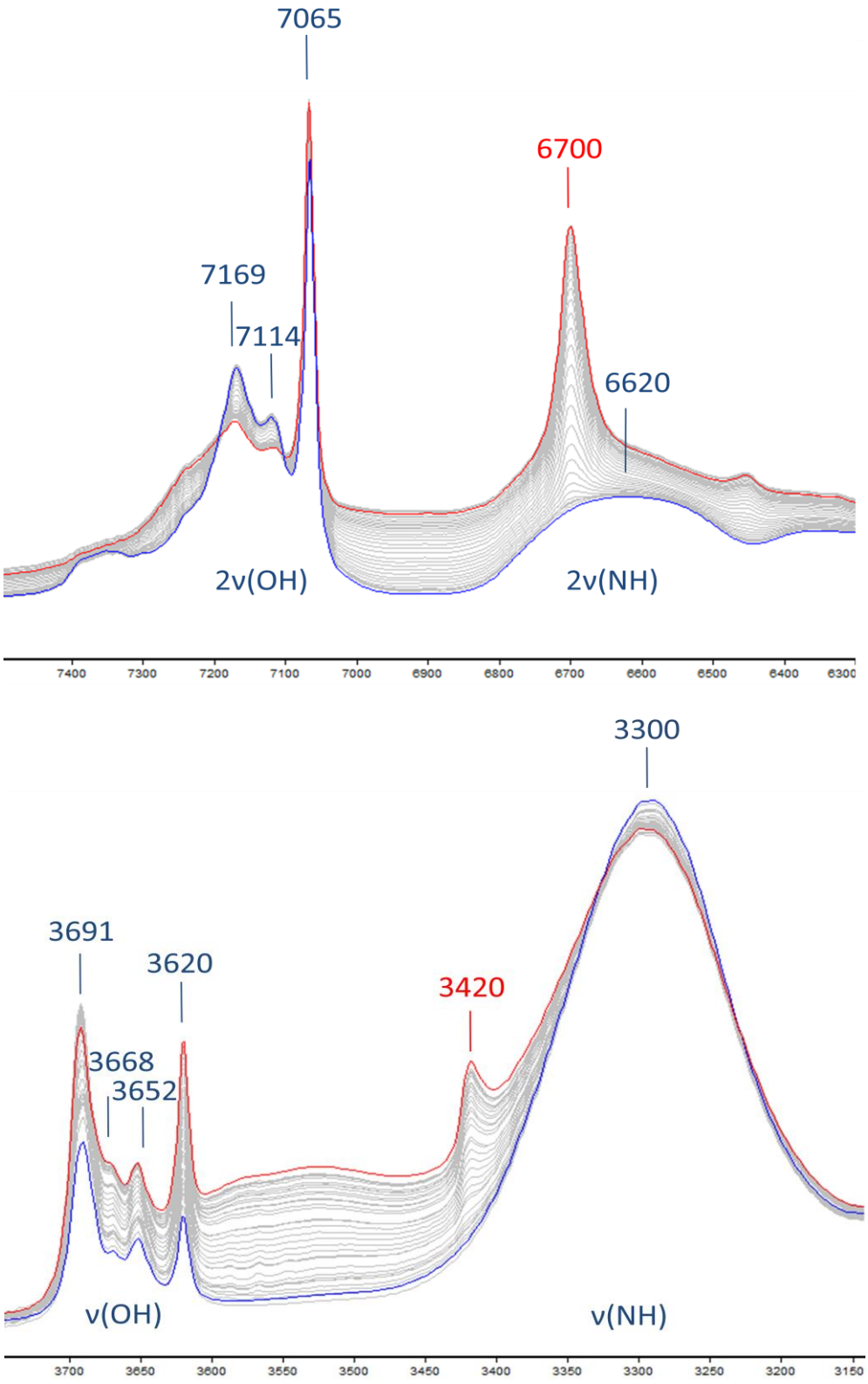

Figure 3.1. NIR (upper) and ATR (lower) absorbance spectra of KGa-1b/NMF intercalation at 30 °C in the 2ν(OH) and 2ν(NH) range recorded over a total period of 49h. The initial spectrum is depicted in blue and the final in red.

In the NIR region three spectral areas were investigated thoroughly for monitoring purposes during the 49h intercalation of KGa-1b with NMF, the first of which includes the 2ν(OH) bands of kaolinite (7200-7020 cm^{-1}, Fig. 3.2, upper), the second the 2ν(NH) bands of NMF (6800-6600 cm^{-1}, Fig. 3.2, middle) and the third the Amide A+III and ν+δ(OH) combinations (4680-4480 cm^{-1}, Fig. 3.2, lower). 2nd derivatives were chosen in order to eliminate the broad bands and amplify the intensity of the narrow peaks. The development of the two new peaks at 6700 and 4640 cm^{-1} due to intercalated NMF is clearly observable in the 2nd derivative spectra. However, the spectral signature of kaolinite displays small changes. The overtone of the inner OH stretching mode at 7065 cm^{-1} seems to slightly shift (to 7066 cm^{-1}) and broaden (by 1 cm^{-1}), whereas the intensity of the bands attributed to inner surface OH (7200-7100cm^{-1}) decreases. The effect of intercalation is much stronger on the position of the ν+δ combination mode of the inner OH. This band, originally at 4527 cm^{-1} is replaced by a new one at 4519 cm^{-1} (Δν=-8 cm^{-1}), due to the displacement of the inner OH bending fundamental vibration which was reported to shift from 911 cm^{-1} to 903 cm^{-1} (Δν=-8 cm^{-1}) [Den02, And18].

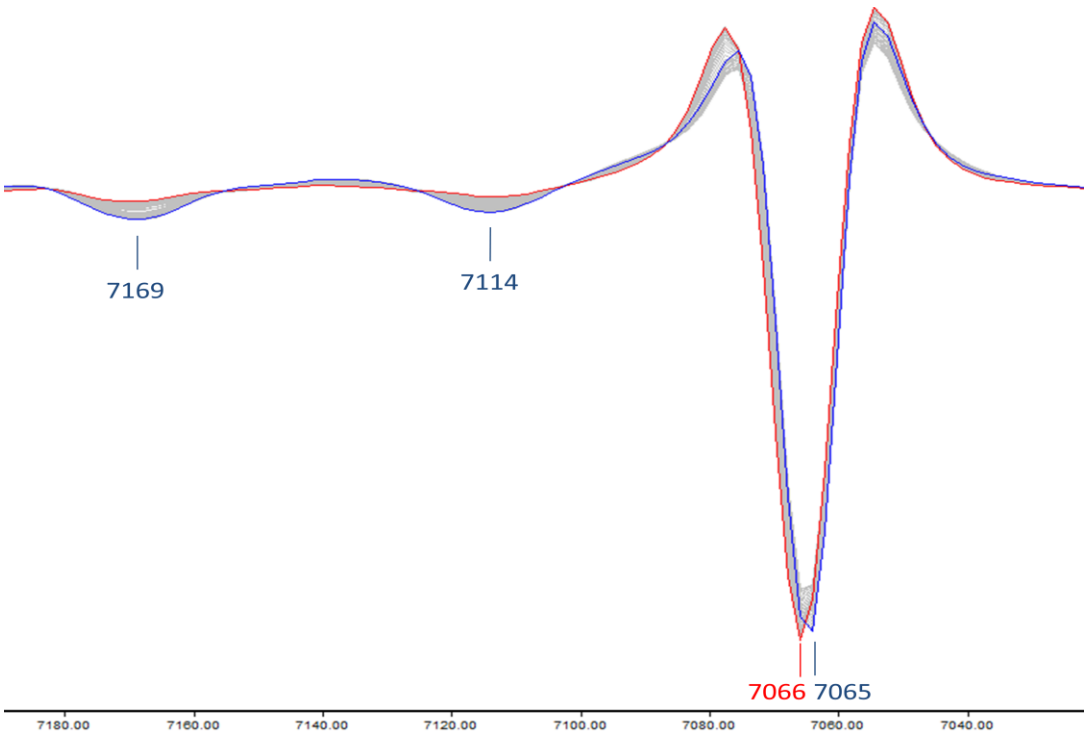

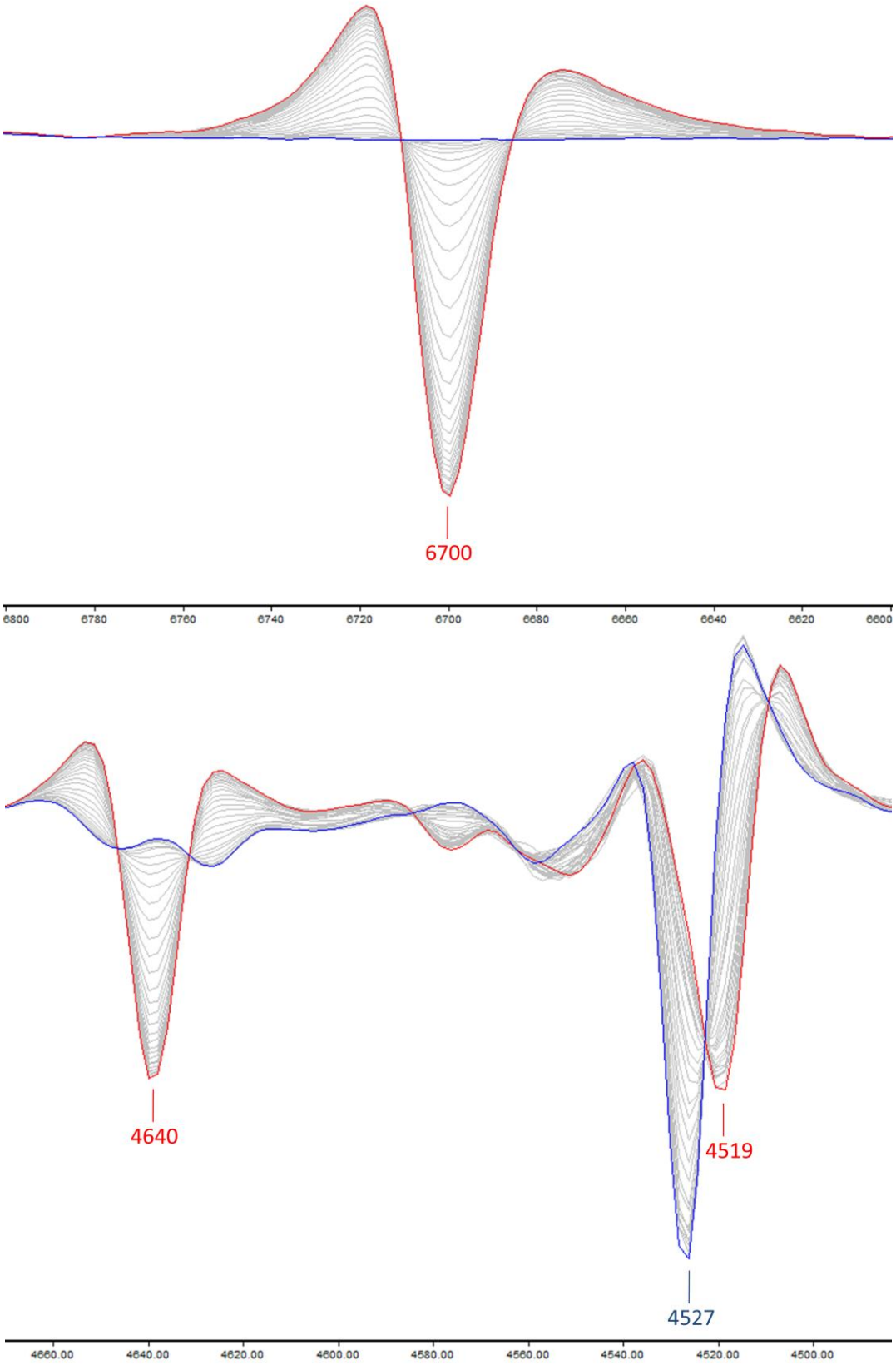

Figure 3.2. 2nd derivative with 9 points smoothing(Δν=2 cm^{-1})of NIR spectra of KGa-1b/NMF intercalation at 30 °C in the 2ν(OH) (upper), 2ν(NH) (middle) and Amide A+III and ν+δ(OH) (lower) range recorded over a total period of 49h.The initial spectrum is depicted in blue and the final in red.

3.2 Selection of kinetic proxies

Reaction kinetics are usually studied spectroscopically by monitoring the increasing or decreasing intensity of proxy bands assigned to the product or reactant, respectively. Ideally, these bands should be conveniently isolated from adjacent features, sloping background, etc. In the present case, the most appealing candidate for monitoring the formation of the intercalate is the sharp 2ν(NH) band at 6700 cm^{-1}. The band grows against a nearly null background because the adjacent broad and weak 2ν(NH) envelope of the liquid at ~6620 cm^{-1} has negligible contribution to the 2nd derivative spectrum (Fig. 3.2, middle) and appears stable in terms of position and width during the reaction. Potential proxies for the quantification of intercalated NMF could be either the integrated intensity of the band after subtracting the zero-time spectrum (Fig. 3.3, left) or its 2nd derivative amplitude (Fig. 3.3, right). The latter is more practical when the spectra are of good quality but requires that the width of the band remains constant during the reaction, and among reactions on similar materials.

The same proxy can be used for investigating the intercalation kinetics for KGa-2, too (Fig. 3.3, lower). The two Georgia kaolinites have similar spectra, except for a small portion of impurities that are contained in KGa-2, e.g. Fe^{3+} with a spectral contribution at 7018 cm^{-1} corresponding to 2νAlFeOH vibrations [Pet99]. Actually, the behavior of KGa-2/NMF (1:1 wt) spectral signature observed in 2ν(OH) and 2ν(NH) area is almost identical to that of KGa-1b: the bands attributed to the inner surface OH (7169, 7114 cm^{-1}) are decreasing in intensity, whereas the 2ν(NH) peak at 6700 cm^{-1} is increasing. More importantly, the widths of the 2ν(NH) band in the KGa-1b and KGa-2 series are constant during intercalation and identical within the resolution of our experiments (Fig. 3.4). This proves that the intermolecular interactions of NMF in the interlayer remain constant during intercalation and are independent of kaolinite type. Compared to KGa-1b, KGa-2 shows smaller change of the diagnostic peaks, indicating smaller NMF uptake, but this will be examined later on the thesis (Ch. 4).

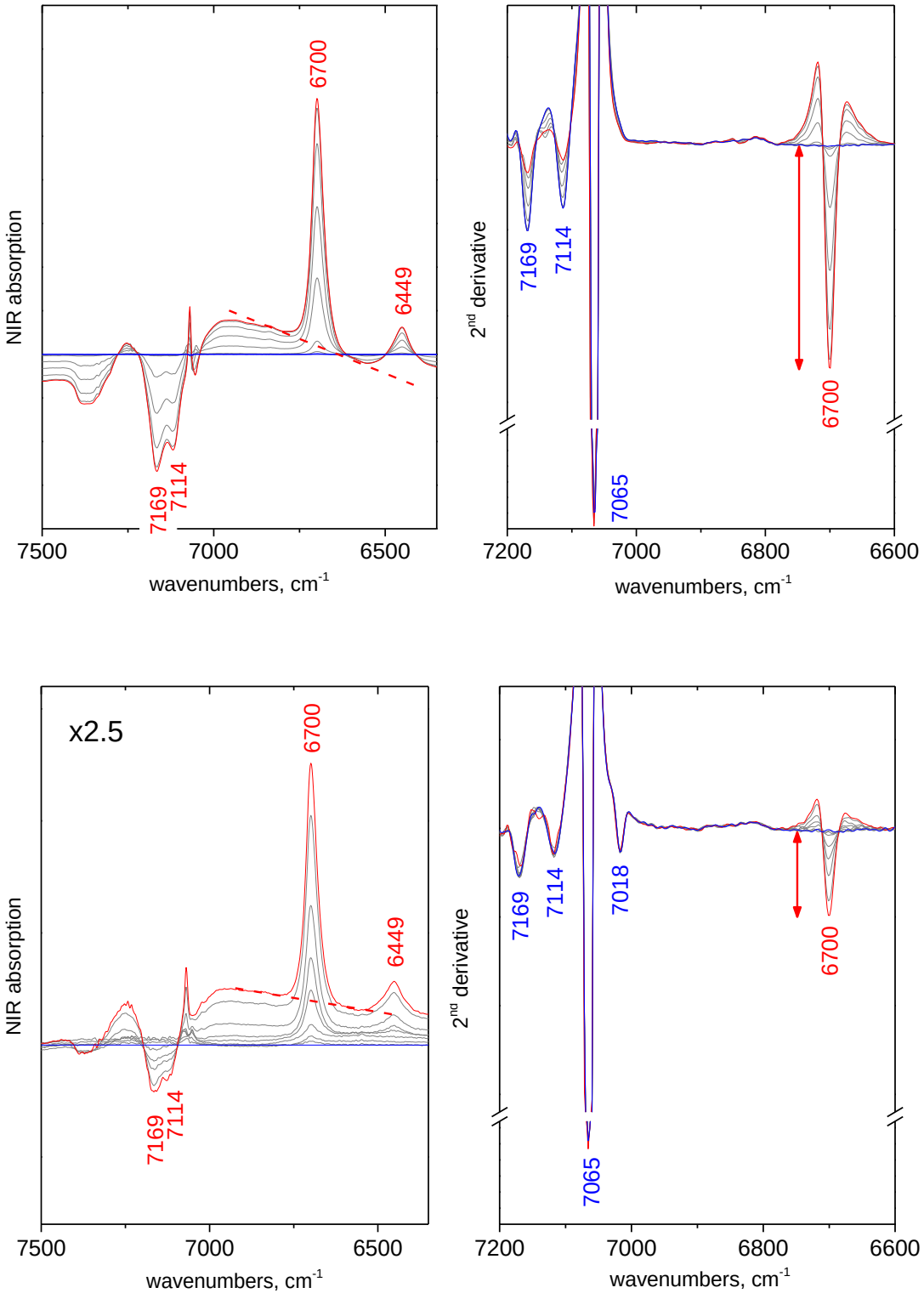

Figure 3.3. Selected NIR spectra of KGa-1b/NMF (upper) and KGa-2 (lower) during intercalation at 30 °C in the 2ν(OH) and 2ν(NH) region: (left) difference after subtracting the spectrum at zero time and (right) 2nd derivative with 9 points smoothing ($\Delta\nu$=2 cm^{-1}). Notice the break of the y-axis in the right panel.

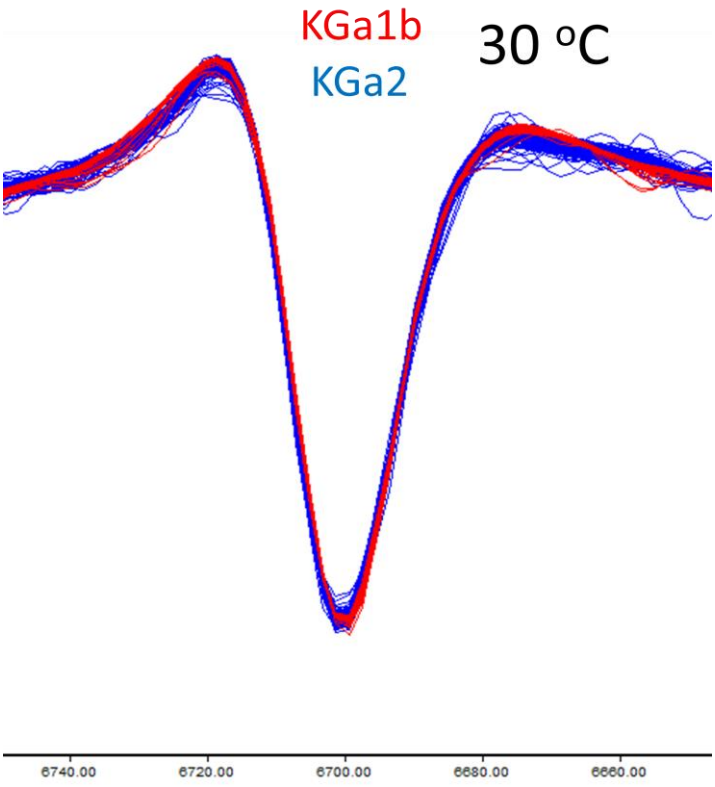

Figure 3.4. 2nd derivative with 9 points smoothing (Δν=2) of the 2ν(NH) mode vector normalized at the displayed frequency range for KGa-1b (red) and KGa-2 (blue) intercalation kinetics with NMF at 30˚C. The initial 10-20 spectra of each series were not included in the comparison because they were noisy due to low intensity.

3.3 Kinetics at 30 °C

Intercalation kinetic NIR experiments of dry KGa-1b and KGa-2/NMF (1:1 wt) pastes were performed at 30 °C over a period of >2 days with a sampling frequency of 30min. The resulting spectral series were analyzed by the integral and 2nd derivative methods. In order to compare the kinetics recorded by each method, the integrated area and the 2nd derivative intensity data were normalized to their respective long-term asymptotic values (see below, Fig. 3.6), yielding an apparent degree of intercalation (apparent reaction progress), α_{app}. In both reactions, α_{app} obeys sigmoidal time-dependence, which is practically independent from the proxy employed (Fig. 3.5). The matching between the integral- and derivative-based data series suggests that the effects of changing baseline or width of the 2ν(NH) mode are negligible.

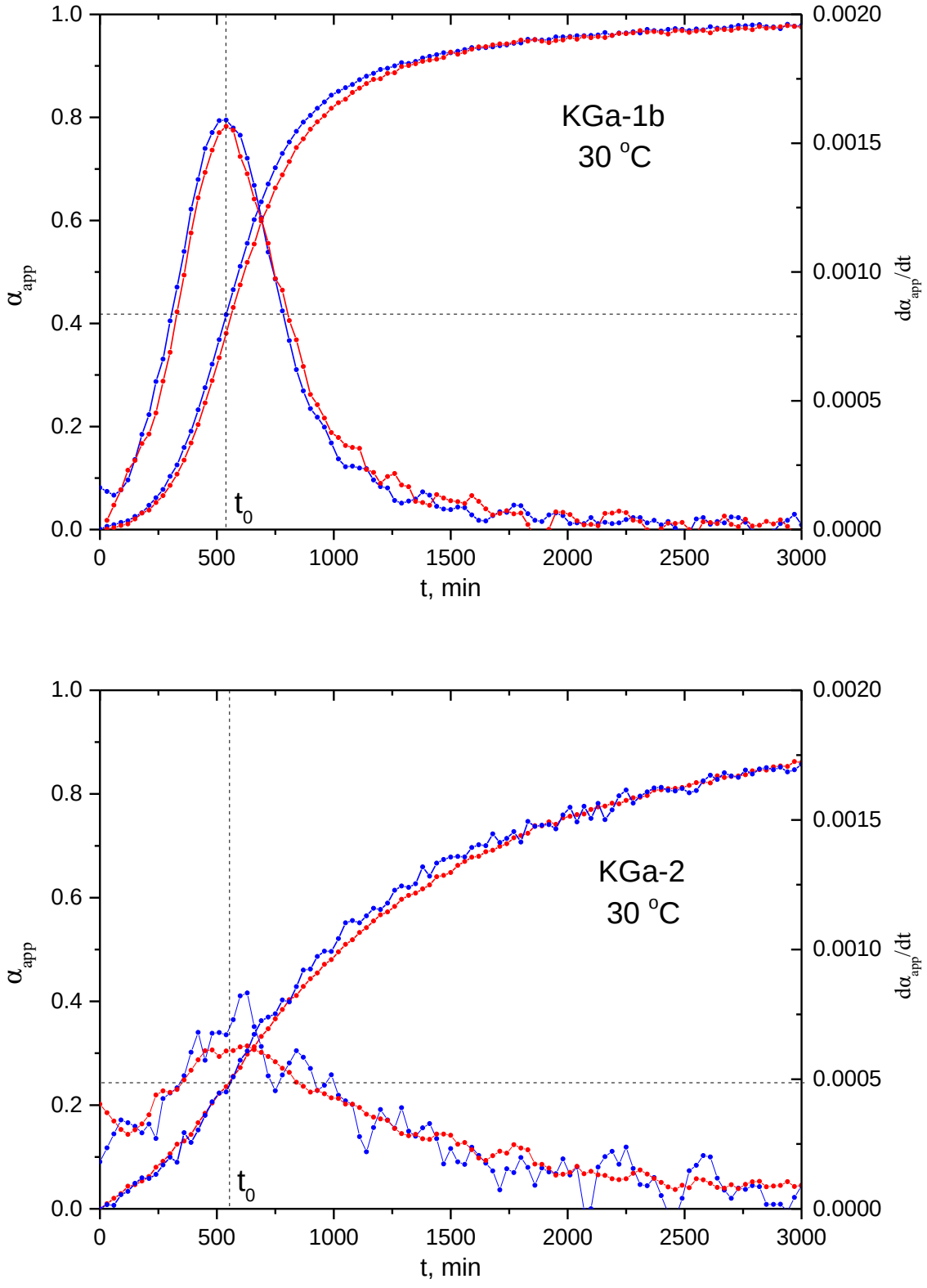

Figure 3.5. NIR intercalation kinetics of dry KGa-1b/NMF (upper) and dry KGa-2/NMF (lower) at 30 °C by the integral (red) and 2nd derivative (blue) proxies. α_{app} and $d\alpha_{app}/dt$ are the apparent degree and rate of the reaction, respectively.

During the first ~500-600min the reaction is accelerating. The rate of the subsequent deceleration is smaller than the acceleration's, so that the sigmoidals appear steeper in the beginning than in the end. Although both kaolinites display S-shape kinetics, the characteristics of each curve are different. In the case of KGa-2 the sigmoidal is less steep and more asymmetric than in KGa-1b. This asymmetry is better observed in the $d\alpha_{app}/dt$ rate (Fig. 3.5), expressed by a skewed curve with a maximum at t_0, equal to ~550min in KGa-2 versus ~520min in KGa-1b. The apparent reaction progress is ~0.24 and ~0.42 for KGa-2 and KGa-1b, respectively. After two days at 30 °C, KGa-1b has reached a plateau in α_{app}, indicating that intercalation has reached asymptotically its final state. On the other hand, KGa-2 intercalation continues, albeit with a very slow rate.

As the kinetic experiments in Fig. 3.5 were performed under identical conditions, the differences observed between the KGa-1b and KGa-2 systems must reflect some material property of the particular kaolinites employed. In order to examine further the systematics of intercalation and their dependence on the type of kaolinite, variable-temperature studies were accomplished for both kaolinites.

3.4 Temperature dependence

Sealed samples of dry KGa-1b/NMF (1:1 wt, paste) placed in a thermostatic bath were examined at twelve temperatures in the 30-75 °C range (Fig. 3.6, upper). Similarly, dry KGa-2/NMF was investigated at six temperatures in the 25 to 70 °C range (Fig. 3.6, lower). Intercalation is clearly faster when the temperature increases, e.g. in KGa-1b kinetics are almost complete after ~30h at 30 °C, ~10h at 45 °C or ~3h at 70 °C. For that reason, the time resolution of monitoring ranged between 30 and 5 min, respectively. Altogether, the kinetics in Fig. 3.6 represent cumulative data acquisition of ~1month. In the case of KGa-2, intercalation needs more time to evolve. All sigmoidals are more flattened than their KGa-1b counterparts and, at most temperatures studied, they don't reach a clear plateau. A plateau is observed at the highest temperature, e.g. after ~10-12h at 70 °C intercalation. Due to the widely different time-range of the experiments, the effect of temperature is more conveniently studied in a log-time scale (Fig. 3.7).

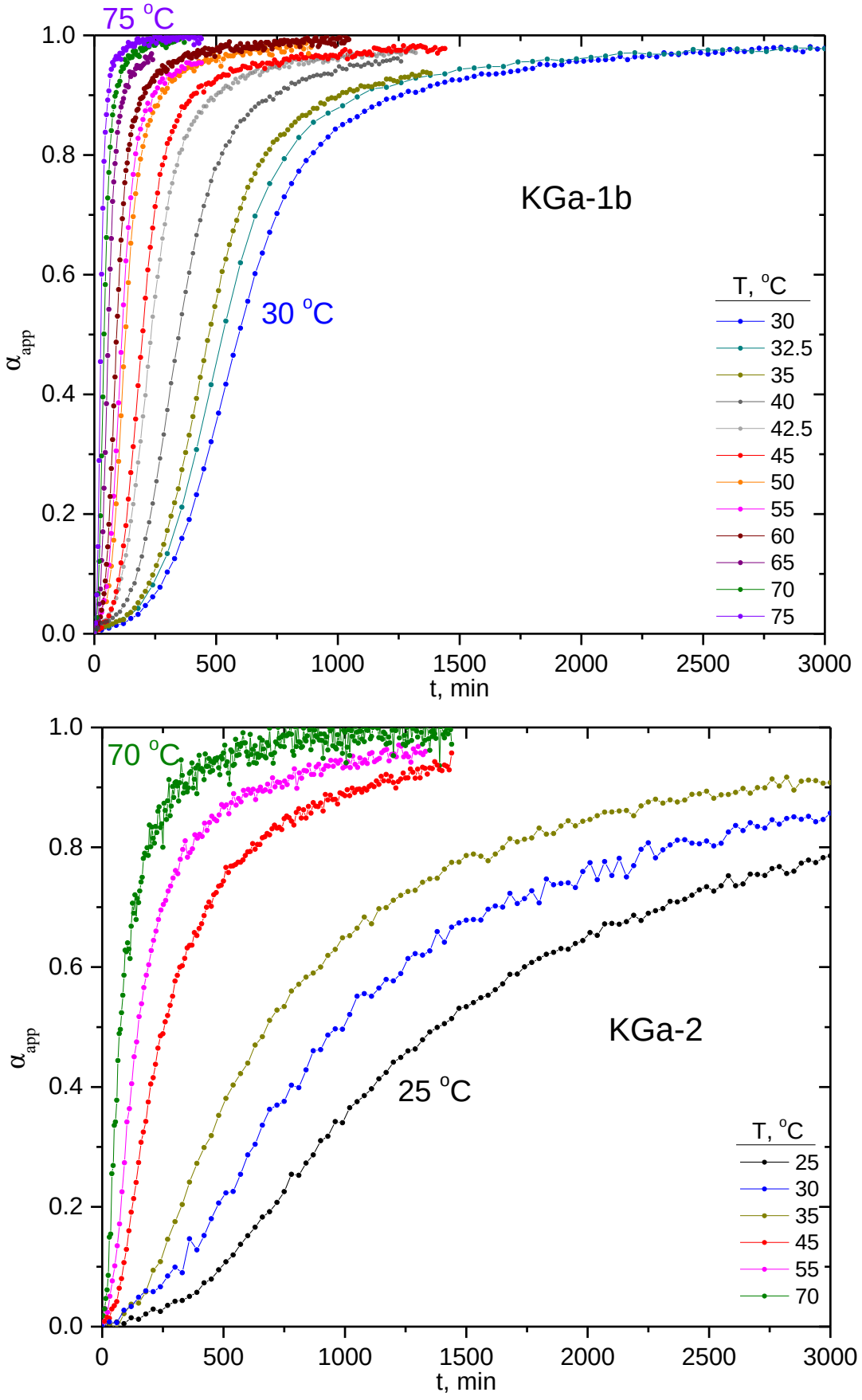

Figure 3.6. NIR intercalation kinetics of dry KGa-1b/NMF (upper) in the 30-75 °C range and dry KGa-2/NMF (lower) in the 25-70 °C range.

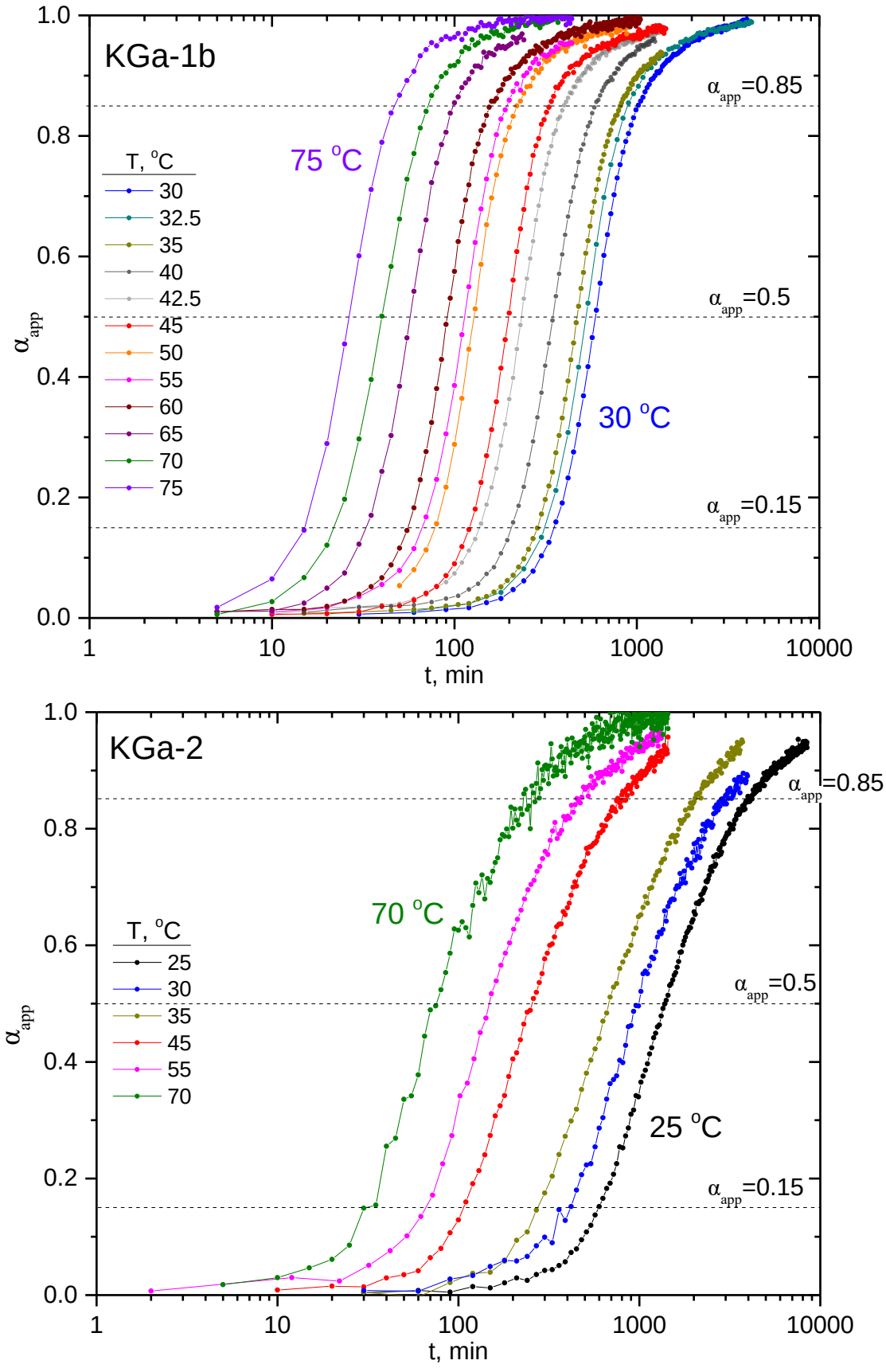

Figure 3.7. Dry KGa-1b/NMF (upper) and dry KGa-2/NMF kinetics (lower) depicted in Fig. 3.6 in a log-time axis.

In the log-time scale, the S-shape of the kinetics which is specific for each kaolinite appears to be maintained over the whole range of temperatures (Fig. 3.7). The increase in temperature appears to result only in a parallel shift of the curve towards shorter times. Moreover, the sigmoidals that were clearly asymmetric in the linear-time scale (Fig. 3.6) appear symmetric in the log-time scale (Fig. 3.7), an observation that will be explored in more detail later in this thesis.

In order to closely examine the effect of temperature on the shape of the sigmoidals, the data were plotted versus reduced time, t/t_0, where t_0 is defined as the time of maximum rate, $d\alpha_{app}/dt$ (Fig. 3.5). This type of time reduction (or any other type, e.g. at fixed α_{app}) merged the twelve sigmoidal curves of KGa-1b or the six for KGa-2 into well defined time-temperature superposition masterplots (Fig. 3.8). The shape of the intercalation masterplot is unique for each type of kaolinite in the examined temperature range (30-75 °C for KGa-1b and 25-70 °C for KGa-2), the characteristics of which differ in terms of steepness, asymmetry and approach to the final asymptotic state.

Further evidence for the quality of the time-temperature superposition can be provided by calculating the activation energy of intercalation at various values of α_{app} [Sta03] for the two kaolinite systems. Assuming that the kinetic data obey an Arrhenius equation:

$$lnt_f = \frac{E_\alpha}{RT} + C \qquad Equation\ 3.1$$

where t_f is the time needed to reach a certain reaction degree, E_α the activation energy, R the universal gas constant, C a constant depending on the kinetic model and the reaction stage and T the absolute temperature [Sta03], the activation energy was estimated from the Arrhenius plots (Fig. 3.9) for α_{app}=0.15, 0.5 and 0.85. All three calculations, as well as an additional one based on the time for $d\alpha_{app}/dt=0$, resulted in the same activation energy: E_α=60±2 kJ/mol (0.62±0.02 eV, 14.3±0.5 kcal/mol) (Fig. 3.9, upper).

Surprisingly, the same exercise in KGa-2 yielded E_α=57±3 kJ/mol (Fig. 3.9, lower), which is identical within error to KGa-1b.

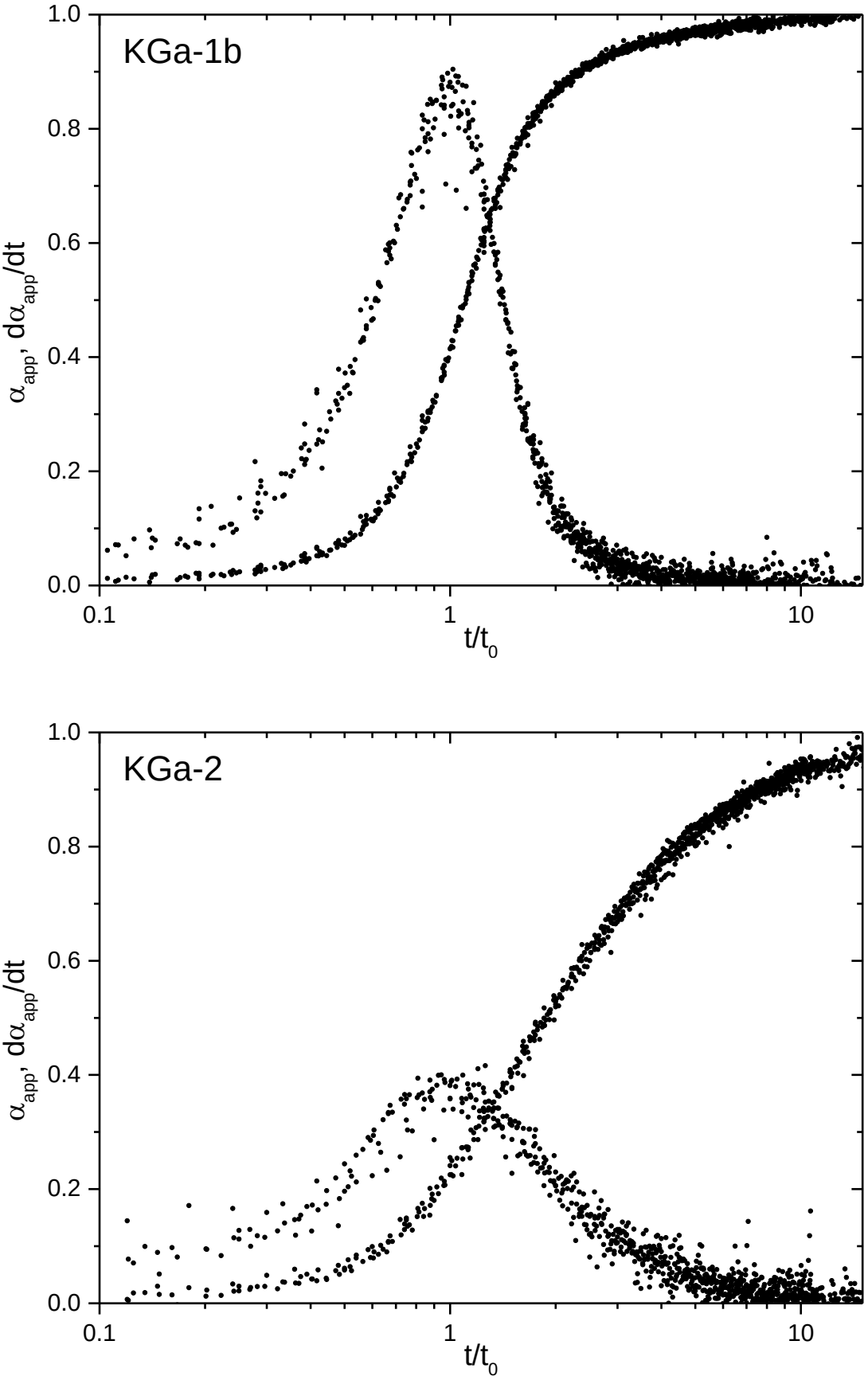

Figure 3.8. NIR-based time-temperature superposition of the kinetic data of KGa-1b (upper) for Fig. 3.7 upper and KGa-2 (lower) for Fig. 3.7 lower. Reduced t/t_0 times are used.

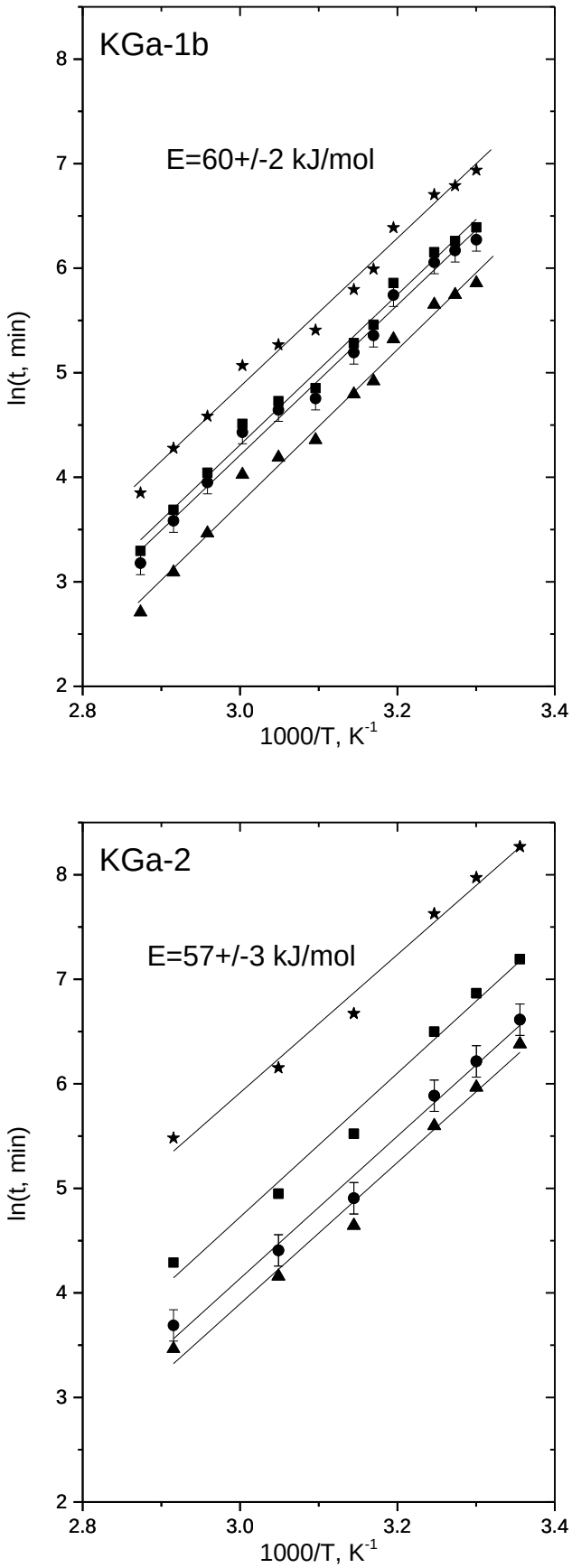

Figure 3.9. Arrhenius plots for KGa-1b (upper) and KGa-2 (lower) of t_0 values (circles) and α_{app}=0.15 (triangles), 0.5 (squares) and 0.85 (stars). Straight lines are least-square fits.

3.5 XRD vs. NIR sigmoidal kinetics

The sigmoidal time-dependence progress of kaolinite intercalation extracted by NIR (Fig. 3.8) has been already observed by XRD, albeit *ex-situ* [Wei63, Ole68, Hac69, Ole70, Cas15, Mak19]. In fact, it has been typically observed for all primary intercalating molecules, e.g. urea, DMSO etc. The degree of intercalation (α_{XRD}) at a given time t was estimated by the ratio:

$$a_{XRD}(t) = \frac{\mathrm{A_N(t)}}{\mathrm{A_N(t) + A_K(t)}} \qquad Equation\ 3.2$$

where $A_N(t)$ and $A_K(t)$ are the time-dependent integrated intensities of the *001* diffraction peaks of the intercalated and pristine kaolinite, respectively [Ole68, Wie69].

The first effort to study the kinetics of intercalation was done by Weiss [Wei63] with urea, formamide and hydrazine as guest molecules under different environmental conditions (Fig. 3.10).

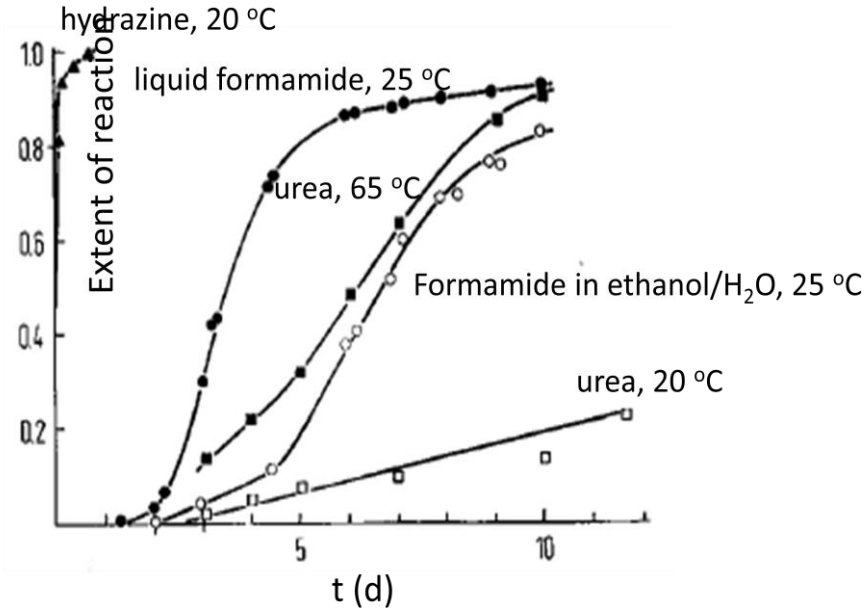

Figure 3.10. Rate of intercalation of urea (squares), formamide (circles) and hydrazine (triangles) in kaolinite. Reproduced from Weiss [Wei63] by permission.

Although the data were very few and the time-scale was in days, the sigmoidal behavior was clearly observed in most samples. However, the evolution of very quick reactions (e.g. intercalation with hydrazine) could not be recorded.

XRD studies of NMF intercalation were reported in the literature [Hac69, Ole70, Mak19]. Among them, only Hach-Ali and Weiss [Hac69] and Makó [Mak19] examined the temperature dependence of the kinetics.

Hach-Ali and Weiss [Hac69] studied the 2-4 μm fraction of a commercial kaolinite designated as KIS. They mixed 0.6 g of kaolinite, dried at 110 °C, with 2 ml of NMF, and the sealed vial was kept at the applied temperature for the necessary time. The samples were examined at 7, 25, 45 and 65 °C, all of which presented sigmoidal intercalation kinetics. The time needed for almost complete intercalation was ~3d, 13h and 3h at 25, 45 and 65 °C, respectively. The final reaction degree was estimated to exceed >95% according to Eq. 3.2, but the authors considered the use of Eq. 3.2 problematic. When using Eq. 3.2 for quantification purposes it is assumed that the structure factor and the Lorentz polarization for the reflections of pristine and intercalated kaolinite are equal, which was not confirmed. The authors tried to correct the results by measuring known mixtures of "fully intercalated" and non-intercalated kaolinite and concluded that the actual final degree of reaction is smaller (~90%), i.e. Eq. 3.2 overestimates α.

Olejnik et al. [Ole70] used the <2 μm equivalent spherical diameter fraction of a kaolinite from Mesa Atla, New Mexico (No. 9 of API project No. 49) in the Na^+ saturated form. They studied suspensions (2 ml of NMF in 20 mg of kaolinite) shaken at 20±2 °C for various lengths of time. For the XRD kinetics, the sample was spread on an unglazed porcelain tile to form a uniform thin layer and then it was covered with a polythene film. The final degree of intercalation, as defined by Eq. 3.2, was over 90% and was reached after ~3d. In fact, the sigmoidal shape was not confirmed in this study due to limited data in the beginning of the reaction.

Makó et al. [Mak19] used a commercial Zettlitz kaolinite (Czech Republic), which contained ~90 wt% of medium-defect kaolinite with a Hinckley index of ~0.8, versus ~1 in KGa-1b and ~0.2 in KGa-2. The raw sample was mixed with the intercalated reagent and distilled water at room temperature and then aged for 1 and 24h at different temperatures (20, 40, 50, 60, 70 and 80 °C). The maximum

intercalation degree was calculated at 95%. Full kinetics were reported only at two temperatures, 20 and 60 °C. The time needed to reach the final reaction degree was estimated ~10h at 20 °C and <1h at 60 °C. The kinetic curves consisted of a few data points and the sigmoidal at 60 °C was clearly undersampled.

Overall, the reaction times of the present NIR-based kinetic study agree favorably with the XRD-based ones in the literature and any differences may be tentatively attributed to the different geological origin of kaolinite, the particle size, and the preparation of the sample.

However, it is fascinating and a bit counterintuitive that both NIR and XRD display similar sigmoidal kinetics, despite the fact that they probe very different aspects of intercalation. Without considering interstratification or layer distortion effects, XRD-derived kinetics respond to the progressive increase of the coherence of expanded interlayers along *001*. Strictly speaking, the interlayers must contain some critical number of intercalated guest molecules to be expanded but do not need to be full. On the other hand, a NIR-based degree of reaction corresponds to the growing concentration of intercalated species in the interlayers. Therefore, the NIR-based curve could be expected to be smoother than its XRD counterpart. In fact, it could be expected to lack the initial incubation period that causes the sigmoidal shape. This is because the intercalated guests may be observed by spectroscopy as they populate along *ab* before the requirement for coherence along *c* is met by interlayer expansion. Moreover, a stack of fully expanded interlayers, which would produce 100% intercalation in XRD experiments, may not necessarily be fully populated by guest molecules, yielding <100% intercalation in NIR spectroscopy. The similarity between the NIR- and XRD- based sigmoidals may imply that NIR also probes expansion along *c* and not diffusion along *ab*. The latter may be too fast to be observed leading to a two-state description of the system consisting of non-intercalated and fully intercalated entities and lacking partially intercalated interlayers.

3.6 XRD vs. NIR activation energy

Despite the differences in the kinetics between KGa-1b and KGa-2, both samples display one single activation energy, ~60 kJ/mol (Fig. 3.9). Previous efforts to estimate activation energy of kaolinite intercalation with NMF by XRD claimed values of ~150 kJ/mol [Hac69] and ~72 kJ/mol [Mak19]. In both cases activation energy was extracted from a limited number of thermostatic experiments and the kinetics (considered to obey an Avrami-Erofeev model) were based on Eq. 3.2 which does not incorporate the influence of the structure factor and the Lorentz polarization on the two reflections. The suitability of Avrami-Erofeev and other models in the literature to fit the kinetic data will be discussed elsewhere in this thesis (Ch. 5). However, we note that, Hach-Ali and Weiss extract E_α ≈150 kJ/mol from the temperature dependence of Avrami-Erofeev slopes based only on the data from the early (accelerating) part of the sigmoidal. Plotting the entire data series vs. log time as in Fig. 3.7 (Fig. 3.11), and calculating E_α in the manner of Fig. 3.9 (Fig. 3.12) yield E_α≈73±3 kJ/mol (0.75±0.03 eV, 17.4±0.7 kcal/mol), i.e. similar to the results of Makó et al. [Mak19] and in reasonable agreement with the present NIR investigation (~60 kJ/mol).

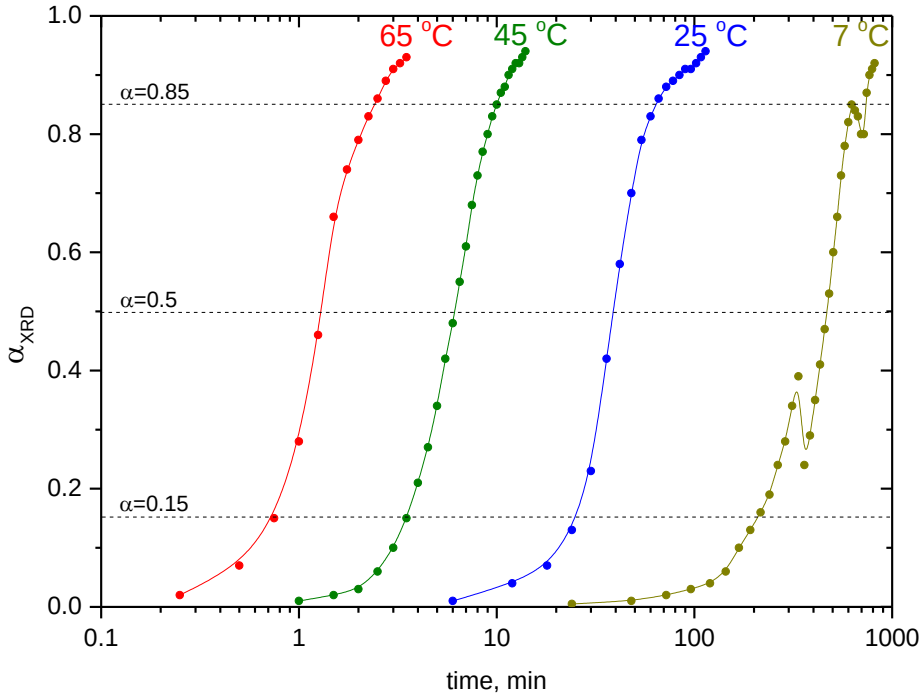

Figure 3.11. Intercalation kinetics of kaolinite/NMF based on the results of Hach-Ali and Weiss [Hac69].

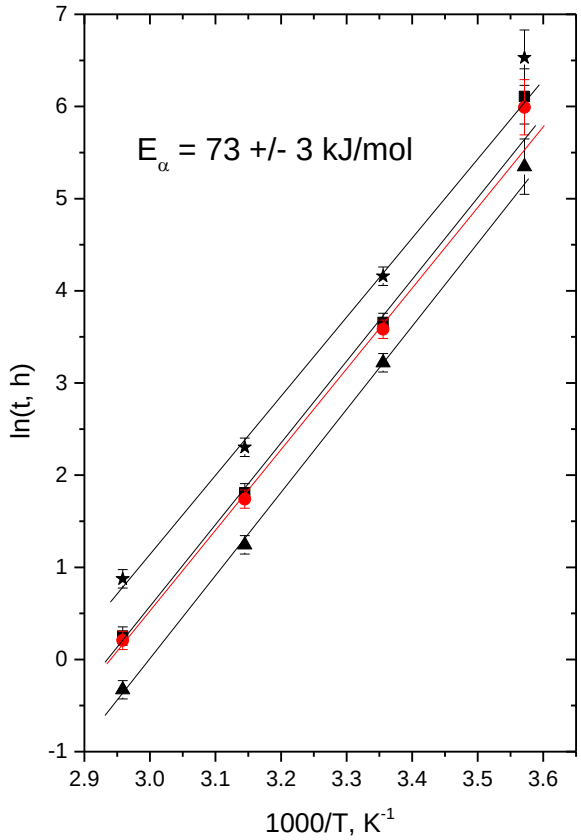

Figure 3.12. Arrhenius plots of t_0 values (red circles) and t at α_{app}=0.15 (triangles), 0.5 (squares) and 0.85 (stars) for the diagrams of Fig. 3.11. Straight lines are least-square fits.

Time-temperature superposition and the independence of activation energy on apparent reaction progress, $\alpha_{app,}$ were demonstrated by the NIR monitoring of two kaolinite/NMF systems. Our findings indicate that the rate-determining step of intercalation is unique throughout the time-temperature window of our experiments and common to both kaolinites. Should there be two processes active during intercalation, as suggested in literature [Hac69, Lag06, Cas15, Mak19], they would exhibit different temperature dependence (activation energy). This is definitely not observed. Remarkably, the same underlying conclusion can be drawn now on the basis of the most XRD data in the literature obtained on a third kaolinite [Hac69], besides KGa-1b and KGa-2.

Chapter 4

Is intercalation complete?

In the previous chapter, the kinetic curves were produced by normalizing the 2nd derivative intensity data to their respective long-term asymptotic values, which yielded an apparent reaction progress, α_{app} -> 1. However, the actual degree of intercalation, α, is not necessarily identical to α_{app}, despite the high purity of both kaolinites (96.4 and ~100% for KGa-1b and KGa-2, respectively, see below) and opposite to the analysis of the XRD data which suggests nearly complete intercalation (90%) for KGa-1b [Tun96].

There are several spectroscopic indications suggesting that $\alpha_{app}<\alpha$. For example, in the case of KGa-1b, quantitative intercalation (α=1) at long times would imply the disappearance of the kaolinite's inner surface 2ν(OH) signature (Fig. 3.3) and the full replacement of the ν+δ(OH) band at 4527 cm^{-1} by the new one at 4519 cm^{-1} (Fig. 3.2, lower). The fact that this is not observed in any of the experiments described in Chapter 3 provides evidence that intercalation was not complete despite having reached a plateau (in the case of KGa-1b). This chapter aims at determining experimentally the true degree of intercalation of each kaolinite in order to enable a subsequent study on the origin of non-intercalated material.

4.1 Kaolinite intercalation by NMF vapors

In the preparative stages of this work, it was realized that intercalated kaolinite could be produced equivalently (and to the same α_{app} at ambient temperature) by exposing kaolinite to liquid NMF (as in Ch. 3) or to gaseous NMF, despite the low vapor pressure of the amide (~0.45 Torr at 25 ^{o}C). The liquid NMF approach offered better control of the reaction conditions and was preferred, but intercalation from the vapor phase offered a better view of the kaolinite spectral changes, because the spectra were free from the contribution of liquid NMF which is particularly strong in the combination range. A small quantity of KGa-1b (~0.1 g) was spread on the integration sphere window of the NIR spectrometer (~2 cm diameter) and was covered by a cup containing a small reservoir of NMF. The inside of the cup was lined by filter paper, also soaked in NMF. This created a small volume (~300 ml) that was totally isolated from the environment and saturated by NMF. This type of intercalation experiment typically lasted for ~4d with a temporal resolution of 30min and was affected by unavoidable variations of the ambient temperature during the measurement period.

The quantification of the reaction progress was based on the analysis of the ν+δ(OH) band by multiple regression (Fig. 4.1 for KGa-1b). Each spectrum at time *t,* S_t, was expressed as a linear combination of the spectra of the α=0 and α=1 states, (S_0 and S_1, respectively), $S_t=(1-\alpha_t)S_0+\alpha_t S_1$, where α_t represents the true degree of intercalation at time *t*. S_0 is measured at the beginning of the experiment, before the onset of intercalation. S_1 was obtained from $S(t_\infty)$ as $S(t_\infty)/\alpha_\infty$. The final degree of progress, α_∞, was calculated by subtracting $(1-\alpha_\infty)S_0$ from $S(t_\infty)$ so that the signature of S_0 is fully eliminated from it. Multiple regression calculated $(1-\alpha_t)$ and α_t independently, and the proximity of their sum to unity was a measure of the quality of the fit.

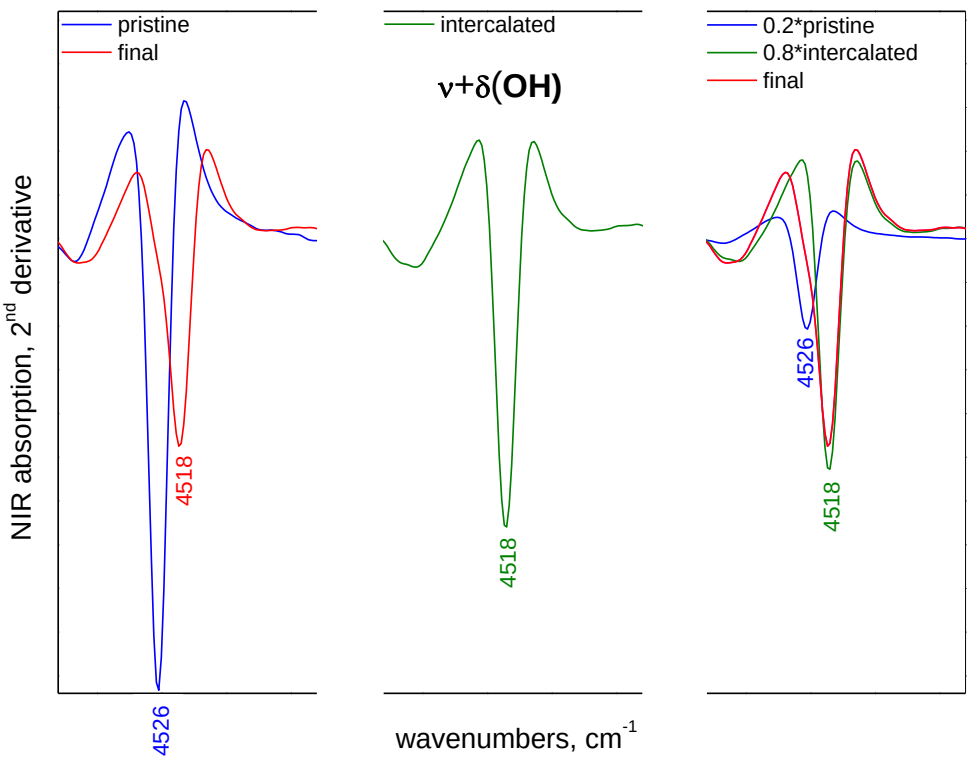

Figure 4.1. Multiple regression principle as derived from the 2nd derivative with 9 points smoothing ($\Delta\nu$=1 cm^{-1}) of NIR spectra of KGa-1b/NMF intercalation at room temperature in the ν+δ(OH) range: (left) S_0 spectrum (blue) and S_t for t=~4d (red), (middle): S_1 spectrum (green), (right): S_t spectrum expressed as a linear combination of S_0, S_1spectra. For details see text.

In the example of Fig. 4.1, the initial spectrum, corresponding to pristine KGa-1b, displays a single peak at 4526 cm^{-1}, whereas the spectrum after ~4d demonstrates a peak at 4518 cm^{-1} with a weak residual component at 4526 cm^{-1} (Fig. 4.1, left). The subtraction of the initial spectrum S_0 from the final, till the contribution of the former is eliminated provided the spectrum of fully intercalated kaolinite, S_1 (Fig. 4.1, middle). All the spectra between the two states (non- or fully intercalated) can be reproduced satisfactorily as a linear combination of the pristine and fully intercalated kaolinite spectra (Fig. 4.1, right). The calculated factors of the linear combination of each spectrum attributing to intercalated or pristine component can provide an estimation of the intercalated or non-intercalated portion, respectively (Fig. 4.2). The sum between the intercalated and non-intercalated sample is always ~1, meaning that the two components S_0 and S_1 are sufficient to describe the system (two-mode system) and suggesting that there is no intermediate phase between the two end-member states.

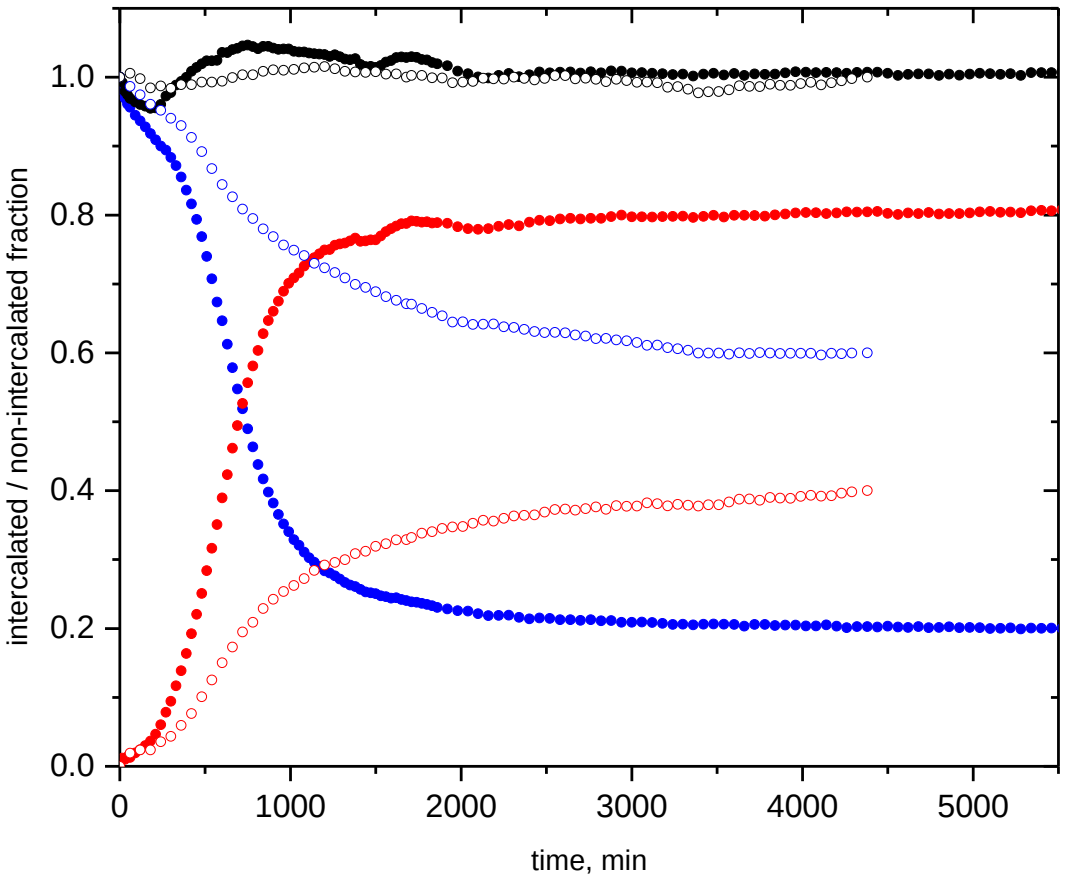

Figure 4.2. Progress of intercalated kaolinitic fraction (red), non-intercalated (blue) and their sum (black) based on the ν+δ(OH) peak for KGa-1b (filled symbols) and KGa-2 (open symbols).

The as-derived kinetics reached a plateau within ~2d yielding an intercalation degree of the order of α=0.8 (Fig. 4.3, upper). By analogy, the final degree of intercalation in KGa-2 did not exceed α=0.4 (Fig. 4.3, lower). Interestingly, the kinetics monitored by the shift of the ν+δ(OH) band are in excellent synchronization with those derived via the intensity of the 2ν(NH) band from the same sets of spectra of both KGa-1b and KGa-2 (Fig. 4.3). Importantly, this suggests that the two proxies of the kaolinite layer and the NMF-hosting interlayer "sense" the same reaction.

The difference between the NMF uptake of KGa-1b and KGa-2 (~94% and ~70%, respectively, based on Equation 3.2) has been reported by Uwins et al. [Uwi93]. This difference was observed despite a pretreatment by hydrazine which is a known enhancer of intercalation [Den03].

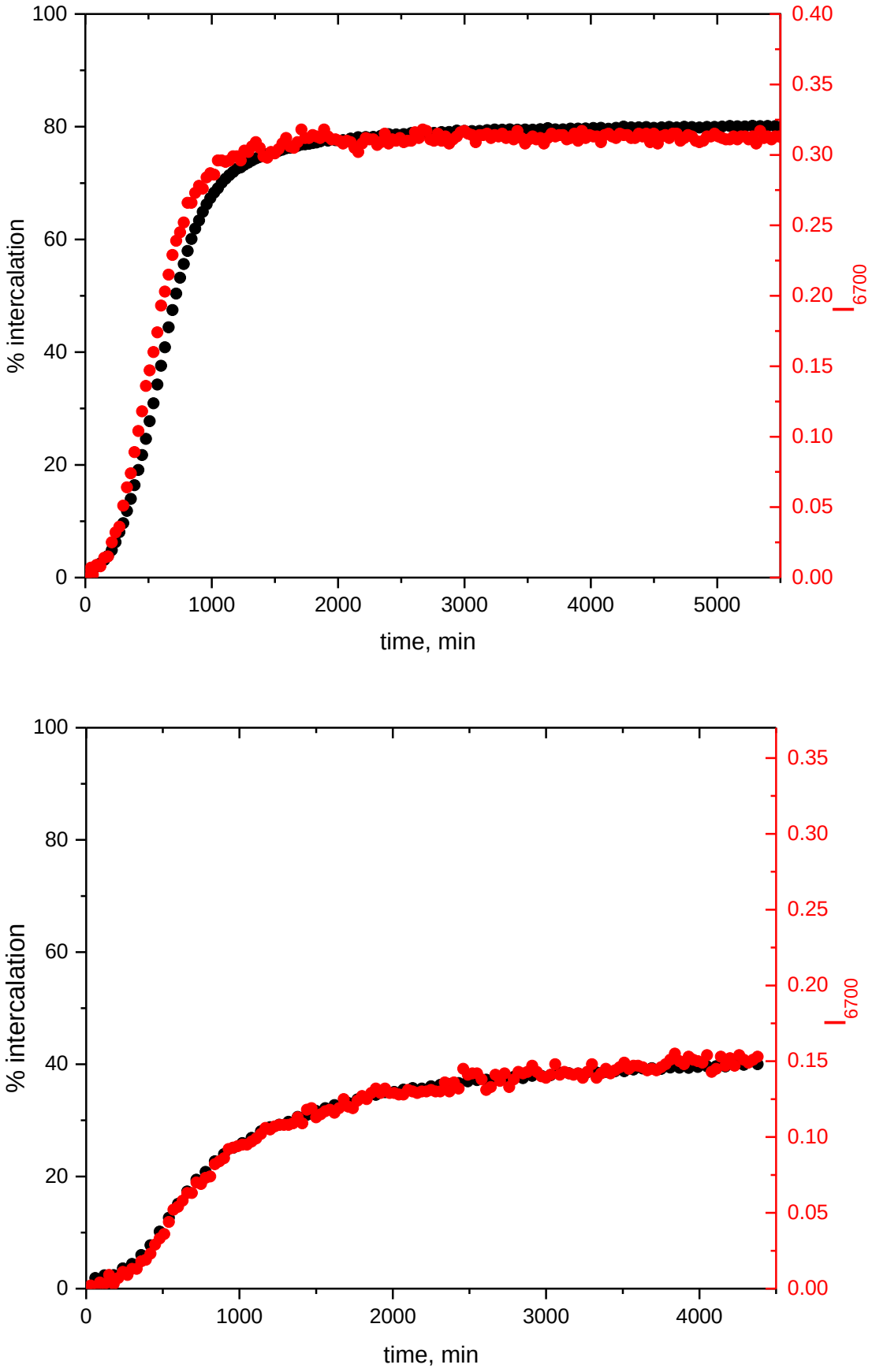

Figure 4.3. % intercalation kinetics based on the ν+δ(OH) (black) and 2ν(NH) indicator (red) in KGa-1b (upper) and KGa-2 (lower).

4.2 Thermogravimetric analysis

As an independent test of the previous results, thermogravimetric analysis (TGA) was performed. A typical TGA diagram of kaolinite displays a mass loss equal to 14% between ~400-600 °C due to dehydroxylation [Dri15] based on the reaction:

$$Al_2Si_2O_5(OH)_4 \rightarrow Al_2Si_2O_7 + 2H_2O\uparrow$$

The observed loss of KGa-1b is 13.5% indicating purity of 96.4%. The corresponding loss in KGa-2 is 14%, therefore it is almost 100% pure kaolinite.

The intercalated samples display, except of the aforementioned loss due to the dehydroxylation of kaolinite at high temperatures, also a loss in the low temperature range corresponding to NMF, liquid and intercalated. The maximum NMF uptake of kaolinite can be calculated according to the stoichiometric formula provided by Adams [Ada78]: in each unit cell of kaolinite ($Al_4Si_4O_{10}(OH)_8$) two NMF molecules maximum are contained. This stoichiometry corresponds to 22.9 g of NMF per 100 g of pure kaolinite. Calculating the NMF mass loss that is attributed to 100 g of pure kaolinite during the heating can provide an estimation of the intercalation degree.

When liquid and intercalated NMF are present in the sample they exhibit overlapping loss in the TGA diagram. As a result, the accurate discrimination of the two components is not straightforward. Thus, the removal of the excess of liquid NMF was employed before TGA analysis. Following Tunney and Detellier [Tun96], the samples were washed with dioxane and then dried at ambient temperature for ~1d. By this method, some intercalated NMF could also be rinsed or evaporated, resulting in the underestimation of the intercalation degree [Lag06]. Samples from NMF vapors experiments could also be analyzed by TGA. The absence of liquid NMF state would lead to avoidance of further processing before the measurements and more reliable results.

A quantity of the dry sample (~10 mg) was placed on the pan, equilibrated at 40 °C and scanned to 800^{o}C at 10 ^{o}C/min, under dry N_2 purging (60mL/min). The recorded TGA diagrams were normalized to 100% kaolinite (14% mass loss).

Dry KGa-1b/NMF and KGa-2/NMF intercalated for ~3d at 30 °C displayed a minimum NMF uptake of ~16.3 and ~6.5 g per 100 g of kaolinite, respectively (Fig.

4.4). Similar values were obtained at KGa-1b/NMF and KGa-2/NMF by NMF vapors after ~3d intercalation. The calculated intercalation degree was ~70% for KGa-1b and ~30% for KGa-2, definitely far from complete intercalation, but comparable to ~80% and ~40%, respectively, that was derived from the study with NMF vapors.

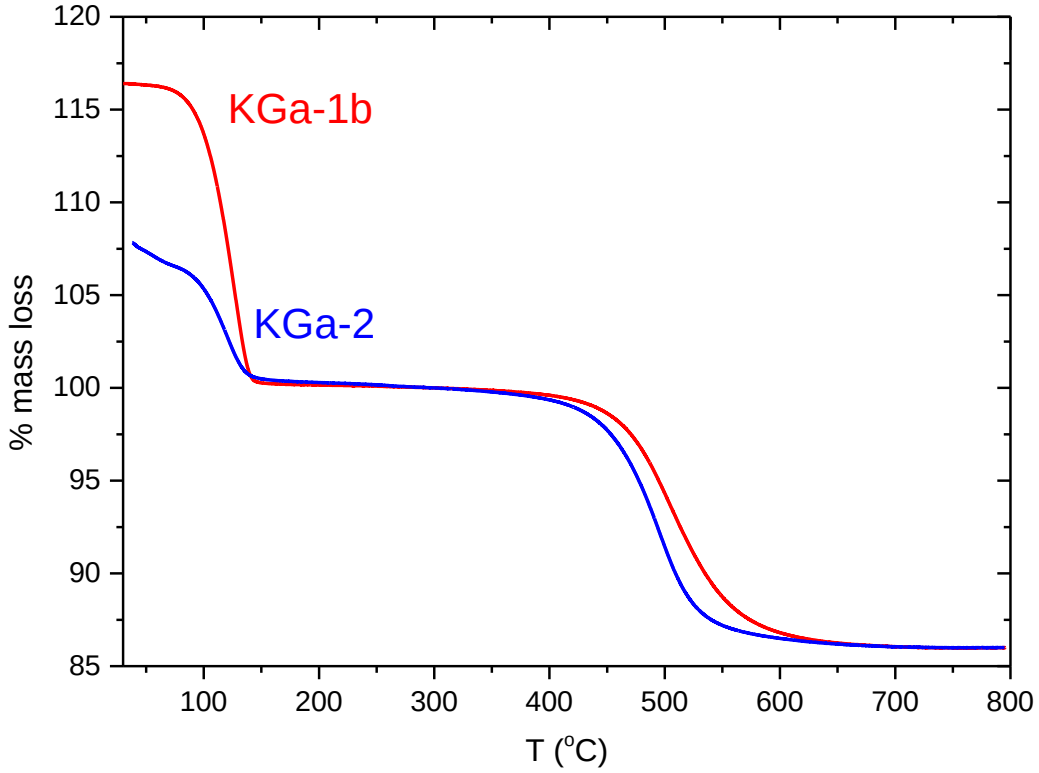

Figure 4.4. TGA diagrams normalized to 100% kaolinite in KGa-1b/NMF (red) and KGa-2/NMF (blue) from pastes after washing with dioxane.

4.3 Preliminary XRD monitoring

In contrast to previous publications by XRD that reported 90% intercalation in KGa-1b using Equation 3.2 [Tun96], the present NIR study provided evidence that the final intercalation degree is lower (~80%) and cannot be approximated as quantitative. One possible reason for this discrepancy could be the overestimation of the degree of intercalation due to improper use of Equation 3.2 (Section 3.5). This is supported by preliminary *in-situ* XRD intercalation experiments performed by our partner (Clay Minerals Laboratory of the Institute of Geological Sciences/Polish

Academy of Sciences) and reported jointly in a recent international conference [And19].

A KGa-1b/NMF paste (1:1 wt) was prepared, spread on the XRD sample holder at ambient temperature (20-22 °C) and measured over the 2-30° 2θ range with a 4h time resolution, over a period of ~40h. The *001* reflections of the pristine and intercalated kaolinite are observed at 12.5° and 8.3° 2θ translating to d_{001}-spacings of ~7.2 Å and 10.9 Å, respectively (Fig. 4.5), and are in agreement with previous reports [Hac69, Ole70, Ada78, Uwi93, Cag10]. Only the peak at 12.5° is observed in the initial diagram. The intensity of this peak decreases with reaction time, while the new peak at 8.3° increases. Changes in the position of the peaks during intercalation were less than 0.02° 2θ which was the resolution of the diffractogram.

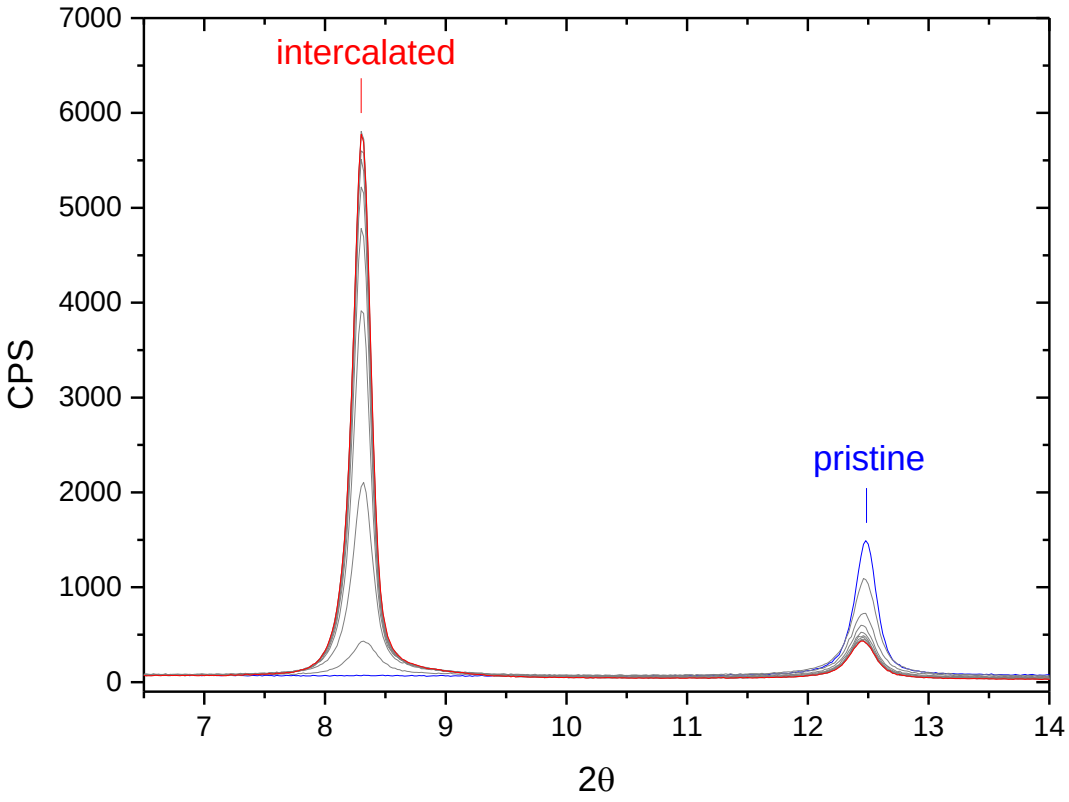

Figure 4.5. XRD diagrams of KGa-1b/NMF intercalation. The initial and last diagrams are depicted in blue and red, respectively.

The application of Equation 3.2 to the final state of the XRD experiment would yield α=0.91 in close agreement with previous XRD studies. However, it is obvious from Fig. 4.5 that the intensities of the peaks indicate that the *001* reflections of the pristine and intercalated phases do not display the same structure and Lorentz-polarization factors. Therefore, the degree of intercalation should not be calculated by Equation 3.2, as has been already suggested by Hach-Ali and Weiss [Hac69]. Instead, assuming that orientation remains stable during the reaction, the final intensity of the pristine kaolinite divided by its initial value can give an estimate of ~33% unreacted kaolinite (intercalation degree, ~67%).

The kinetics of intercalation can be obtained by plotting the progress of the integrated intensity of the peaks of the pristine or the intercalated phase. In order to compare with the NIR-intercalation data (Fig. 3.8), which are based on the formation of intercalated species (Section 3.2), the increase of the integrated peak of intercalated kaolinite was used (Fig. 4.6). The data were normalized to reach unity at the end of the experiment and time-reduced by the inflection point t_0, as in Section 3.4. The inflection point of the XRD series was ~630min versus ~520min at 30 °C (Section 3.3), which can be explained by the different temperature of the two experiments (XRD: 20-22 °C) and the unknown water content of the XRD sample.

The XRD derived kinetics displayed a sigmoidal behavior, in accordance with literature [Wei63, Ole68, Hac69, Ole70, Cas15, Mak19, Section 3.5], regardless of the proxies used. But the most remarkable outcome is the matching between the XRD and NIR kinetic curves (Fig. 4.6). Although further XRD experiments are needed, the matching of the XRD and NIR sigmoidals suggests that the two techniques probe the same aspects of intercalation, which must be related to the expansion along *c*-axis, and not to the propagation within the *ab* plane.

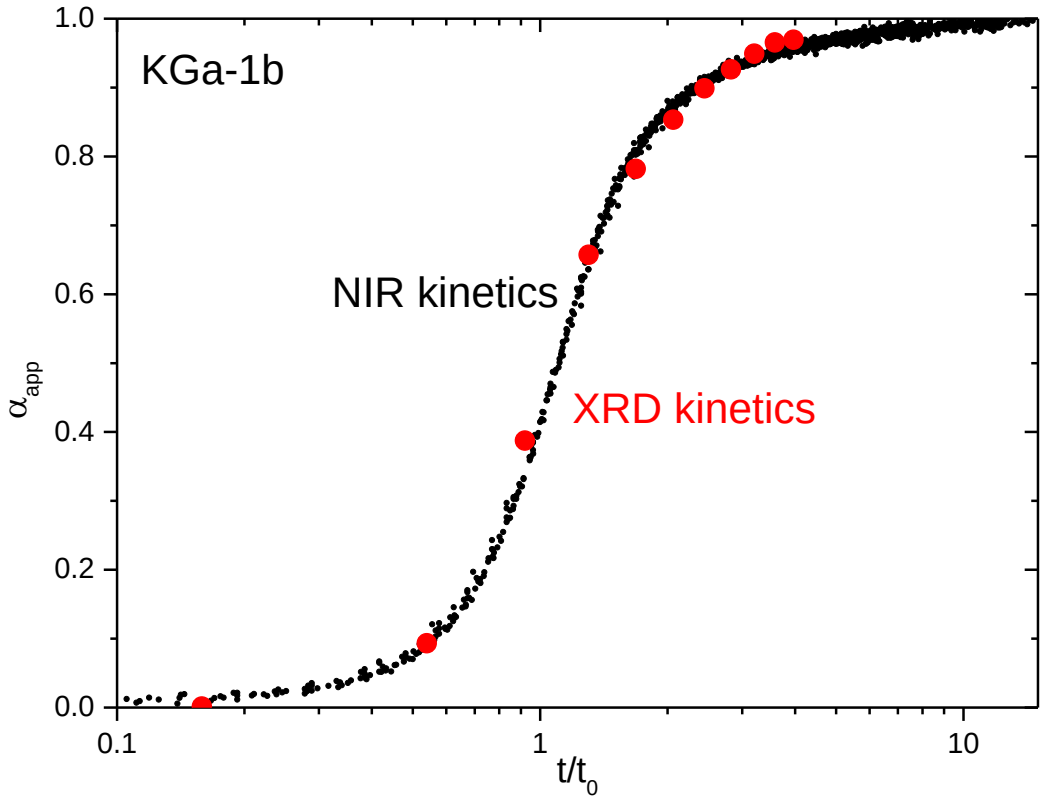

Figure 4.6. NIR-based time-temperature superposition of the kinetic data of KGa-1b/NMF depicted in Fig.3.8 (black) and XRD-based intercalation kinetics (red).

4.4 Supplementary experiments

The aforementioned experiments lead to the conclusion that intercalation is not complete in KGa-1b and it is even lower in KGa-2. Supplementary experiments were performed to exclude the possibility that non-complete intercalation was due to insufficient NMF, or premature termination of the reaction time.

Kaolinite samples were mixed with higher and lower amounts of NMF (1:2 and 1:0.7 wt) and examined with NIR spectroscopy for ~3d at 30 °C in comparison to the usual 1:1 formulations. The kinetic curves were almost independent of the kaolinite/NMF ratio and all reactions had reached a plateau after ~3d. Thermogravimetric analysis that followed after the ~3d infrared investigation yielded nearly the same intercalation degree with 1:1 sample, suggesting that even lower NMF concentration (i.e. 1:0.7 wt) is enough for the completion of intercalation and the doubling of the amount of NMF does not cause any increment. Intercalation was

also studied by adding excess NMF (+1g/1g kaolinite) at the end of a 3d intercalation and noticing no advancement over the following 2d at room temperature. Similarly, sealed 1:1 pastes with KGa-1b and KGa-2 for approximately 1y displayed no advancement of the reaction beyond that reported on the basis of a 3d exposure to NMF.

Taking all the above into consideration, incomplete intercalation is not due to insufficient NMF or lack of time. In both kaolinite samples, there is always fraction which does not respond to intercalation by NMF and this fraction is by no means negligible. Given the purity of the kaolinites investigated, the amount of residual unreacted kaolinite is ~30-20% in KGa-1b and ~70-60% in KGa-2. Such large amounts have to be related to some unknown structural or morphological characteristics that differ between the types of kaolinite. Several possible explanations have been proposed in the literature including the size of the particles or their stacking disorder [Uwi93, Den02] and will be discussed later in this thesis.

Chapter 5

Mechanism of intercalation

Although kaolinite intercalation has been studied through the last fifty years the mechanism of intercalation remains obscure. Previous investigations have examined or assumed several reaction models to explain the sigmoidal process invariably probed by XRD for all types of primary intercalating molecules. Such models include nucleation and growth [Hac69], adsorption and diffusion [Mak19], inserting and rotating [Cas15] or wedging and expanding [Lag06]. Despite the different proposed mechanisms, all of them share one characteristic; two steps are required to describe the sigmoidal intercalation. It is reminded that the NIR-based kinetics were also sigmoidal (to our surprise) and their temperature dependence presented in Chapter 3 did not resolve a second reaction process.

In an attempt to understand better the mechanism of intercalation, it is worth testing the different solid state reaction models on the new NIR-based kinetics which are admittedly more systematic than their XRD-based counterparts. This section intends to examine the suitability of the literature recommended models for the intercalation process as observed by NIR (Fig. 3.8). Additionally, this chapter aims at providing the best fitting model for describing the intercalation of NMF in both KGa-1b and KGa-2. According to Chapter 3, the same general model should describe equally well intercalation in both kaolinites examined.

The kinetic data used for this modelling study were those at 30 °C enriched with all the other temperature data depicted in Figure 3.7 superimposed on the 30 °C data. In this manner, comparisons with literature studies (typically also at ambient temperature) can be made and the asset of time-temperature superposition is

maintained. Kinetics based on the apparent intercalation degree, α_{app}, were used, although the latter does not coincide with the actual intercalation degree (~0.8 in KGa-1b, ~0.4 in KGa-2, Ch. 4), due to the existence of a significant amount that cannot be intercalated (~30-20% in KGa-1b and ~70-60% in KGa-2, Section 4.4). However, if these non-reactive portions were excluded, the progress of intercalation of the remaining material would tend to 1, similar to the apparent degree progress, calculated in Chapter 3 (Fig. 3.7). This approximation is more convenient for modelling owing to the fact that most models are constructed to reach unity at long times. Opposite to the literature, modelling was done on the log-time data to provide equal weight and capture both the onset and the leveling-off of the sigmoidal. For this purpose, a dataset equispaced in log-time by interpolation (typically 0.01 step) was produced.

5.1 Consecutive-reaction models

This type of analysis was performed by Castrillo et al. [Cas15] who studied kaolinite intercalation with dimethylsulfoxide (DMSO) by ex-situ XRD at four temperatures (40, 45, 50 and 60 °C) and used Equation 3.2 for the calculation of reaction progress at different reaction times.

The proposed mechanism was based on a two step model:

$$\text{Kaolinite} + \text{DMSO} \xrightarrow{k_1} \text{B} \xrightarrow{k_2} \text{Kaolinite-DMSO}$$

First, the guest molecules enter between the interlayer space and form complex B in such way that the interlayer does not expand. After that, the guests rotate while inside the interlayers, so that hydrogen bonds are developed between the S=O group and kaolinite's inner surface OH, resulting in a more stable configuration and an increase of the basal spacing.

The model is not very realistic because it assumes an intercalate intermediate with no interlayer expansion, however, it is worth examining as a general scheme involving consecutive reactions.

According to this model, the apparent degree of intercalation can be expressed as a function of time by the following equation [Cas15]:

$$a_{app} = 1 + \frac{1}{k_1 - k_2}\left(k_2 e^{-k_1 t} - k_1 e^{-k_2 t}\right) \qquad Equation\ 5.1$$

where k_1, k_2 are the rate constants for step 1 and step 2, respectively.

Non-linear least squares fitting indicated that Equation 5.1 fails to describe satisfactorily the NIR experimental data, especially in the case of KGa-1b (Fig. 5.1).

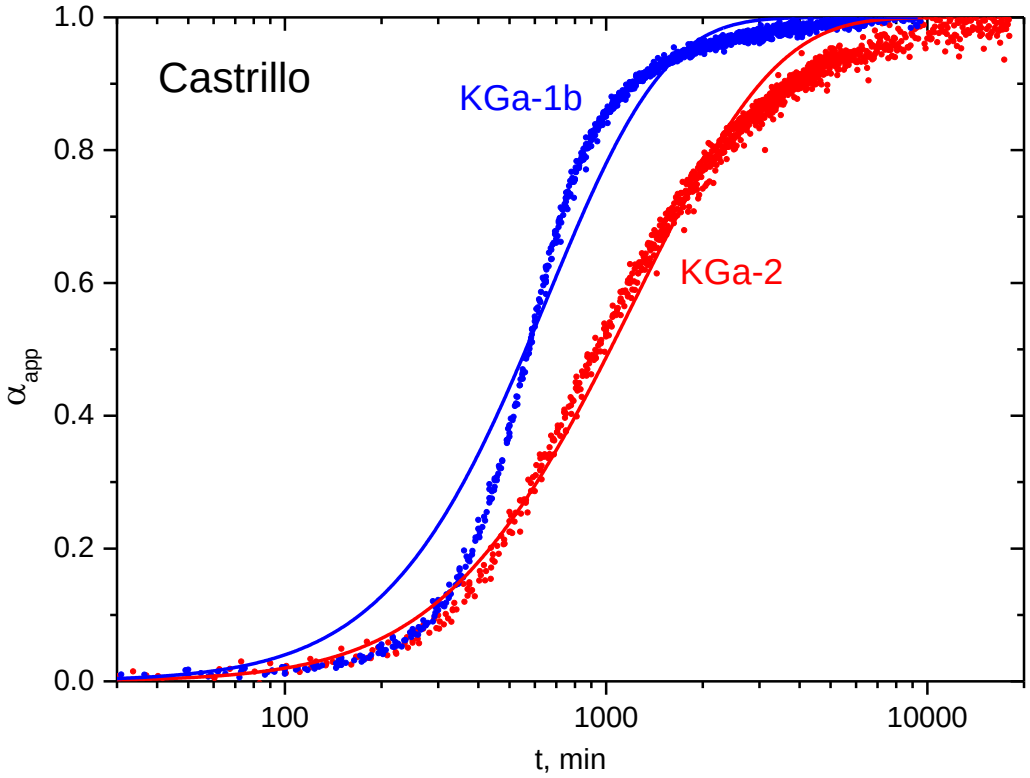

Figure 5.1. Fitted curves (straight lines) obeying Equation 5.1 for KGa-1b (blue) and KGa-2 (red) NIR kinetics (Fig. 3.7) time-temperature superimposed to 30 °C.

Another model based on consecutive reactions has been described by Bentea et al. [Ben17]. In their work they used a two step model, named Finke-Watzky (F-W), to fit sigmoidal curves for growth processes. The two pseudoelementary steps correspond to slow, continuous nucleation and fast, autocatalytic growth, following the sequence:

$$A \xrightarrow{k_1} B$$

$$A + B \xrightarrow{k_2} 2B$$

The model was initially proposed for the formation of iron nanoclusters [Wat97], but since then it has been successfully applied to a wide range of cooperative natural phenomena that display sigmoidal kinetic curves and are involved in many processes, such as aggregation of proteins, solid state phase and solid state photochemical transformations, catalyst phenomena, etc. [Ben17].

The F-W model is clearly relevant to intercalation phenomena. A and B can be thought as representing the free and intercalated states of the guest molecules, respectively. Once A becomes intercalated (B), it facilitates the intercalation of additional A's via the second elementary reaction. This is the simplest description of autocatalytic reactions and it is compatible with the pre-existing theories of mechanism of intercalation [Hac69, Lag06]. The F-W model could therefore be a suitable candidate for describing the sigmoidal kinetics of kaolinite intercalation. The apparent intercalation degree could be expressed as [Ben17]:

$$a_{app} = A\left(1 - \frac{k_1 + k_2 A}{k_2 A + k_1 e^{(k_1 + k_2 A)t}}\right) \qquad Equation\ 5.2$$

where A is a constant between 0 and 1 and corresponds to the fraction of intercalated kaolinite and k_1, k_2 are the rate constants for nucleation and growth, respectively.

The best fitting curves obeying Equation 5.2 are not very satisfactory either (Fig. 5.2). The rate constants k_1 and k_2 of the two steps were found to be 1.8±0.1 x 10^{-4} and 63±1 x 10^{-4} min^{-1}, respectively, in the case of KGa-1b and 6.3±0.1 x 10^{-4} and 16±1 x 10^{-4} min^{-1}, respectively, in the case of KGa-2. The initial step, related to nucleation is much slower than the growth stage (which is intuitively correct), ~35 times slower in KGa-1b but only ~2.5 times in KGa-2.

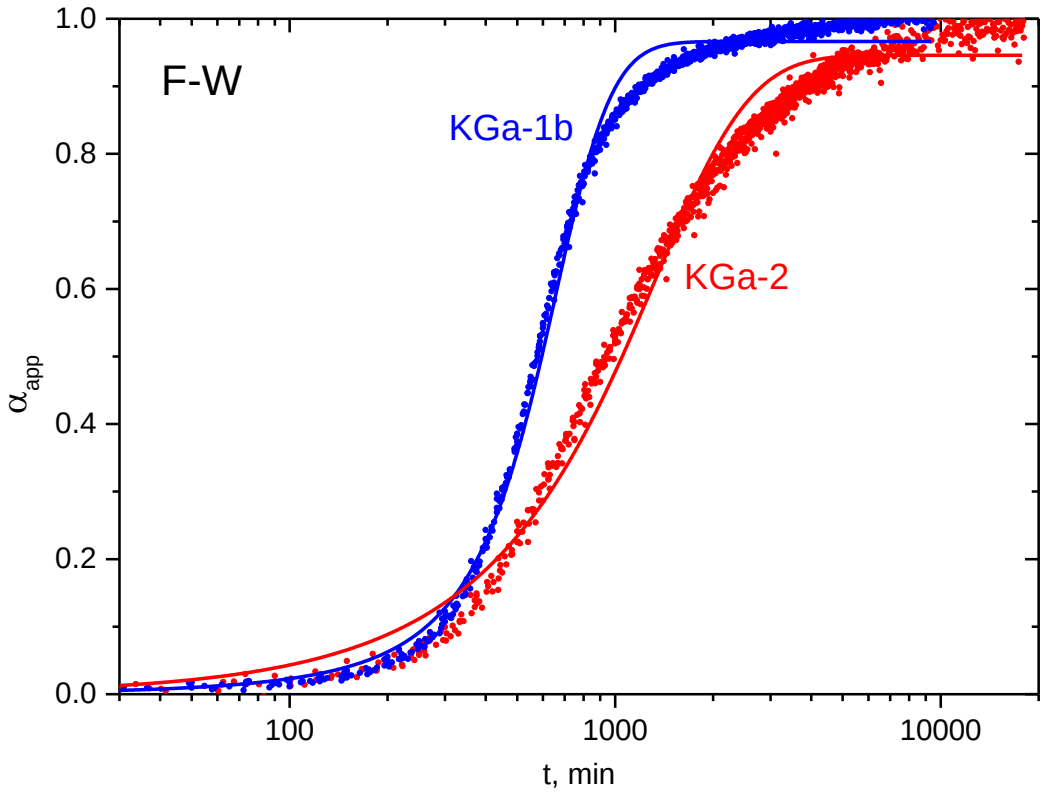

Figure 5.2. Fitted curves (straight lines) obeying Equation 5.2 for KGa-1b (blue) and KGa-2 (red) NIR kinetics (Fig. 3.7) time-temperature superimposed to 30 °C.

5.2 Avrami-Erofeev models

The Avrami-Erofeev or JMAEK (Johnson, Mehl, Avrami, Erofeev, Kholmogorov) model is widely used in many solid state reactions to describe phase changes in materials [Bro80, Kwa06] such as the kinetics of crystallization by nucleation and growth. The conversion fraction, α_{app}, can be expressed as a function of time via the following equation:

$$[-\ln(1-a_{app})]^{\frac{1}{n}} = kt \qquad Equation\ 5.3$$

where n stands for the reaction order and k for the reaction rate constant.

The above model has been explicitly used in the literature to fit the XRD-based kinetics of NMF intercalation in kaolinite [Hac69, Mak19]. Hach-Ali et al. tested the fitting in kinetics at 25, 45 and 65 °C [Hac69], whereas Makó et al. studied the reaction at 20 and 60 °C [Mak19], but the sigmoidal in the latter was

undersampled. Based on this literature, the model was well describing the early stage of the Hach-Ali et al. kinetics (fitted in linear time) for n = 2 (diffusion in two-dimensions) [Hac69] as well as the kinetics at 20 °C of Makó et al. for n = 1.5 (diffusion in one-dimension) [Mak19].

For testing the applicability of the Avrami-Erofeev model on the NIR kinetic data, it is convenient to examine the linearity between the quantities $[-\ln(1-a_{app})]$ and $[t^2]$ (Fig. 5.3) or $[t^{1.5}]$ (Fig. 5.4). No such linear relationships are sustained through the whole range of data in either kaolinite. For that reason, the Avrami-Erofeev equation cannot be considered as an appropriate model to describe the full sigmoidal of the intercalation.

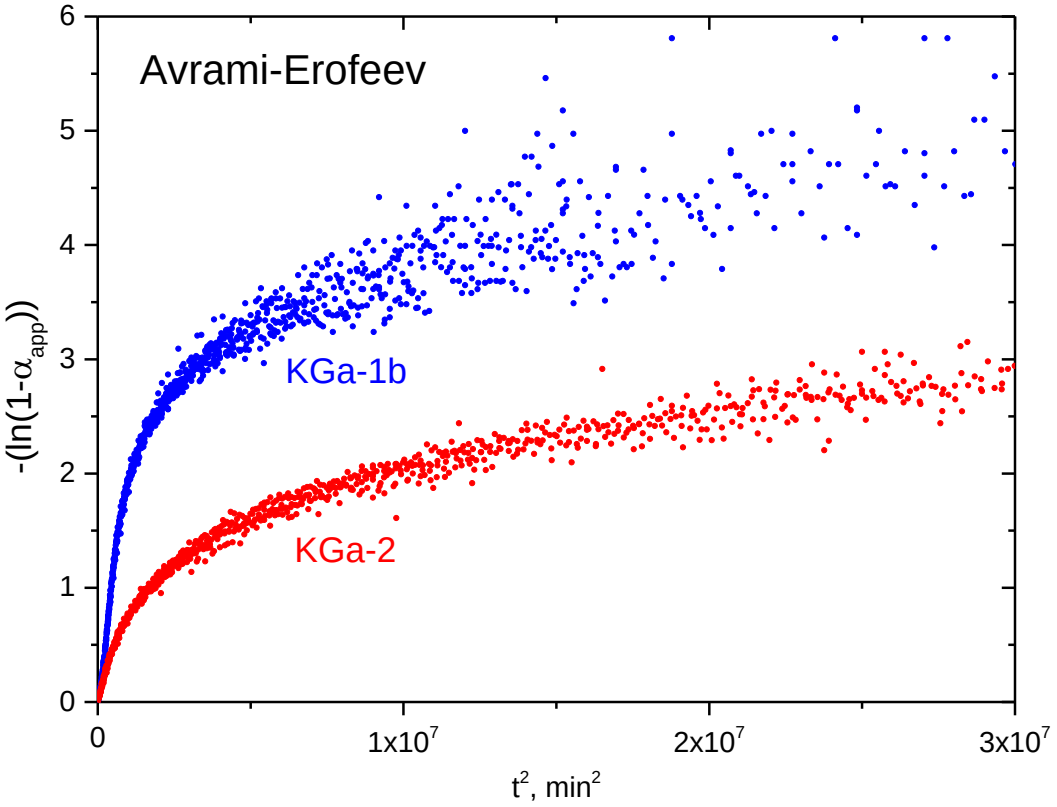

Figure 5.3. Plots of $(-\ln(1-\alpha_{app}))$ vs. t^2 based on Equation 5.3 for KGa-1b (blue) and KGa-2 (red) NIR kinetics (Fig. 3.7) time-temperature superimposed to 30 °C.

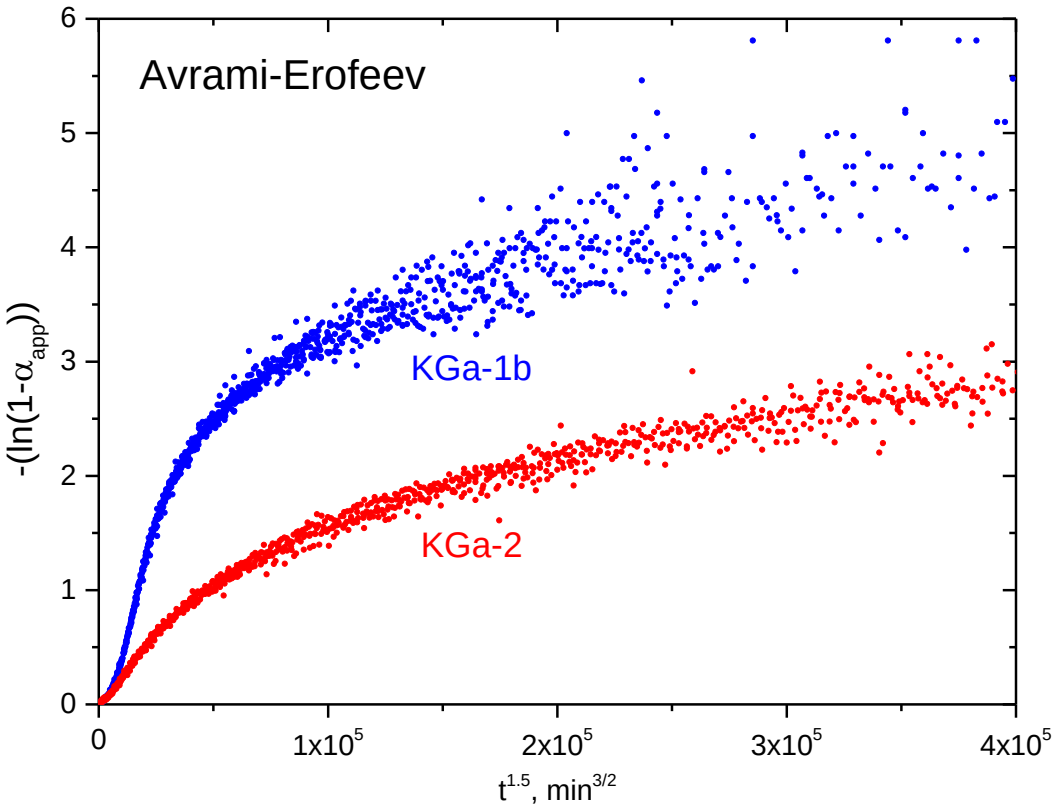

Figure 5.4. Plots of (–ln(1-α_{app})) vs. $t^{1.5}$ based on Equation 5.3 for KGa-1b (blue) and KGa-2 (red) NIR kinetics (Fig. 3.7) time-temperature superimposed to 30 °C.

5.3 Diffusion models

Another model category of solid state kinetics that could be used to describe intercalation is diffusion. Diffusion refers to the filling of the pre-expanded interlayer, i.e. to the step that follows what has been described in the literature as adsorption/nucleation/wedging. In fact, it was our initial hypothesis that diffusion could be the dominant process in kinetics observed by NIR, opposite to XRD.

There are three types of diffusion, based on the direction of extending, that are expressed via the equations [Kwa06]:

1-D diffusion: $$a_{app}{}^2 = kt$$

2-D diffusion: $$(1 - a_{app})\ln(1 - a_{app}) + a_{app} = kt$$

3-D diffusion: $$(1 - (1 - a_{app})^{\frac{1}{3}})^2 = kt \qquad Equations\ 5.4$$

where α_{app} is the apparent intercalation degree and k the rate constant. In the case of intercalation, the 2-D equation is intuitively more suitable. None of these models is suitable for describing a sigmoidal. They are only tested to check whether the longer term evolution of the reaction beyond the initial incubation period can be described as a diffusion process.

Hach-Ali et al. have tested the fitting of the kinetics of NMF intercalation at 7, 25, 45 and 65 °C to all diffusion types [Hac69]. They found poor agreement to the experimental kinetic results, indicating that intercalation is unlikely to obey a diffusion process over the time scale of their experiment.

The failure of diffusion to model XRD-based kinetics does not eliminate the need for testing independently their NIR counterparts (see earlier in this section). A diffusion model would be considered compatible with the mechanism of intercalation if a linear relation existed between the quantities $[{a_{app}}^2]$, $[(1-a_{app})\ln(1-a_{app})+a_{app}]$ or $[(1-(1-a_{app})^{1/3})^2]$ with time [t]. This is definitely not the case as the curves maintain their sigmoidal shape with no tendency to flatten, except of the 3-D diffusion model in KGa-2 (Fig. 5.5). Diffusion is rejected for modelling of NMF intercalation, regardless of whether this is observed in the XRD or NIR scales.

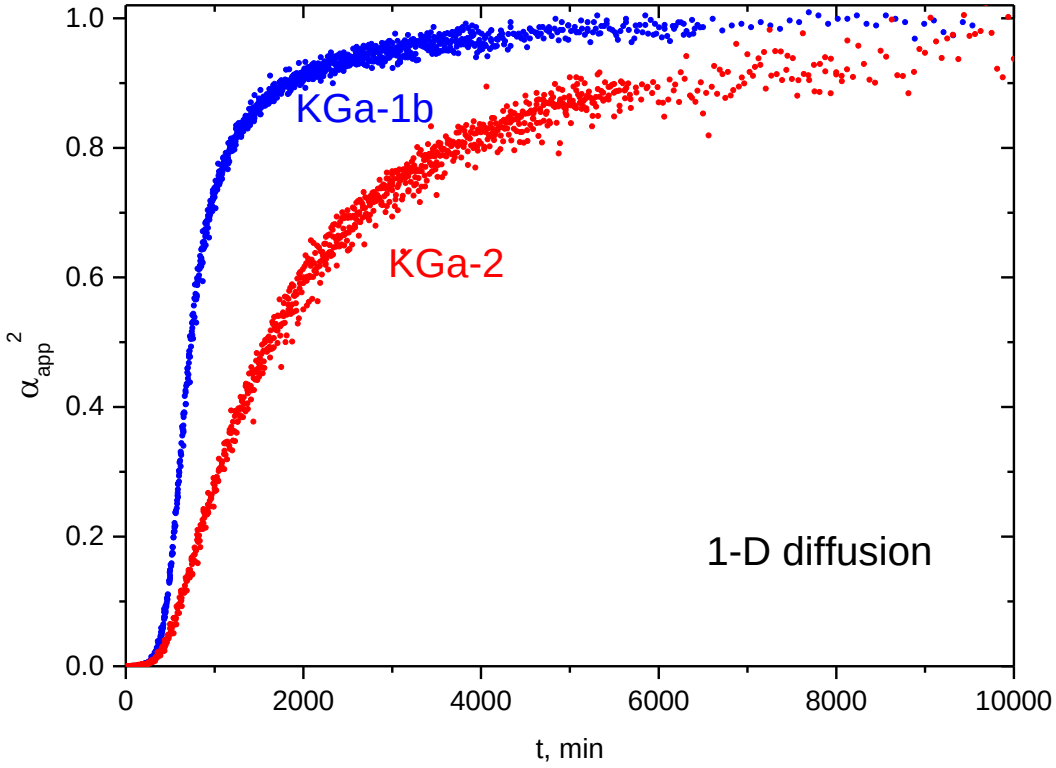
KGa-1b
KGa-2
1-D diffusion
α_{app}^2
t, min
0.0
0.2
0.4
0.6
0.8
1.0
0
2000
4000
6000
8000
10000

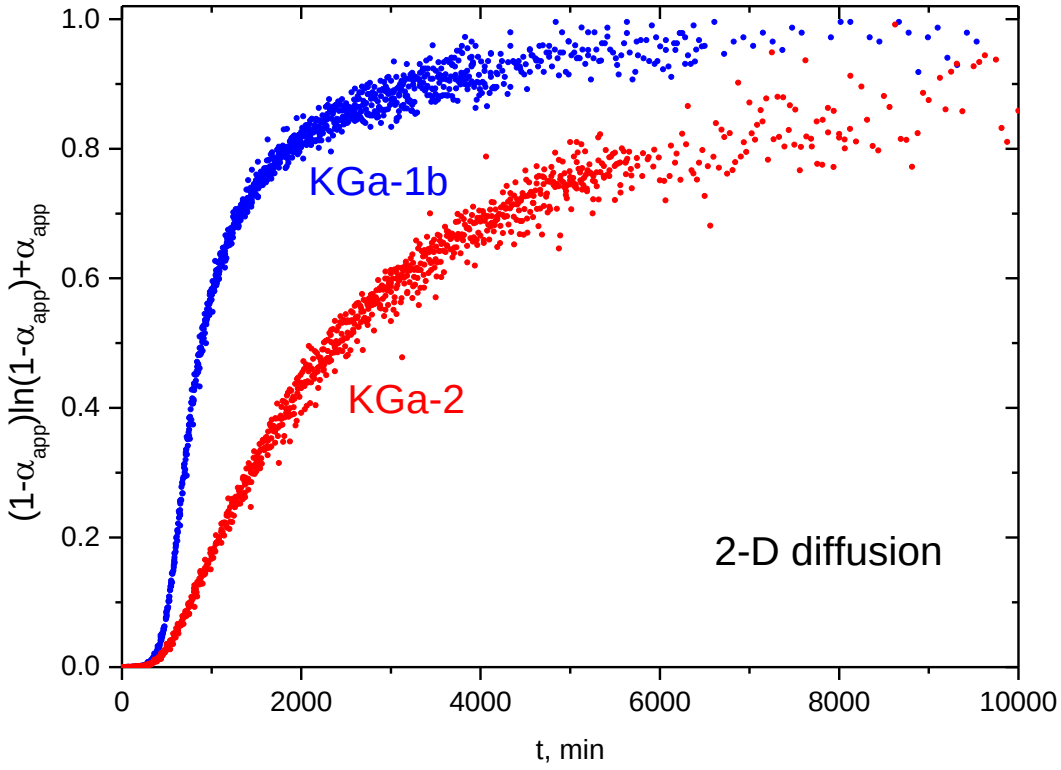
KGa-1b
KGa-2
2-D diffusion
$(1-\alpha_{app})\ln(1-\alpha_{app})+\alpha_{app}$
t, min
0.0
0.2
0.4
0.6
0.8
1.0
0
2000
4000
6000
8000
10000

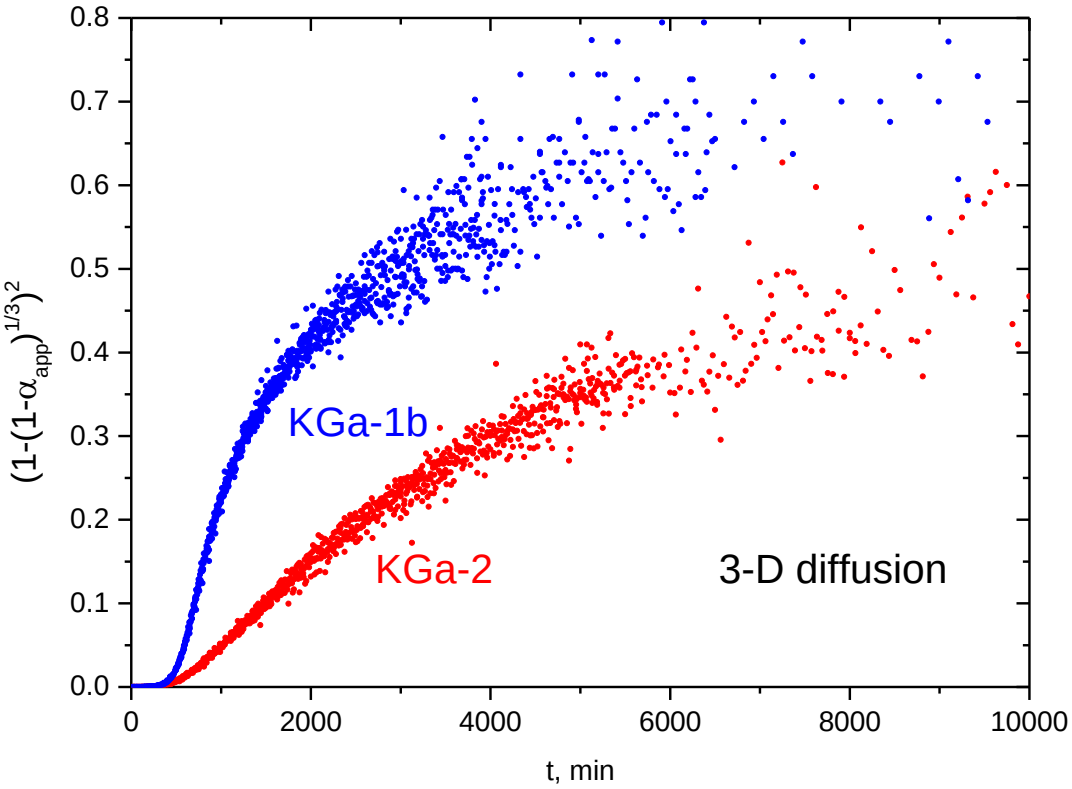

Figure 5.5. Plots of $\alpha_{app}{}^2$ (upper), $(1-\alpha_{app})\ln(1-\alpha_{app})+\alpha_{app}$ (middle) and $(1-(1-\alpha_{app})^{1/3})^2$ (lower) vs. time based on Equations 5.4 for KGa-1b (blue) and KGa-2 (red) NIR kinetics (Fig. 3.7) time-temperature superimposed to 30 °C.

5.4 Prout-Tompkins model and its variants

Among the rate-equations that have been used in the literature to fit sigmoidal-time curves is the Prout-Tompkins (P-T) equation [Pro44, Bro97]. The P-T equation is mathematically identical to the well-known Verhulst logistic equation of population growth [Bro97, Tso02]. It was independently developed to model the kinetics of the thermal decomposition of crystals of potassium permanganate, and it was found to have applications in several different fields, e.g. in solid state kinetics, pharmaceutical studies, irradiation effects, etc. Similar to other models, P-T describes the formation and growth of nuclei and can be expressed as follows [Bro97, Gal99]:

$(derivative\ form)$: $$\frac{da}{dt} = k_B a(1-a)$$

$(integrated\ form)$: $$\ln\left(\frac{a}{1-a}\right) = k_B t + C \qquad Equations\ 5.5$$

where α is the fractional extend of reaction, k_B the so-called "branching" rate constant [Gal99, Kwa06] and C the integration constant. The model represents an autocatalytic reaction, which accelerates proportionally to α and decelerates proportionally to (1-α). The inflection point t_0 is, therefore, obtained at α=0.5. It is reminded that the NIR-based intercalation kinetic data displayed t_0 at α_{app}≈0.42 and α_{app}≈0.24 for KGa-1b and KGa-2, respectively (Fig. 3.5), suggesting that the exact P-T model is not suitable for the present intercalation process, unless it is modified.

Other variants of the P-T model (or, equivalently the logistic equation) are, therefore, worth examining. Most of these variants use different exponents for α and (1-α) which break the symmetry of the sigmoidal and yield t_0 at a≠0.5, and/or introduce an additional decelerating term of the form ln(1-α) inspired from the Avrami-Erofeev.

Models of this type are the so-called modified Prout-Tompkins [Bro97], Pérez-Maqueda [Per06], Cai-Liu [Cai09], Ng [Ng75], Sesták Berggren [Ses71] and the generalized logistic function [Tso02], expressed by the following equations:

Modified $P-T$: $$\ln\left(\frac{a}{1-a}\right) = k_B lnt + C \qquad Equation\ 5.6$$

$Pérez-Maqueda$: $$\frac{\mathrm{d}\alpha}{\mathrm{dt}} = a^m(1-a)^n \qquad Equation\ 5.7$$

$Cai-Liu$: $$\frac{\mathrm{d}\alpha}{\mathrm{dt}} = a^m(1-ka)^n \qquad Equation\ 5.8$$

Ng: $$\frac{\mathrm{d}\alpha}{\mathrm{dt}} = ka^m(1-a)^n \qquad Equation\ 5.9$$

Sesták Berggren: $$\frac{\mathrm{d}\alpha}{\mathrm{dt}} = ka^m(1-a)^n(-\ln(1-a))^p \qquad Equation\ 5.10$$

generalized logistic: $$\frac{\mathrm{d}\alpha}{\mathrm{dt}} = ka^m(1-a^n)^p \qquad Equation\ 5.11$$

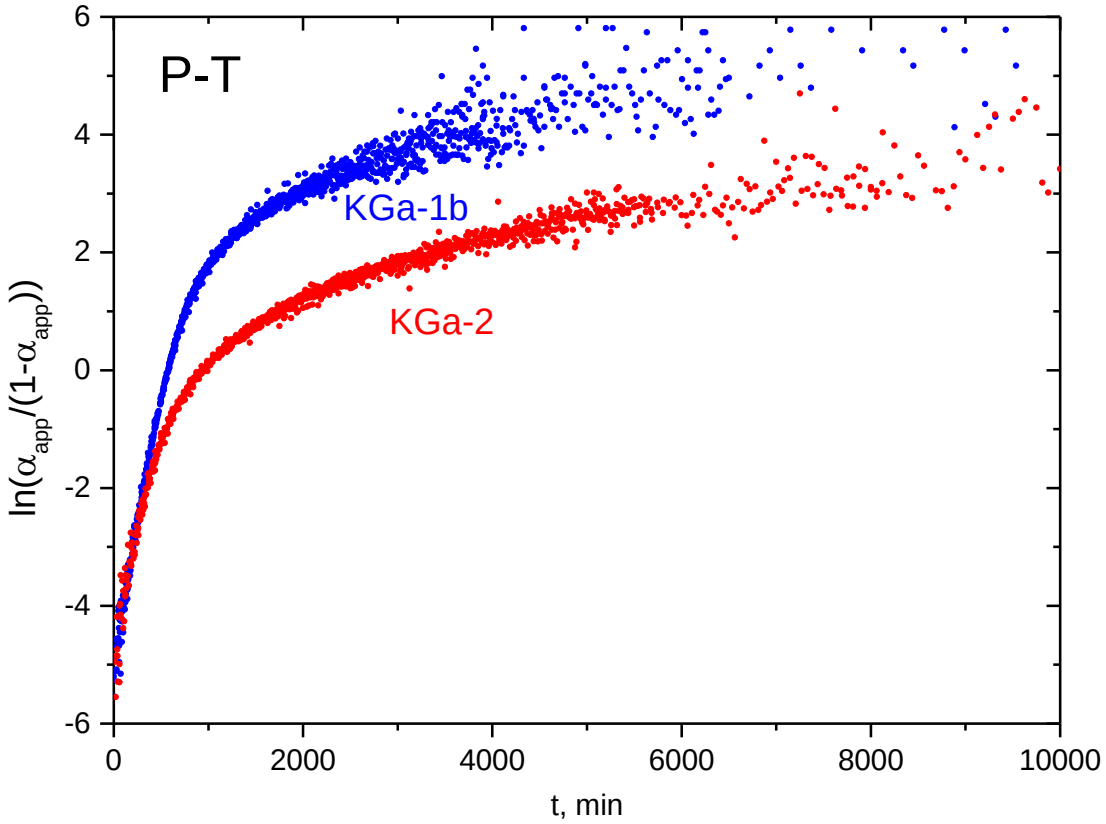

Figure 5.6. Plots of $\ln(\alpha_{app}/(1-\alpha_{app}))$ vs. time based on Equations 5.5 for KGa-1b (blue) and KGa-2 (red) NIR kinetics (Fig. 3.7) time-temperature superimposed to 30 °C.

Attempts to fit our data with the suite of the various P-T model modifications indicated that the fitting is getting better as the number of the parameters in the examined equation increase. Whereas the original single-parameter P-T model (Eq. 5.5) was completely incompatible with the NIR-based kinetics (Fig. 5.6), the four-parameter (k, m, n, p) generalized logistic (Eq. 5.11), displayed almost perfect matching (Fig. 5.8). In the latter case the fitting was performed on the $d\alpha_{app}/dt$ vs. α_{app} curve, with α_{app} values equispaced by interpolation (0.01 step) (Fig. 5.7). The fitted $d\alpha_{app}/dt$ curves in Fig. 5.8 were obtained from the calculated parameters k, m, n, p and Equation 5.11 and the $\alpha_{app}(t)$ sigmoidal was produced by numerical integration.

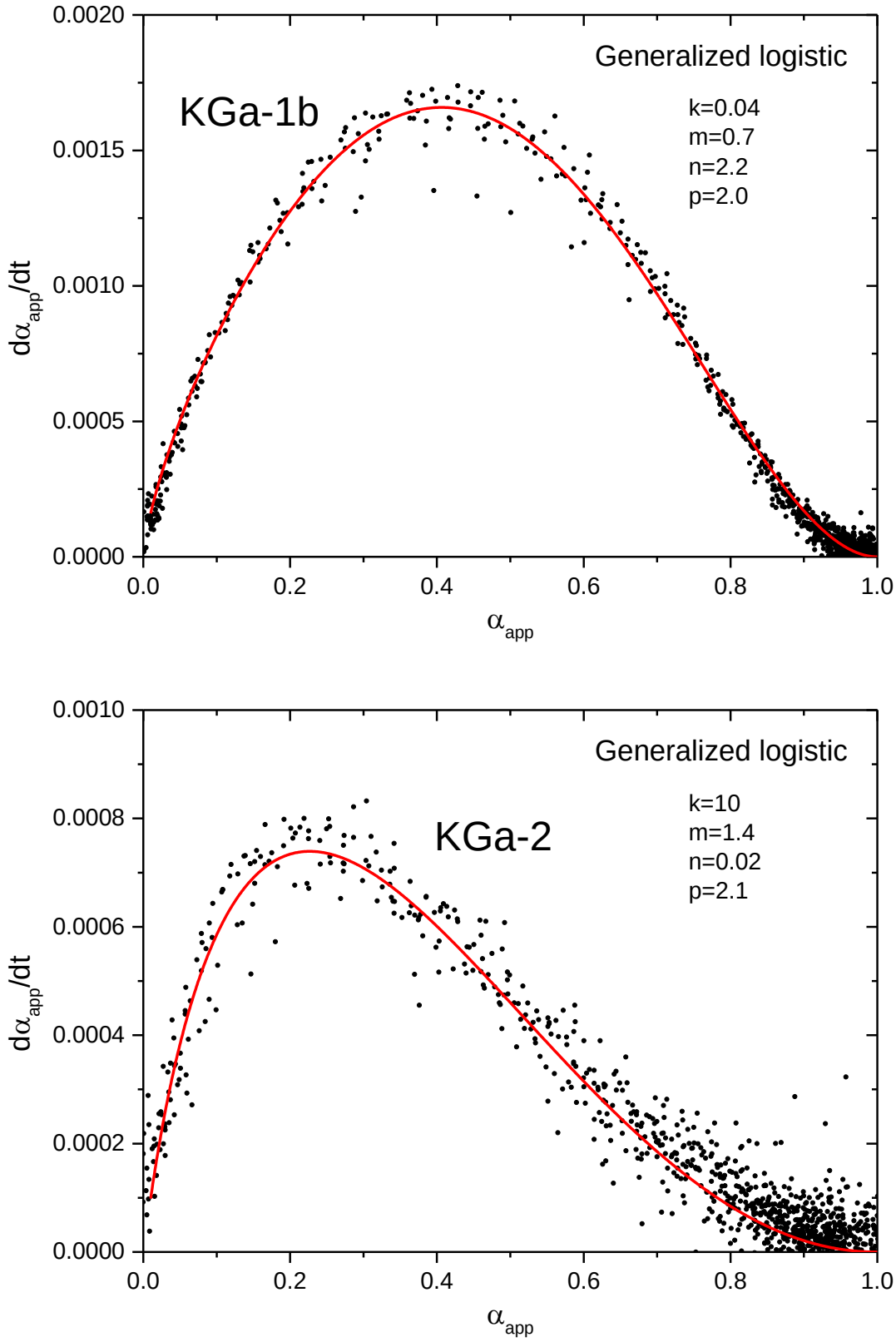

Figure 5.7. Fitted curves (straight lines) obeying Equation 5.11 for KGa-1b (upper) and KGa-2 (lower) NIR kinetics (Fig. 3.7) time-temperature superimposed to 30 °C.

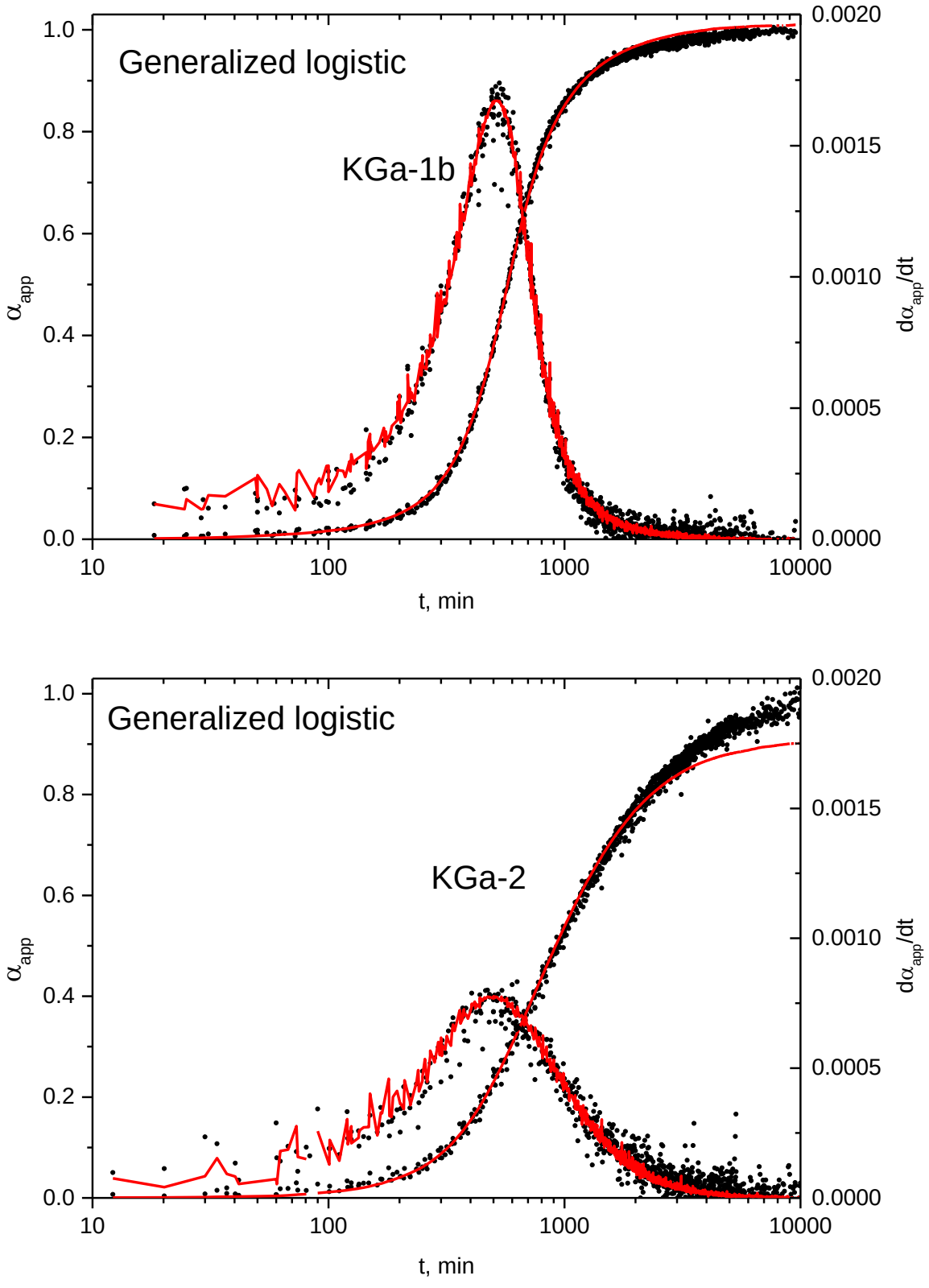

Figure 5.8. Fitted curves (straight lines) obeying Equation 5.11 for KGa-1b (upper) and KGa-2 (lower) NIR kinetics (Fig. 3.7) time-temperature superimposed to 30 °C.

5.5 From chemistry to statistics

The success of the generalized logistic function in fitting the intercalation results (Section 5.4) came at a price: the model lacks physical content due to the large number of parameters and does not contribute to the fundamental understanding of the sigmoidal process. A different approach is clearly needed to rationalize the origin and systematics of the sigmoidal intercalation.

A remarkable outcome of the NIR data analysis is their failure to record the diffusion of the guest molecules in the interlayer. Diffusion would be detectable by spectroscopy not only by the increasing concentration of the intercalated guests, but also by the progressive change of the guest-guest intermolecular interactions during the course of the reaction. In addition, the partial filling of expanded interlayers would imply the existence of a third type of inner surface OH which would be “free”, and not interacting with either NMF (as in fully intercalated interlayers) or the adjacent tetrahedral sheet (as in non-intercalated kaolinite). No such indications are provided by the vibrational spectra, despite their sophisticated analysis: Time dependent guest-guest intermolecular interactions involving NMF would imply a progressive change in the position and width of the 2ν(NH) band. Instead, the data depicted in Figure 3.4 indicate that the position and width are remarkably constant during intercalation process and independent of the type of kaolinite. Similarly, the changes in the kaolinitic signature during intercalation are always described by the linear combination of two spectra, one of which is the spectrum of non-intercalated kaolinite (Fig. 4.2).

Based on the present NIR data, the intercalation of NMF in kaolinite can be described as a switching between two well-defined states. No partially filled state would be well-defined, i.e. time- and material-independent. As a result, the intercalated entity (i.e. the interlayer or the particle) appears either empty or full. The XRD data are also indicative of a two-state system. To my knowledge, there is no XRD reference to partial interlayer filling.

The above are not evidence for the absence of interlayer diffusion. They simply mean that the filling of the interlayer is too fast to be observed by any of the two techniques, XRD and vibrational spectroscopy, even at the lowest practical

temperatures investigated. Once the interlayer is expanded, it becomes fully occupied by intercalated NMF instantaneously. This is compatible with the preliminary finding that XRD and NIR produce identical sigmoidal curves despite their different diagnostic structural scale (Fig. 4.6).

What is then the nature of the process activated at ~60 kJ/mol which is common to both kaolinites (Fig. 3.9) despite their different intercalation "kinetics" (Figs. 3.7, 3.8)? Based on the above, this process must correspond to the switching of the interlayer from the pristine to the fully intercalated states, which is distributed over time.

Opposite to chemical reactions between well-defined compounds, kaolinite consists of particles with single or bimodal log-normal particle size distribution (Dri15, Uwi93, see also Chapter 2). This translates to a distribution of interlayers which, when exposed to the intercalating agent, intercalate instantaneously but at distributed time intervals from the onset of their exposure to NMF. According to this approach, the sigmoidal cannot represent the true kinetics of intercalation. Instead, it is now considered to reflect the distribution of the “incubation” times of individual interlayers or particles. Given the observed symmetry of the sigmoidals when plotted versus log-time (Fig. 3.7), the log-normal distribution would be the most suitable candidate for fitting the data.

The probability density function (PDF) and the cumulative distribution function (CDF) of the log-normal distribution are expressed via:

$$(PDF): \qquad f(x) = \frac{1}{x\sigma\sqrt{2\pi}}\exp\left(-\frac{1}{2\sigma^2}(logx-\mu)^2\right)$$

$$(CDF): \qquad f(x) = \frac{1}{2} + \frac{1}{2}\mathrm{erf}\left(\frac{logx-\mu}{\sqrt{2}\sigma}\right) \qquad Equations\ 5.12$$

where σ is the standard deviation, μ the median and erf the error function.

Both, log-normal and normal (Gaussian) distributions, are used to describe procedures that are based on phenomena that act independently of each other. In case these are additive the distribution is normal, whereas for multiplicative phenomena the distribution turns to log-normal. The log-normal distribution was first reported in 1834, and since then its applications include a wide range of

scientific areas, such as geology, ecology, biology, medicine, toxicology, economics, etc. [Lim01]. It is also preferred when dealing with properties of populations or with their response to external stimuli. For example, the age of first marriage in Western civilization or the body weight follow log-normal distributions [Lim01, Gua19]. Of great interest are the applications in microbiology, such as the sensitivity to fungicide in populations [Lim01].

One significant application is in the study of the collective response of a population to contamination, poisoning, etc. For infectious diseases, the incubation period (the time between infection to illness onset) has been demonstrated to follow log-normal distribution. A famous result of this type was the log-normally distributed incubation period of serum hepatitis in a population of ~6000 soldiers who were inoculated the same day with the same batch of faulty vaccine. This led to the infection of ~1000 soldiers with a mean incubation period of 100 days [Lim01]. One of the most recent applications of log-normal modelling was in the study of the 2019 novel coronavirus (COVID-19) [Lin20]. Given the high infection and mortality rates associated with this coronavirus and the huge impact in global economy and humanity, it was critical to determine the time period required from infection to illness onset. The authors examined a sample population from Wuhan, China, and concluded that the incubation period follows a log-normal distribution, with a mean of ~5d. Based on this study, the incubation period ranges with 95% confidence between 2 and 14 days, implying that a ≥14-day quarantine is need to contain the disease.

It can be proposed that intercalating the interlayers of kaolinite is not conceptually different from counting the response of a population to an external chemical or biological agent. In both cases, each member of the respective populations can be in one of two states: intercalated vs. non-intercalated, healthy vs. ill, alive vs. dead. In both cases, the “kinetic” experiment involves measuring the time-evolution of the infected population, and not the evolution of the symptoms within one individual. Additionally, the description of both systems can include a subset of the original population that is “immune” to the external agent, such as the fraction of kaolinite that does not respond to NMF intercalation (Section 4.4).

Inspired by this analogy, the sigmoidals of KGa-1b and KGa-2 were fitted by the log-normal function. The cumulative distribution function was tested to fit the NIR-based intercalation data, equispaced at a log-time scale. The mean, μ, was found to be 2.8 (~630 min) for KGa-1b and 3 (~1000 min) for KGa-2 (Table 1). The standard deviation, σ, was calculated 0.2 (i.e. 400-1000 min) for KGa-1b and 0.4 (400-2500 min) for KGa-2 (Table 5.1).

In both kaolinites the log-normal function seems to fit very well the NIR-intercalation data. Specifically, the matching is perfect in the case of KGa-2, (Fig. 5.9, lower), and a bit less successful in KGa-1b (Fig. 5.9, upper). This may be related to the fact that KGa-2 demonstrates only one particle size distribution, unlike KGa-1b which displays two [Dri15]. Based on this consideration, the fitting of the KGa-1b intercalation data could be improved by introducing a second log-normal function (Fig. 5.9, upper). Whether this improvement has physical meaning or not requires further investigation.

Table 5.1. Calculated parameters of the fittings of KGa-1b and KGa-2 NIR kinetics (Fig. 3.7) time-temperature superimposed to 30 °C with the log-normal function.

Log-normal		
	KGa-1b	**KGa-2**
μ	2.8	3
σ	0.2	0.4

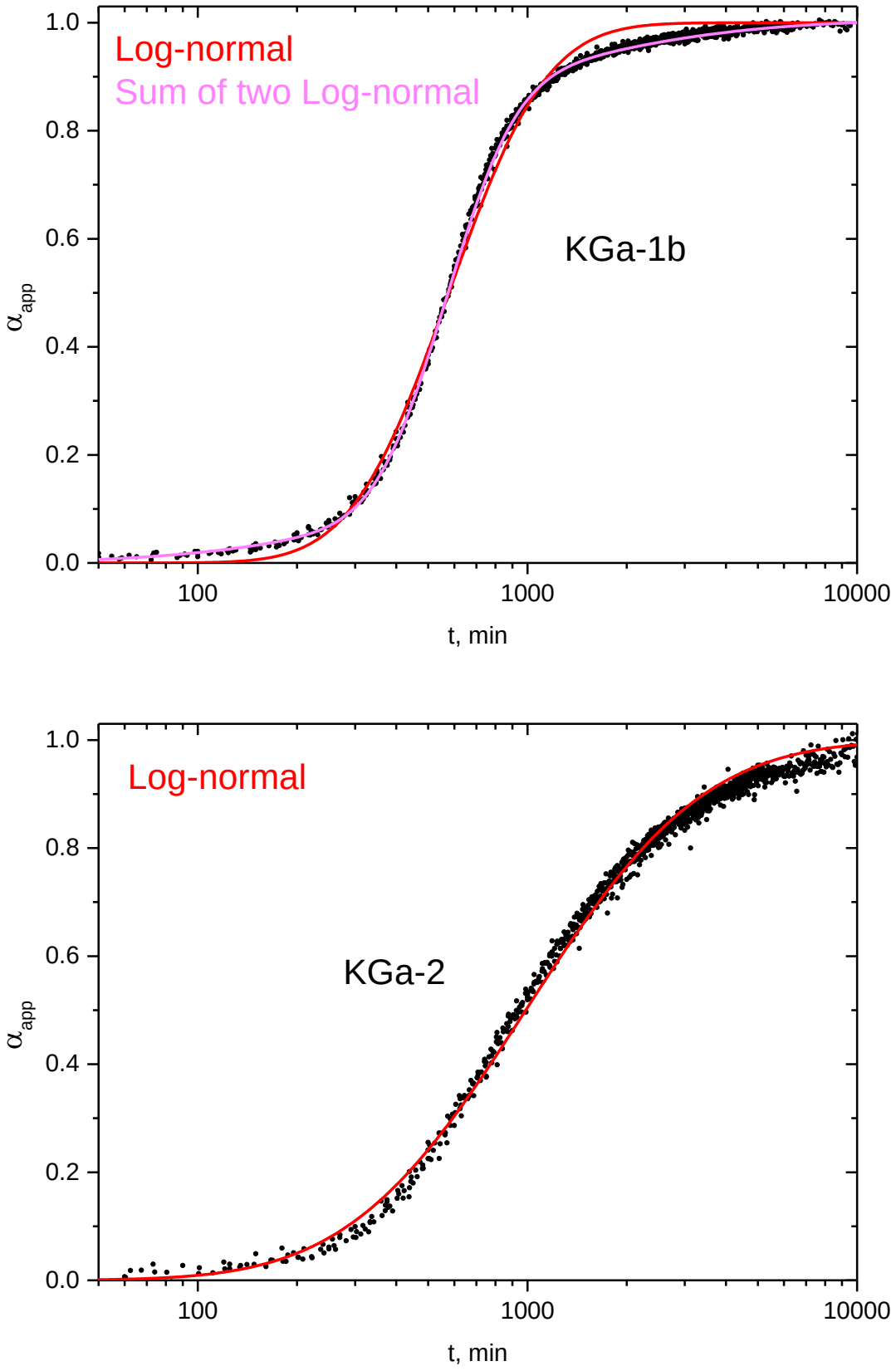

Figure 5.9. Fitted curves (straight lines) obeying Equations 5.12 for KGa-1b (upper) and KGa-2 (lower) NIR kinetics (Fig. 3.7) time-temperature superimposed to 30 °C.

To the best of our knowledge, this is the first time that the temporal evolution of intercalation in kaolinite has been handled as a time-distributed response of an ensemble of kaolinite interlayers exposed to an intercalating agent. This alternative description is been forwarded not only because the data were fitted successfully by a log-normal distribution function, nor because other “chemical” models in the literature were found to perform poorly, but also after recognizing that the observed process involves the “instantaneous” switching from empty to full interlayers and not the progressive filling of the interlayer.

Chapter 6

Effect of H_2O on intercalation

Previous XRD investigations have reported changes in the kinetics of kaolinite intercalation due to the presence of H_2O in the solution of the intercalated solvent, although H_2O itself has never been observed inside the interlayer space. Olejnik et al. reported a non-monotonic effect of increasing H_2O content on reaction rate and incubation time, while recording the kinetics of intercalation by XRD (Eq. 3.2), with DMSO [Ole68], formamide and NMF guest molecules [Ole70]. The final intercalation degree was also perturbed by water content [Mak19].

This effect was studied to some extent in my early study of NMF intercalation kinetics [And18] which was based on the progress of the intensity of the NIR-active 2v(NH) band as described in Section 3.2. *In-situ* experiments of KGa-1b/NMF:H_2O (1 g of kaolinite mixed with 1 g of NMF:H_2O solution) for ten different water molar fractions, x_w, (from 0.07 to 0.85) were performed at ambient temperature with a temporal resolution of 30 min via an integrating sphere technique. A small amount of H_2O in the solution increased the rate of intercalation, V_{int} (defined in the time interval between the end of the incubation and the onset of the plateau), with a maximum rate at 3-10 wt% H_2O ($0.2 \leq x_w \leq 0.35$) (Fig. 6.1, left). Larger H_2O contents caused deceleration of the reaction and, beyond ~30 wt% H_2O in NMF ($x_w > 0.6$) the intercalation became so slow that it was not practical to be recorded in real-time or did not start at all. Similarly, incubation time, t_i, is shorter for x_w between 0.2 and 0.5 (Fig. 6.1, right).

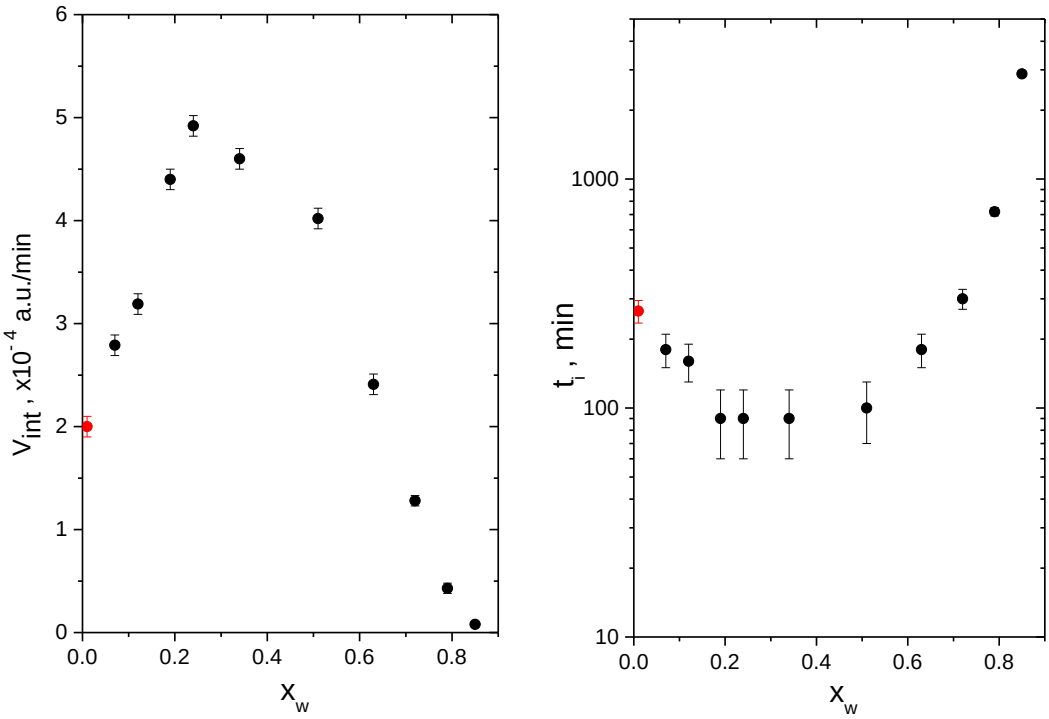

Figure 6.1. Effect of water on the rate (left) and incubation period (right) of KGa-1b intercalation with NMF at ambient temperature. Adapted from [And18]. Highlighted data introduced from the present study of KGa-1b with dry NMF at 30 °C.

According to Olejnik et al. [Ole68, Ole70], the addition of water or other polar molecules, such as methanol or ethanol, in liquid NMF breaks down the extensive network of intermolecular interactions in the pure liquid and facilitates the entry of individual molecules (instead of molecular clusters) into the interlayer space of kaolinite. Thus, the intercalation rate increases and the incubation time decreases. However, for low NMF concentration in the solution, the probability or successful intercalation decreases. In that case, the dependence of intercalation rate and incubation period on H_2O is reversed. The competition between the two phenomena yields the non-monotonic dependence of the kinetics on the molar fraction of water.

In the context of the present study, it is of interest to investigate how H_2O affects the shape of the kinetic curves of KGa-1b and KGa-2, whether H_2O itself intercalates, the activation energy of intercalation, as well as whether the presence of water allows for distinguishing more than one elementary processes in any of the two kaolinites. For this purpose, the kinetic studies of Chapter 3 were repeated using NMF:H_2O solutions instead of pure NMF, while maintaining the kaolinite to liquid mass ratio constant (1:1).

6.1 Intercalation kinetics with a 90NMF-10H_2O wt% solution

Full NIR kinetic experiments were performed in KGa-1b/NMF:H_2O pastes with a 90%NMF-10%H_2O solution (hereafter 90:10) for twelve temperatures in the range of 20-80 ^oC (Fig. 6.2, upper). Similarly, NIR kinetics were recorded for KGa-2/NMF:H_2O pastes for six temperatures in the range 30-80 ^oC (Fig. 6.2, lower). It is reminded that the 90:10 solution was found to induce maximum intercalation rate and minimum incubation period at ambient temperature [And18].

Sigmoidal evolutions are observed in all cases. In KGa-1b all sigmoidals display almost identical shape when plotted in the manner of Fig. 3.7, which is temperature independent. The curves have maintained their symmetry in the log-time axis and they are shifted parallel to each other towards shorter times with increasing temperature. Comparing to the dry samples examined in Section 3.4 (Fig. 3.7), the presence of water caused a reduction of the time required for the completion of intercalation, that is implied from the onset time of the final plateau of the sigmoidal. Reactions are almost finished after ~20h at 30 ^oC, ~7h at 45 °C and ~2h at 70 °C, instead of ~30, 10 and 3h, respectively, for the 100% NMF solution (hereafter 100:0).

The KGa-2 intercalation kinetic curves, demonstrate a similar behavior. In the low temperature region (T<60 ^oC) the sigmoidals seem to have almost identical shapes. However, as the temperature increases the absolute intensity of the 2ν(NH) band becomes lower, leading to a significant deterioration of the S/N ratio (e.g. 70 and 80 ^oC in Fig. 6.2, lower).

As a result of the aforementioned observations, the KGa-1b and KGa-2 90:10 sigmoidals are perfectly time-temperature superimposed (in the manner described in Section 3.4) over the whole temperature range investigated, and their master curves are nearly indistinguishable from those obtained with dry NMF (Fig. 6.3, c.f. with Fig. 3.8).

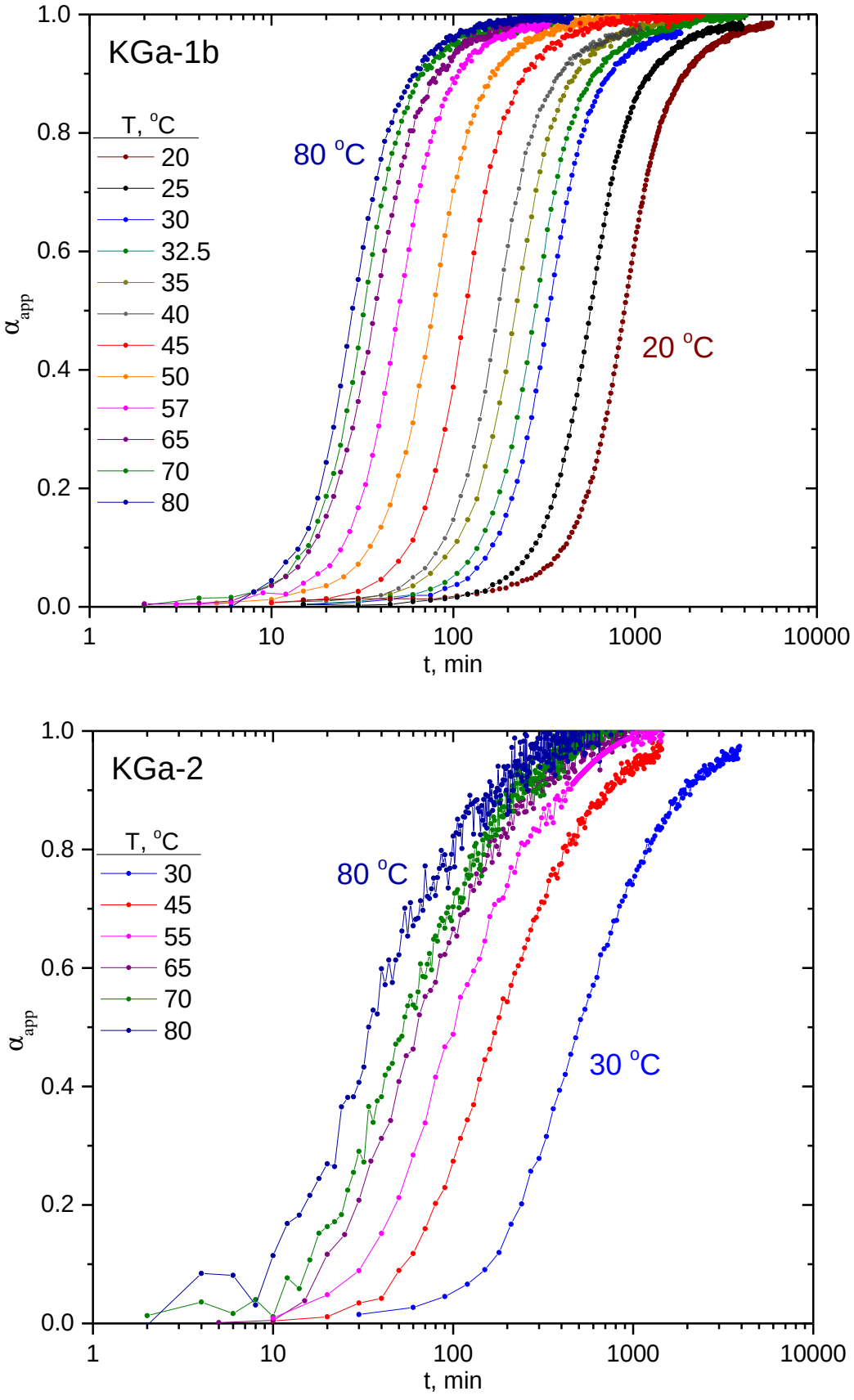

Figure 6.2. KGa-1b (upper) and KGa-2 (lower) intercalation kinetics with 90:10 solution depicted in a log-time axis.

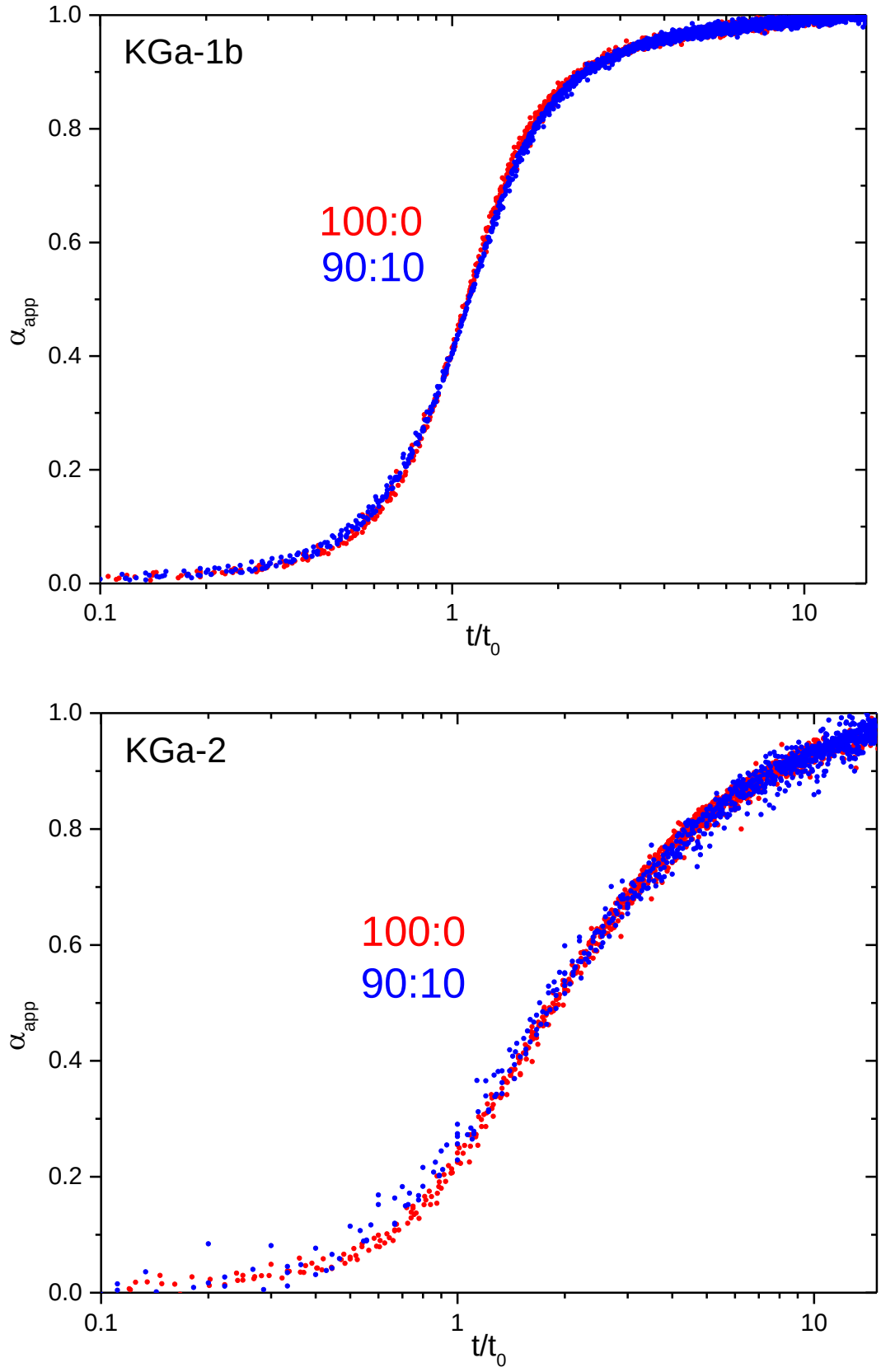

Figure 6.3. 90:10 NIR-based time-temperature superposition of the kinetic data (blue) of KGa-1b for 20-80 °C (upper) and KGa-2 for 30-80 °C (lower) from Fig. 6.2. Dry NMF data are included for comparison (red). Reduced t/t_0 times are used.

In summary, the use of a 90:10 solution instead of pure NMF shifts the sigmoidals to smaller times over a broad temperature range and maintains the shape of the time-temperature superposition master curve in both KGa-1b and KGa-2. At the highest temperatures studied, the sigmoidal kinetics of KGa-2 became noisy, suggesting a decrease of the amount of (the already low, Chapter 4) intercalated material in this clay. This is possibly an indication for the presence of a different intercalation mechanism which is induced by the presence of H_2O and influences KGa-2 more than KGa-1b.

6.2 Intercalation in the presence of higher H_2O wt%

As the effect of H_2O content is non-monotonic (Fig. 6.1), kinetics need to be also studied with more dilute NMF solutions. A full list of the experiments performed can be found in Table 6.1. Notably, measurements at both high temperature and high H_2O content yielded sigmoidals that are no longer superimposable on the master curves of Fig. 6.3. For example, a comparison of the normalized sigmoidals of KGa-1b intercalated with an 80:20 solution at 30, 45 and 70 ^oC shows that the 70 ^oC curve is slower in reaching the final plateau and appears deformed in a reduced-time scale (Fig. 6.4). In other words, an unknown H_2O-induced high temperature process is observed in both KGa-1b and KGa-2.

The systematics of the data in terms of time-temperature superposition are summarized in Table 6.1. They are also illustrated by means of the activation energy plots in Fig. 6.5. Superimposable sigmoidals fall on straight lines of $\ln t_0$ vs. 1/T with $E_\alpha \approx 60$ kJ/mol. Therefore, data over the green temperature-H_2O field of Table 6.1 for both KGa-1b and KGa-2 are governed by the same process, which is independent of H_2O-content. The high-temperature, high-H_2O concentration abnormalities are manifested by the apparent decrease of E_α values (Fig. 6.5). Given the fact that the corresponding sigmoidals are non-superimposable, the decrease of E_α is considered an artifact, which is presumably due to changes of the 2ν(NH) intercalation proxy at high temperature and high H_2O content and calls for its systematic investigation.

Table 6.1. List of NIR-monitored kinetic experiments of KGa-1b (upper) and KGa-2 (lower) as a function of temperature (°C) and composition of intercalating solution (NMF:H_2O wt%). Time-temperature superpositions are valid over the range highlighted green and deviations are observed over the range highlighted red.

KGa-1b

	100:0	90:10	80:20	70:30
20		✓		
25		✓		✓
30	✓	✓	✓	✓
32.5	✓	✓		
35	✓	✓		
37				✓
40	✓	✓		
42.5	✓			
45	✓	✓	✓	✓
50	✓	✓		✓
55	✓			✓
57		✓		
60	✓			
65	✓	✓		
70	✓	✓	✓	✓
75	✓			
80		✓		

KGa-2

	100:0	90:10	80:20	70:30
25	✓		✓	
30	✓	✓	✓	✓
35	✓			
45	✓	✓	✓	✓
55	✓	✓	✓	
65		✓		
70	✓	✓	✓	
80		✓		

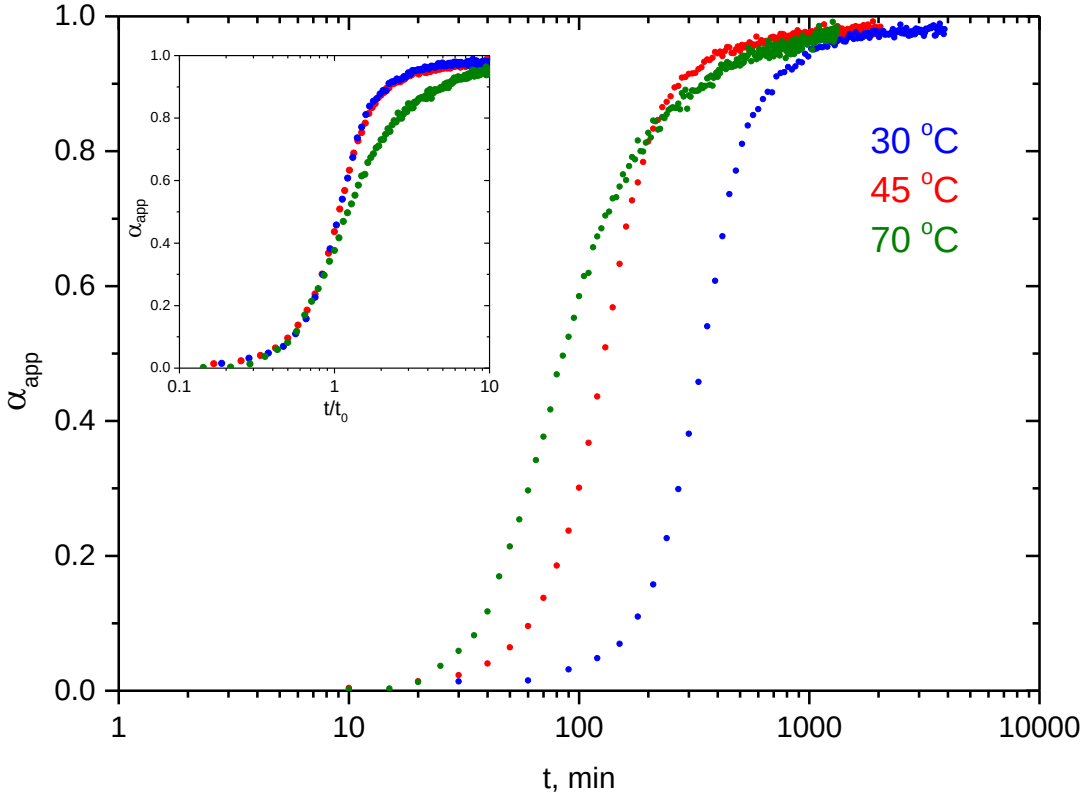

Figure 6.4. KGa-1b intercalation kinetics with 80%NMF-20%H_2O solution depicted in a log-time axis. Insert: time-temperature superposition of the kinetic data in reduced t/t_0 axis.

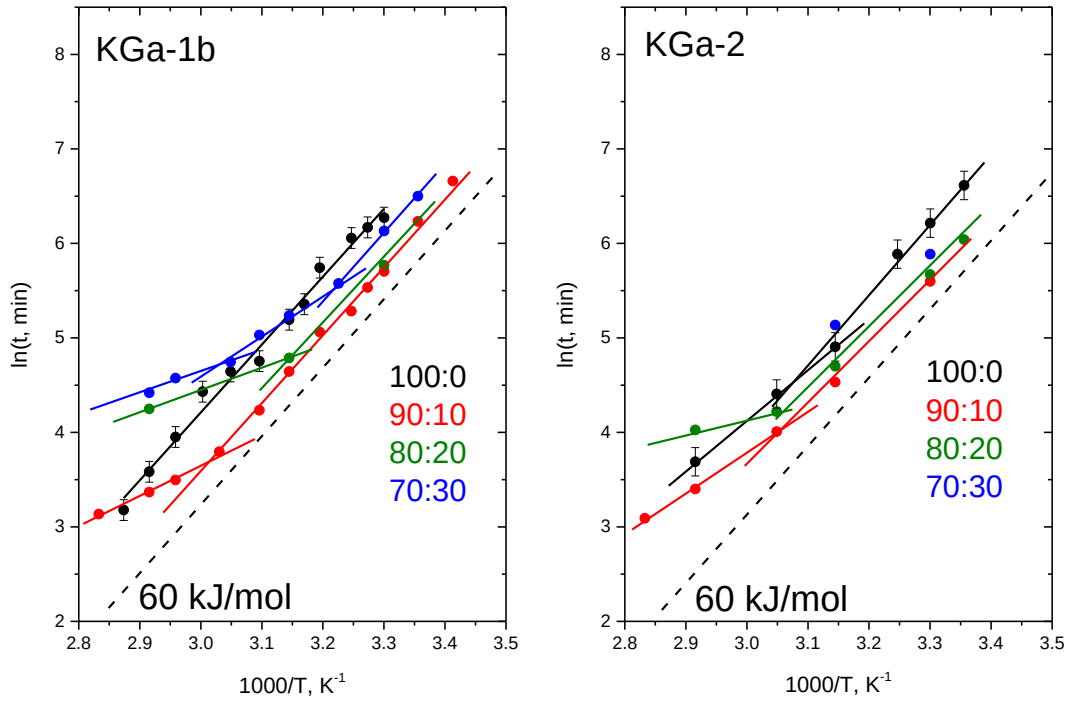

Figure 6.5. Arrhenius plots of t_0 values for KGa-1b (left) and KGa-2 (right) intercalated with 100:0 (black), 90:10 (red), 80:20 (green) and 70:30 (blue) NMF:H_2O. Note the high temperature deviation of $logt_0$ at high H_2O contents. Dashed lines represent E_α=60 kJ/mol.

6.3 Effect of temperature and H_2O content on the 2ν(NH) proxy

The first issue to be addressed is the effect of water content on the 2ν(NH) proxy, especially at the high temperature range in which the abnormalities of the kinetic shape are observed. For that reason, the vector normalized 2nd derivatives of the 2ν(NH) band in KGa-1b intercalated with 100:0, 90:10 and 80:20 solutions were compared at 30 and at 70 °C (Fig. 6.6). Note that the 30°C data in Fig. 6.6 (upper) are from time-temperature superimposable sigmoidals, whereas the 70 °C data run across the green and red fields of Table 6.1.

It is observed that at any given temperature, the position and the width of the band are independent of the presence and amount of water contained in the intercalating solution. If H_2O was present in the interlayer space, it would have interacted with the intercalated NMF causing changes in the shape of the 2ν(NH) band. No such changes are observed in our experiments. This means that the NMF molecules are inserted selectively in the interlayer space, whereas H_2O interacts only with the kaolinite edges/surfaces outside the interlayer. It is therefore concluded that a change in the intermolecular interactions of NMF cannot be the cause of the non-monotonic trends in Fig. 6.1, or the high-temperature deviations in Figs. 6.4, 6.5. The latter are possibly due to concentration and temperature dependent NMF-H_2O interactions with the outer surface of kaolinite (i.e. edges).

The negative evidence about the existence of interlayer H_2O is in support of the description of intercalation by a two-state model (coexistence of fully- and non-intercalated interlayers) as proposed in Sections 4.1 and 5.5: A partially occupied and slowly filling interlayer by NMF would immediately invite interlayer H_2O, as long as the intercalating solution is not anhydrous. This would cause the time-dependence of the vibrational signature due to the variable NMF:H_2O interlayer composition, and would by no means result in identical band positions and widths, as observed in Fig. 6.6.

KGa-2 displays exactly the same behavior as KGa-1b, as it is shown in Fig. 6.7 under all intercalating conditions investigated, implying that the interlayer environment is the same as KGa-1b.

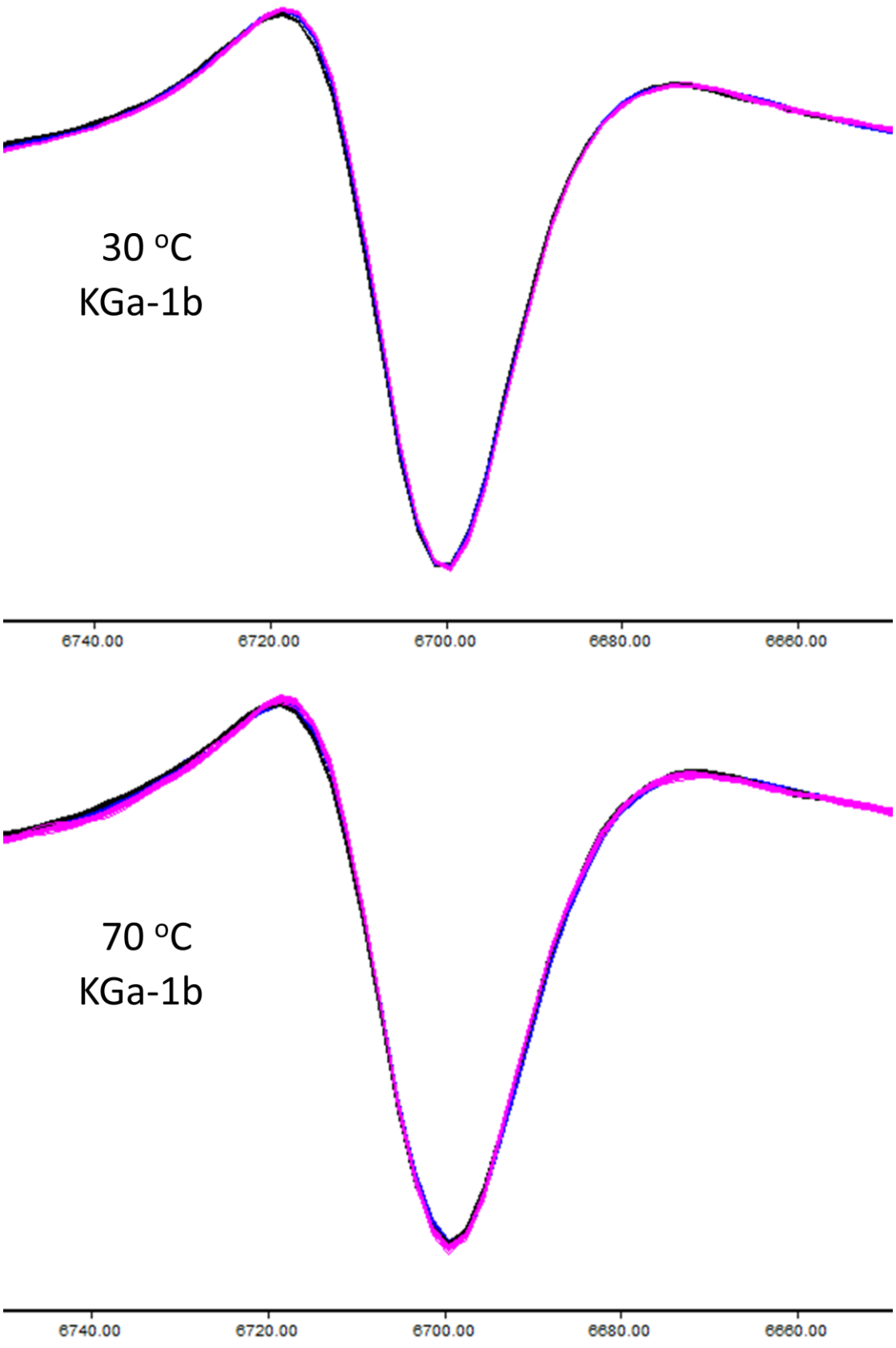

Figure 6.6. Vector normalized 2nd derivative spectra over the 2ν(NH) range for KGa-1b intercalated with 100:0 (black), 90:10 (blue) and 80:20 (magenta) NMF:H_2O at 30 °C (upper) and 70 °C (lower). Note that the bandshapes are independent of H_2O content.

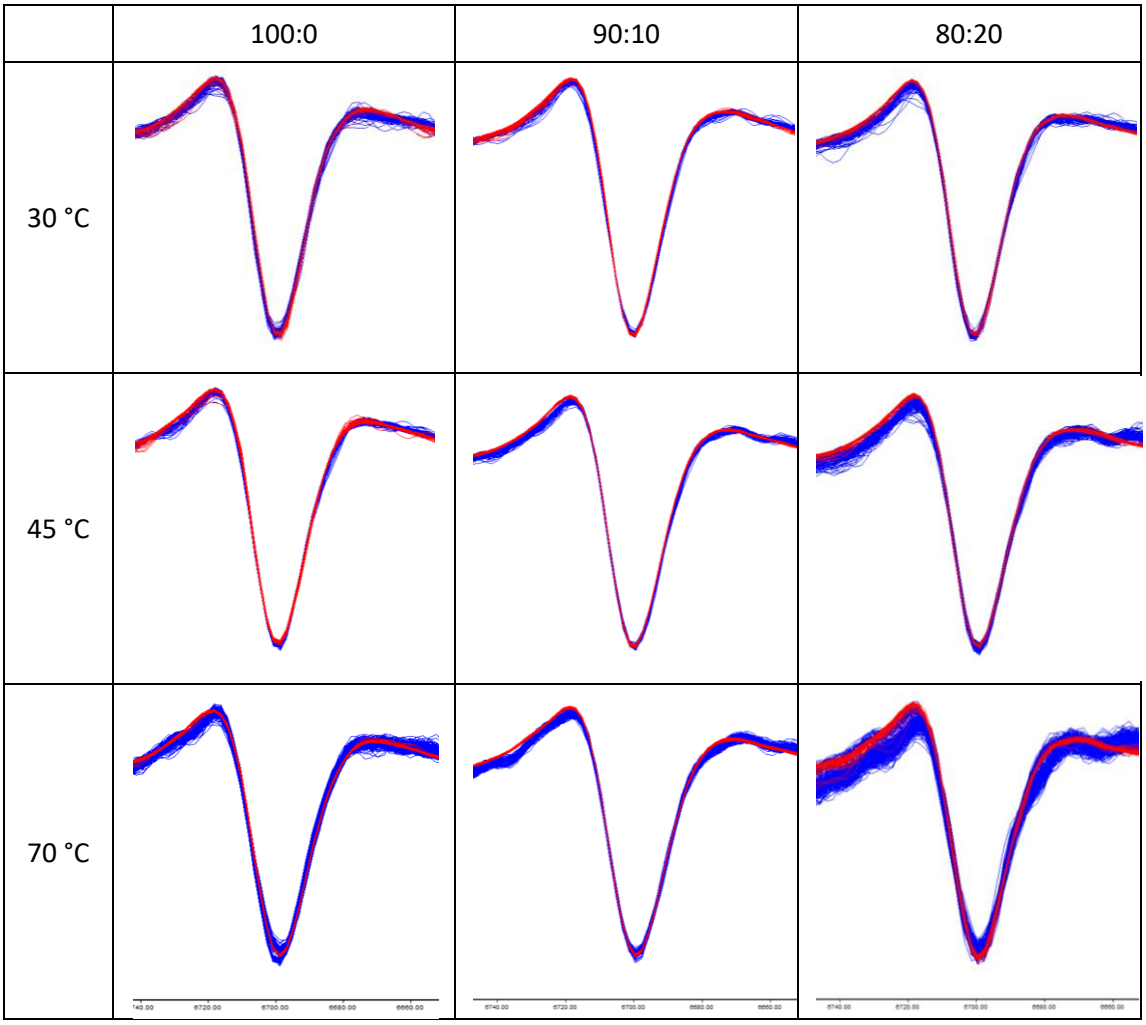

Figure 6.7. Timeseries of the 2nd derivative of the 2ν(NH) band of KGa1b (red) and KGa-2 (blue) intercalated with 100:0, 90:10 and 80:20 NMF:H_2O solutions at 30, 45 and 70 °C. Note that KGa-1b and KGa-2 exhibit the same bandshapes at any temperature-H_2O content conditions.

The next issue to be addressed is the effect of temperature on the position and width (hence, the intensity) of the 2ν(NH) proxy. The vector-normalized 2nd derivatives of the 2ν(NH) band in KGa-1b intercalated with 100:0 and 80:20 solutions were compared at 30, 45 and 70 °C (Fig. 6.8). The change in position is practically negligible. However, a broadening of the band is observed as the temperature increases and this would lead to a decrease of the intensity at high temperatures. The latter decrease should be taken into account explicitly if data from different temperatures need to be compared.

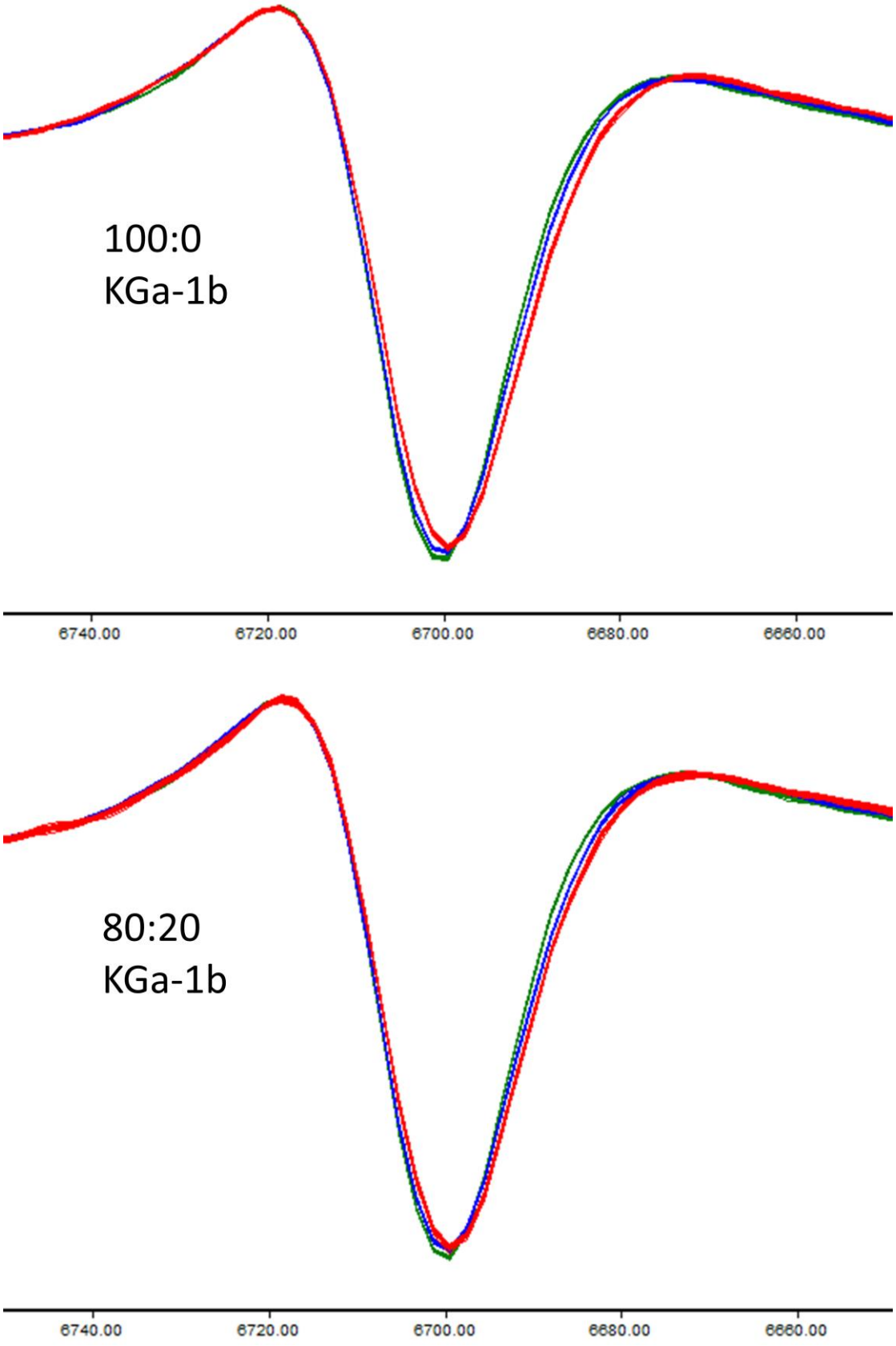

Figure 6.8. Vector normalized 2nd derivative spectra over the 2v(NH) range for KGa-1b intercalated with 100:0 (upper) and 80:20 (lower) NMF:H_2O at 30 °C (green), 45 °C (blue) and 70 °C (red). Note the band broadening with temperature.

In order to calibrate the effect of temperature on the intensity of the 2ν(NH) probe, an exhaustively intercalated KGa-1b/70:30 sample (>3m intercalation at ambient temperature) was equilibrated at different temperatures in the range 20-80 °C and measured by NIR while sealed (Fig. 6.9). Starting from 20 °C, a systematic broadening with increasing temperature is observed (Fig. 6.9a), as indicated by the data shown in Fig. 6.8. The changes in width lead indeed to the intensity decrease of the 2nd derivative of the band, as expected (Fig. 6.9b). A correction derived from the data in Fig. 6.9b is, therefore, needed in order to compare semiquantitatively the progress of intercalation as a function of temperature. This approach is based on the assumption that no deintercalation takes place upon increasing temperature. Evidence for the validity of this assumption is provided in the next section.

A more robust correction for temperature effects would involve the ratioing of the 2ν(NH) intensity to an internal reference band in the spectrum. A suitable candidate is the 2ν(OH) band at 7065 cm^{-1} attributed to the inner hydroxyls of kaolinite. This is the band of kaolinite which is least affected by intercalation in terms of position, width and intensity (Fig. 3.2). The temperature dependence of the intensity of this band (Fig. 6.9c), also defined by the amplitude of the 2nd derivative, is proportional to that of the 2ν(NH) band (Fig. 6.9b), resulting in a constant intensity ratio of the two peaks (Fig. 6.9d):

$$r = \frac{Intensity\ 2\nu(OH)}{Intensity\ 2\nu(NH)} \qquad Equation\ 6.1$$

The ratio, r, is approximately constant for all intercalating solutions investigated (r=6.0±0.2 for the 100:0 solution, 5.8±0.1 for the 90:10, 6.5±0.1 for the 70:30). The progress of intercalation under all intercalating conditions investigated can, thus, be estimated semiquantitatively by the 2nd derivative intensity of the 2ν(NH) band normalized by the corresponding intensity of its inner-OH 2ν(OH) counterpart (Eq. 6.1).

KGa-1b with 70:30 solution

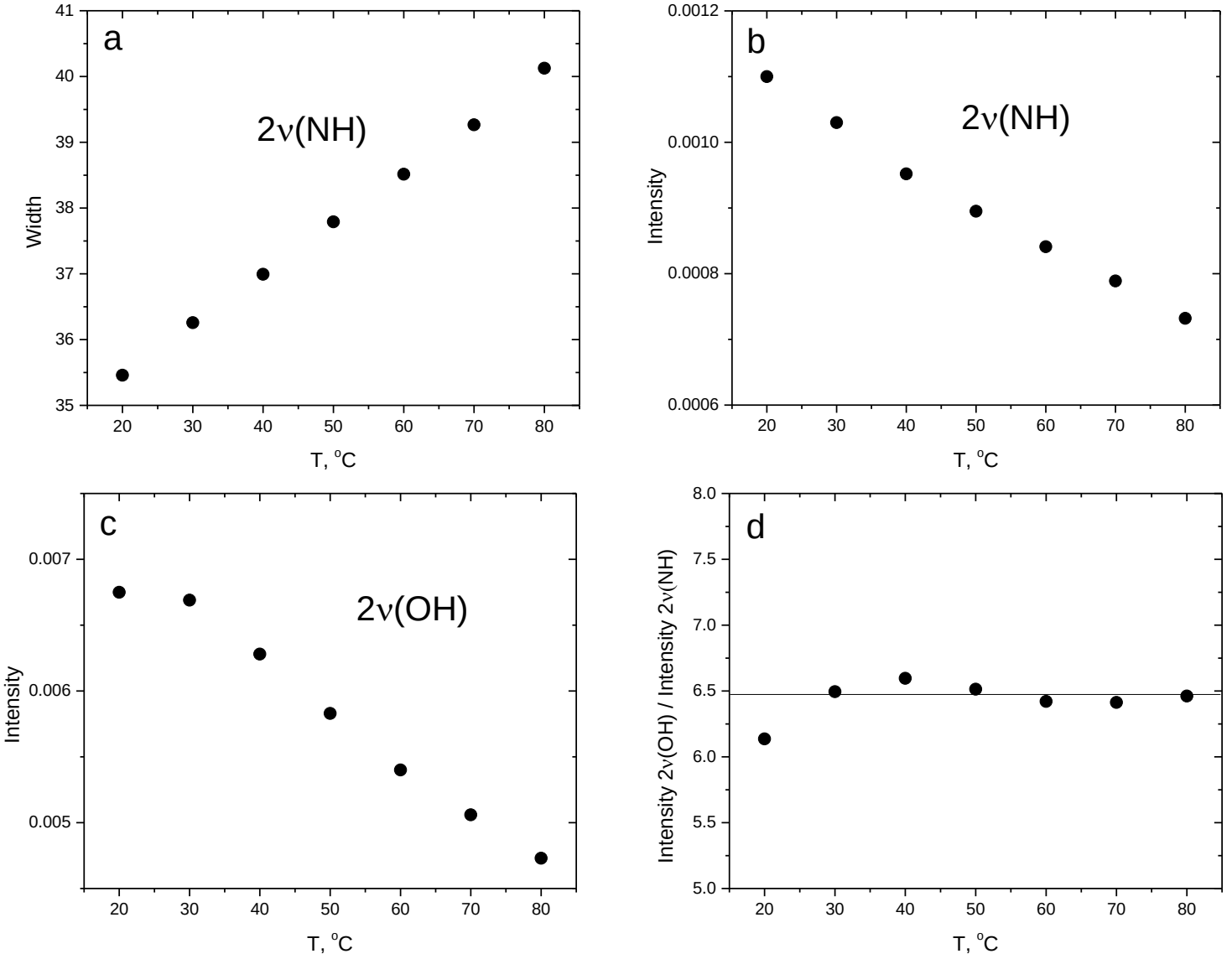

Figure 6.9. a) Width and b) intensity (lower) of the 2nd derivative of the 2ν(NH) band, c) intensity of the 2nd derivative of the 2ν(OH) band and d) ratio of the 2nd derivative intensities of the 2ν(OH) band to the 2ν(NH) band of a final-state intercalated KGa-1b sample with 70:30 NMF:H_2O as a function of temperature in the 20-80 °C range.

6.4 Semiquantitative aspects of intercalation

The proxy refined in the previous section is now employed for studying semiquantitatively the effect of temperature and H_2O content on the kinetics of intercalation as well as on the amount of intercalated NMF. Eight systems were investigated in this manner (KGa-1b and KGa-2, intercalated with 100:0, 90:10, 80:20 and 70:30 solutions). Each of the eight systems was subjected to the following three independent intercalation experiments:

a) Isothermal heating at 30 ^oC for ~3 days (measurements every 30 min)

b) Isothermal heating at 45 ^oC for ~24 h (every 10 min),

c) Isothermal heating at 70 ^oC for ~24 h (every 5 min), followed by isothermal heating at 45 ^oC for ~24 h (every 10 min), followed by isothermal heating at 30 ^oC for another ~24h (every 30 min). Temperature changes were instantaneous by transferring the NIR fiber with the fitted sample to a second thermostated bath.

A plot of the three experiments was produced for each of the eight systems (Figs. 6.10 and 6.11 for KGa-1b and KGa-1, respectively). Each panel represents data acquisition of more than 7d. Comparing the intercalation data of the eight systems allows for the following remarks:

Under any conditions investigated, KGa-2 is observed to reach lower final degree of intercalation and a poorly defined plateau compared to KGa-1b, in agreement with Ch. 4 regarding the anhydrous system.

No differences are observed between the 100:0 and 90:10 solutions in terms of the NMF uptake at any temperature (Figs. 6.10a,b, and 6.11a,b). A small decrease of the final NMF uptake is observed though upon increasing temperature. The sigmoidals maintain their shape and the 90:10 systems are shifted to lower times, in agreement with Section 6.1. Up to 10 wt% H_2O it appears to catalyze intercalation, as suggested by Olejnik et al. (Ole68).

Further increase of water content causes a pronounced reduction of the final NMF uptake at 45 ^oC and especially 70 ^oC, which is accompanied by the loss of the final plateau (Figs. 6.10c,d, and 6.11c,d). The effect of water at high temperatures is stronger in KGa-2 than in KGa-1b. In fact no intercalation is observed when KGa-2 is exposed in a 70:30 solution at 70 ^oC.

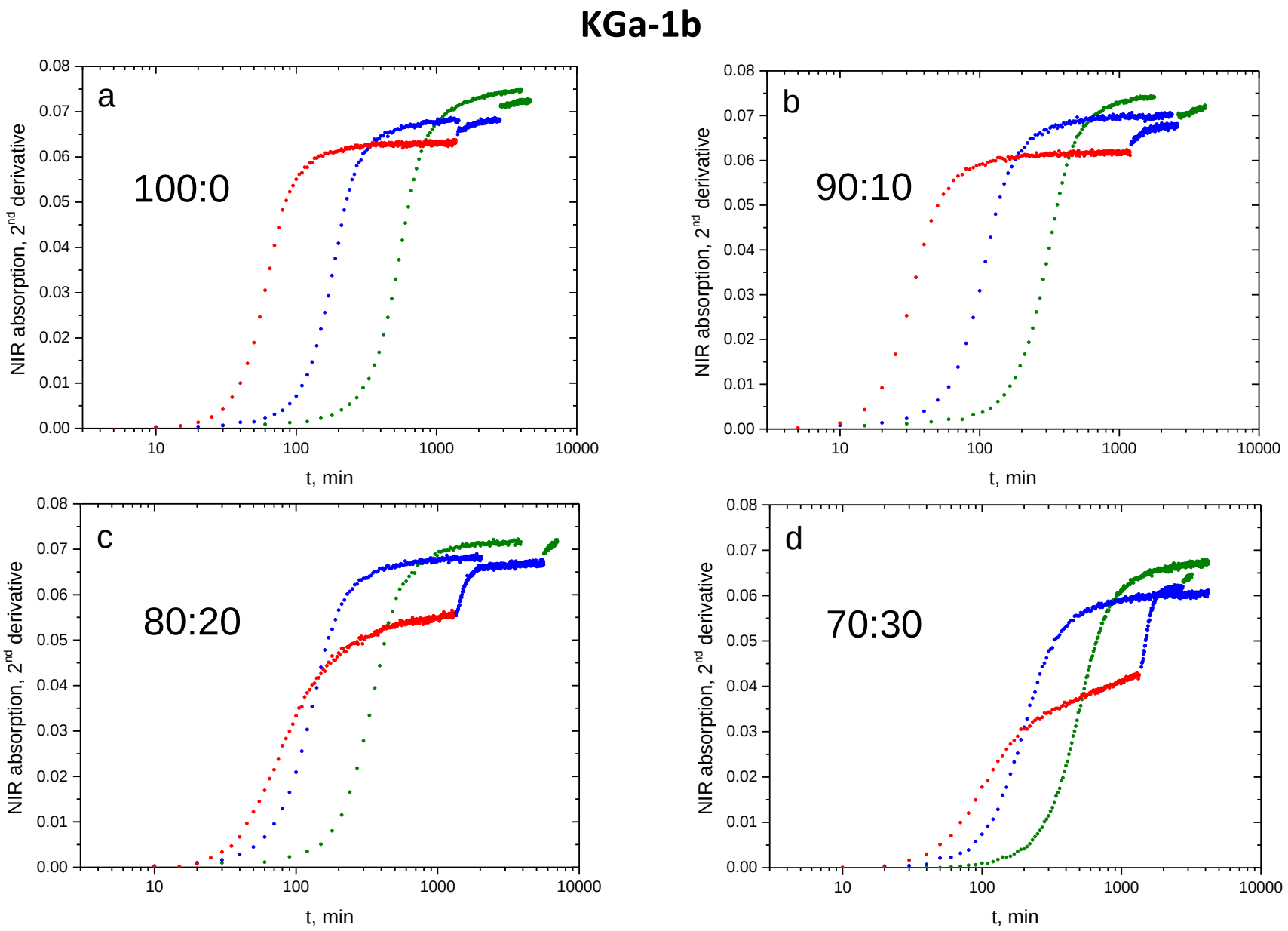

Figure 6.10. 2nd derivative intensity of the 2ν(NH) band normalized by the 2ν(OH) inner for KGa-1b intercalated with a) 100:0, b) 90:10, c) 80:20 and d) 70:30 NMF:H_2O at 30 °C (green), 45 °C (blue) and 70 °C (red). For details see text.

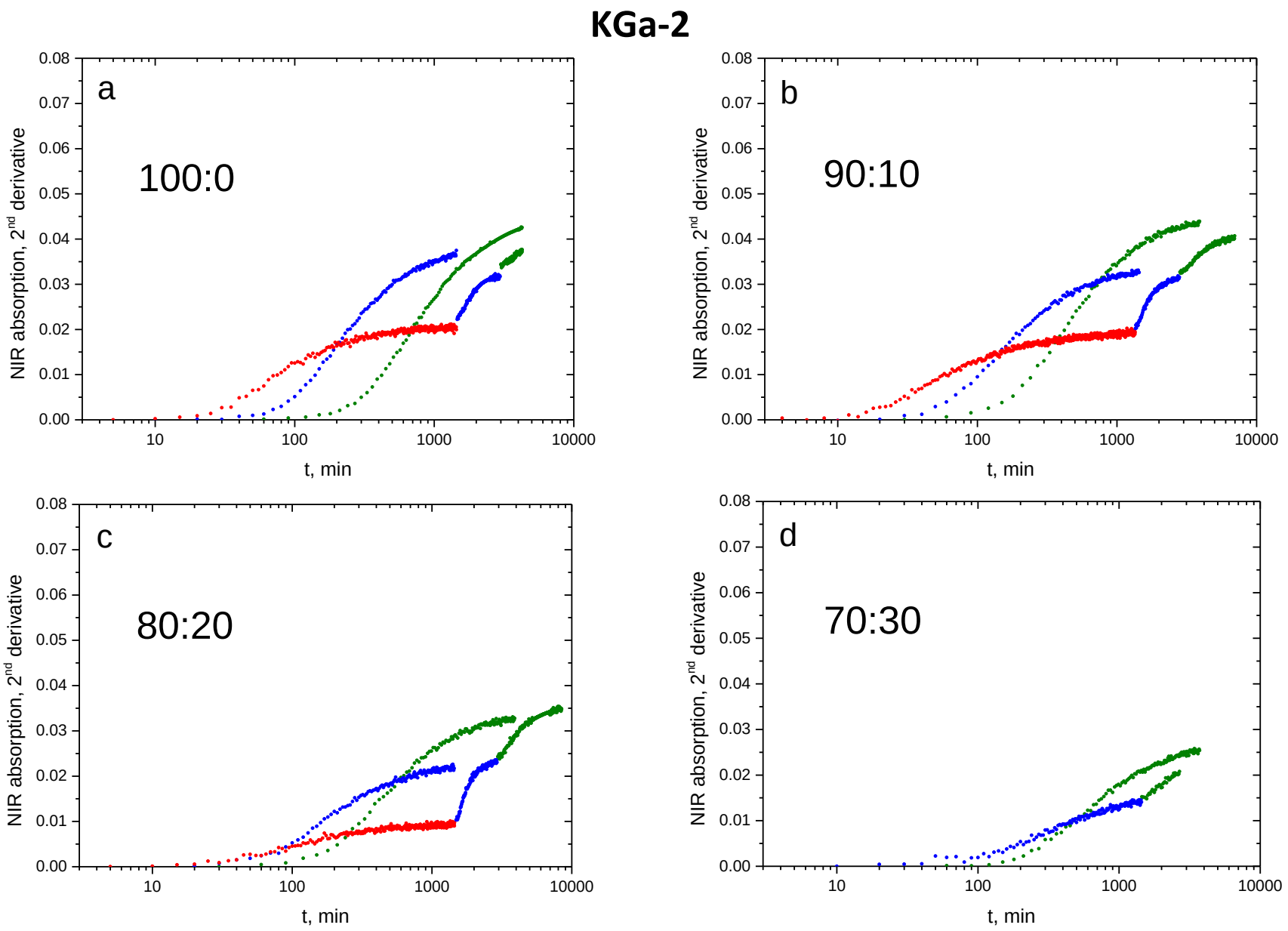

Figure 6.11. 2nd derivative intensity of the 2ν(NH) band normalized by the 2ν(OH) inner for KGa-2 intercalated with a) 100:0, b) 90:10, c) 80:20 and d) 70:30 NMF:H_2O at 30 °C (green), 45 °C (blue) and 70 °C (red). For details see text.

The trends in the final degree of intercalation obtained by NIR at the various intercalating conditions investigated (Figs. 6.10, 6.11) are supported by independent thermogravimetric experiments performed at a temperature range of 40-800 ^{o}C with a 10 ^{o}C/min rate. The recorded TGA diagrams were normalized to 100% kaolinite (14% mass loss).

Samples of KGa-1b and KGa-2 intercalated with 100:0, 90:10, 80:20 and 70:30 solutions were left to react for 3d at 30 °C, or for 1d at 70 °C. At the end of these reaction periods, the excess unreacted NMF was removed as described in Section 4.2.

The degrees of intercalation estimated by TGA (Fig. 6.12) imply that the increase of temperature or/and the H_2O content in the solution cause a decrease of the NMF uptake, in accordance with the results of the NIR analysis. To my knowledge this is the first report of decreasing intercalation with increasing temperature. High temperatures are usually recommended to speed up intercalation (e.g. [Lag06]) but the present findings suggest that this may lead to a higher fraction of non-intercalated material.

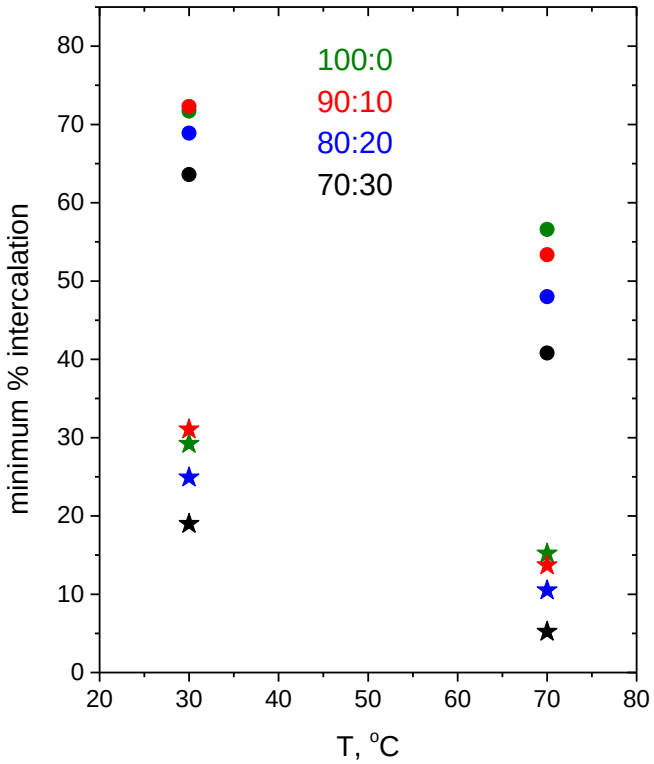

Figure 6.12. Minimum % intercalation in KGa-1b (circles) and KGa-2 (stars) under different intercalating conditions.

Remarkably, the data in Figs. 6.10 and 6.11 demonstrate that switching to 45 ^{o}C and then to 30 ^{o}C after a long-term exposure to 70 ^{o}C results in the revival of the hindered intercalation. This is observed in all systems, but is especially pronounced at high water content, i.e. when intercalation at 70 ^{o}C was more suppressed. The limiting uptake of these 45 and 30 ^{o}C segments are in good agreement with that of the corresponding single-temperature kinetics. In fact, reaching the plateau by isothermal heating at 30 ^{o}C can be faster than by sequential heating at 70-45-30 ^{o}C.

In a closed system such as that investigated here, the dependence of the final NMF uptake on temperature could be the result of a thermodynamic equilibrium governing the partition of NMF between the intercalating liquid and the interlayer. If that were the case, intercalation would be reversible and its extent would depend solely on temperature and not on thermal history. This is not observed: It was found that any closed system subjected to exhaustively intercalation at 30 ^{o}C does not deintercalate upon increasing the temperature to 70 ^{o}C for several hours. This means that in a closed kaolinite/NMF/H_2O system, temperature-dependent equilibria take place between the liquid and the outer surface of the mineral particles, and these may involve the relative participation of NMF and H_2O to chemisorption. This equilibrium favors the chemisorption of NMF at low temperatures and low H_2O contents. Under these conditions, the interlayers can pop to their fully expanded state, but cannot deintercalate NMF back to the liquid.

Chapter 7

Effect of particle size on intercalation

Based on the analysis presented in Chapter 5, it was suggested that the sigmoidals do not represent a diffusion process but the distribution of the time needed for the switching between two states (from non-intercalated to fully intercalated interlayers). Sigmoidal distributions are different in the two kaolinites examined (Ch. 3) and are not stable in the presence of H_2O at high temperatures (Ch. 6). The distributions contain non-reactive material in KGa-1b and KGa-2 (Ch. 4). The existence of inert, non-intercalating material in specific types of kaolinite has been also reported in literature [Fro02, Lag06], yet the origin of this behavior remains a puzzle.

One possible explanation for the observed differences in the shape of the sigmoidals and the final NMF uptake could be related to the existence of particles with different sizes along *ab*-plane (distributed log-normally) in bulk kaolinite. It is reminded that KGa-1b displays a bimodal particle size distribution with maxima at 3 and 22 μm and KGa-2 a broad unimodal distribution with mean size of ~10 μm [Dri15] (Section 2.1). As it was proposed in previous XRD studies, particle size could play an important role on intercalation: the smaller the particles, the more reduced the intercalation yield [Uwi93, Den02].

In this chapter, the effect of particle size on intercalation is examined by the usual NIR recording of NMF intercalation kinetics.

7.1 Natural particle size fractions

Fractions of naturally occurring particles were derived by gravity and centrifugal sedimentation, by the Clay Research Group in Krakow, following the method by Tanner and Jackson [Tan48]. Bulk kaolinite was dispersed in deionized water under ultrasonic vibrations. The dispersed sample was then poured into a big plastic beaker, which was filled up with deionized water. Based on the time required for a particle with a certain diameter to precipitate, the grains were separated in >10 μm and 10-4 μm fractions. The remained suspension was centrifuged for 4 minutes at 1000 RPM to precipitate the 2-4 μm particles. At the end of the procedure, all the fractions were dried at 60 °C. Using this method, >95% of the total mass was recovered with the >10 μm particles and the rest <5% into <10 μm particles.

Due to the small quantity of finer fractions, full NIR kinetic experiments were performed only at 45 °C using ~0.05 g of kaolinite with 90%NMF-10%H_2O solution in a 1:1 wt mixture and a miniature version of the reactor fitted to the NIR probe (Fig. 7.1). Intensities of the 2nd derivative of the 2ν(NH) band were normalized to the corresponding intensities of 2ν(OH) band of inner OH groups as described in Section 6.3 (Eq. 6.1) in order to provide a semiquantitative estimate of NMF uptake. Data acquisition lasted ~24h in each experiment, which was sufficient for recording a well-defined end-point in KGa-1b at this temperature (see Fig. 3.7).

In both kaolinites, there are distinct differences between the kinetics recorded for the >10 μm and the <10 μm particles. As it is shown in Fig. 7.1, the kinetics of bigger particles display the same behavior as the bulk sample, which was expected because the bulk consisted mainly of >10 μm particles. The kinetics of finer fractions demonstrate longer incubation period and lower intercalation rate. In fact, the reactivity to intercalation is so slow in the small particles (2-4 and 4-10 μm) that 24 h at 45 °C are not enough for the KGa-1b sigmoidals to reach a plateau, whereas in KGa-2 the sigmoidal is completely lost. The effect of particle size on intercalation is more pronounced in KGa-2, where NMF uptake and reaction rate are progressively reduced with decreasing particle size. In the case of KGa-1b, the differences between the kinetics of the 2-4 and 4-10 μm fractions are small, possibly due to particle agglomeration which results in poor separation.

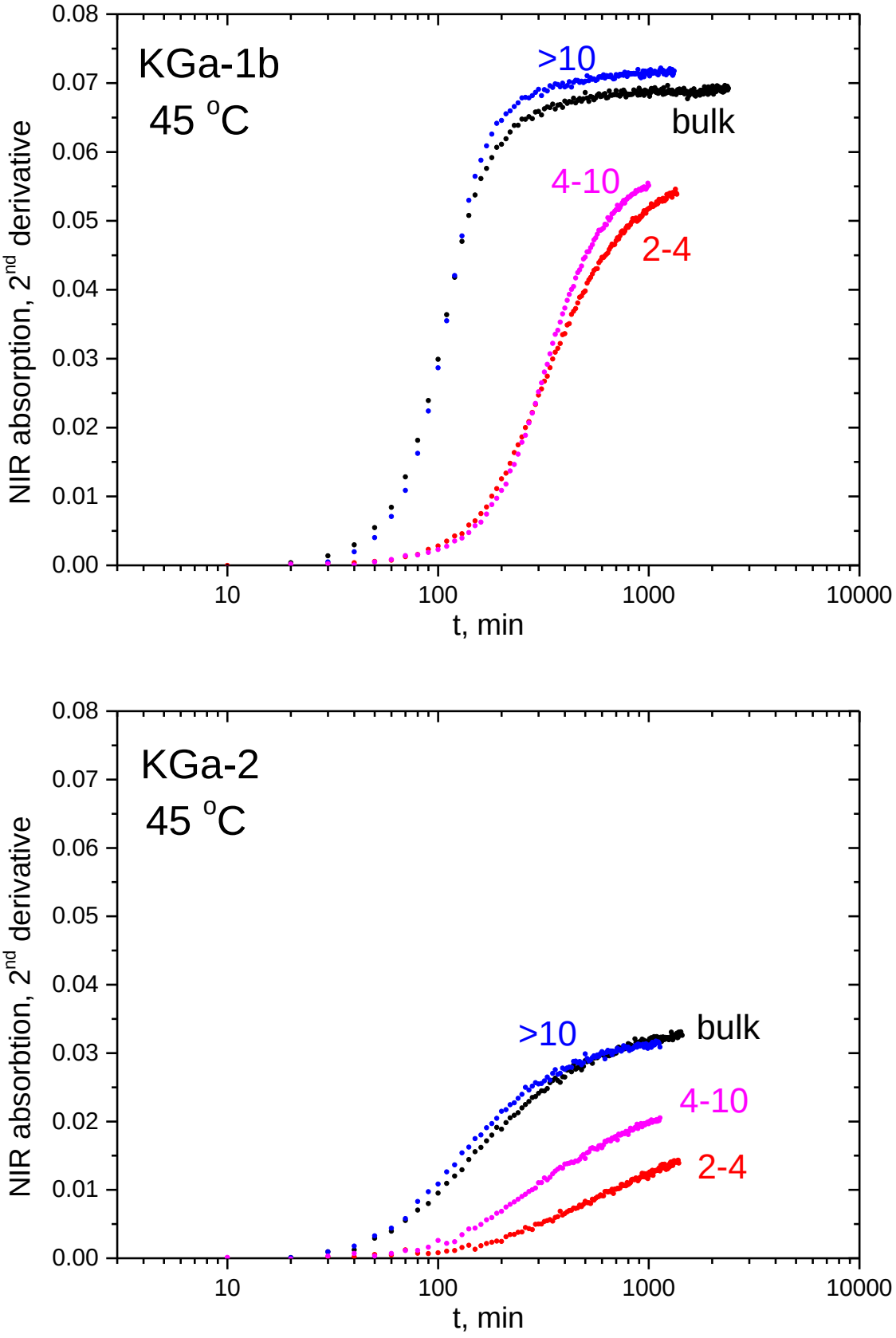

Figure 7.1. NIR-based intercalation kinetics at 45 °C for the natural particle size fractions 2-4 (red), 4-10 (magenta) and >10 µm (blue) of KGa-1b (upper) and KGa-2 (lower) compared to bulk (black).

For this reason, separations were repeated in the case of KGa-1b by treating the sample with a well-known dispersant (Calgon) prior to sedimentation, similarly to Mackinnon et al. [Mac93]. The main difference between the two methods is that the dispersant acts by binding to the outer surface of the particles, and therefore prevents them from forming aggregates, but it may have an effect on intercalation. Four fractions were separated in this manner: >10 μm (51%), 4-10 μm (22%), 2-4 μm (25%) and <2μm (2%).

The experimental processing and kinetic recording were the same as in the study of the previous particle size separation. Kinetics derived from the intercalation of these fractions (Fig. 7.2) display the same general characteristics (progressive reduction of the rate and the degree of reaction with decreasing size) with the previous samples (Fig. 7.1). The finer segregation led to a better discrimination between the kinetics of particles with different size. The sigmoidal shape is observed in all the >2 μm size fractions, but not in the case of <2 μm particles, which exhibit very low reactivity to intercalation. The amount of non-reactive material increases progressively with the decrease of the size from >10 μm to <2 μm.

The linear combination of the kinetics weighted by the % wt of each fraction depicted in Fig. 7.2 is very similar to the kinetics of the bulk sample, albeit with a small shift towards longer times (Fig. 7.3), which could be related to a small change in H_2O content in the sample or to an unknown Calgon effect.

The differences between the shape of the kinetics of the various particle size fractions are better observed when plotting the data normalized to their respective long-term asymptotic values versus a reduced time axis (t/t_0 values) (Fig. 7.3), as described in Section 3.4. The sigmoidals of the >4 μm particles perfectly superimpose with the bulk sample kinetics, despite the discrepancy in the amount of non-reactive kaolinite, whereas the rest display deviations regarding the intercalation rate. As it can be figured out, the sigmoidal of the 2-4 μm particles could be reproduced as a linear combination of the 4-10 and <2 μm fractions. This would imply that the 2-4 μm distributed as a band with a peak at 3 μm in a log-scale axis (Fig. 2.1) is a mixture of the other two populations.

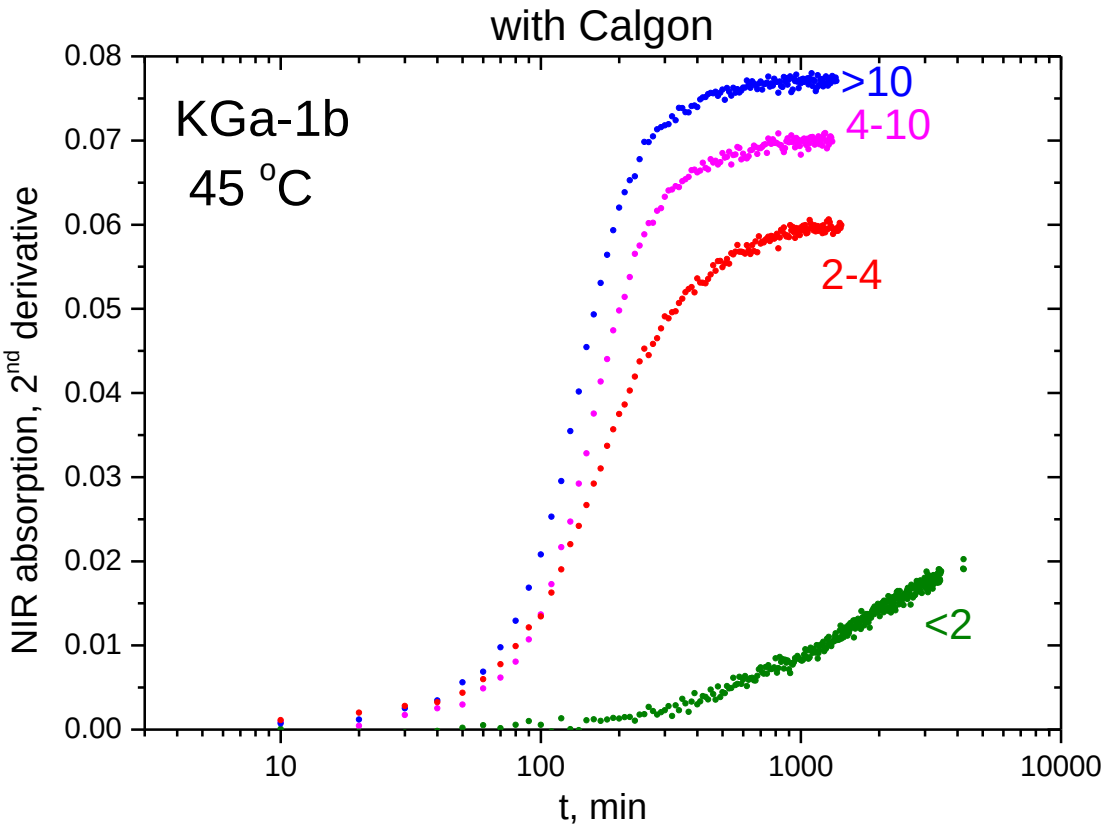

Figure 7.2. NIR-based intercalation kinetics at 45 °C for the particle size fractions with Calgon <2 (green), 2-4 (red), 4-10 (magenta), >10 μm (blue) of KGa-1b.

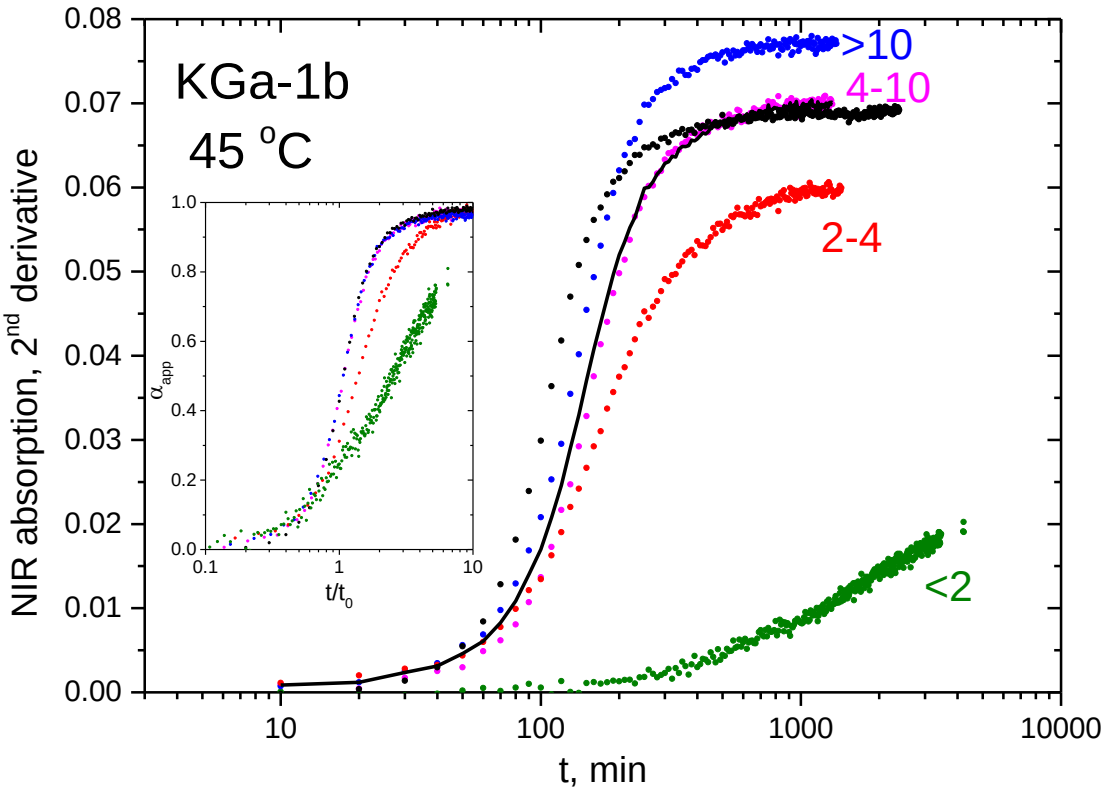

Figure 7.3. Comparison of the kinetics depicted in Fig. 7.2 to the bulk (black dots) and to their linear combination weighted by the % wt of each fraction (black line). Insert: time-temperature superposition of the normalized kinetic data in reduced t/t_0 axis.

It could be argued that the reason for the reduced reactivity of the smaller particles is a different interlayer environment, less favorable for NMF. To test this hypothesis it is important to check the signature of NMF during intercalation in large and small particles. The width of the 2nd derivative of the 2ν(NH) peak is identical within the resolution of our experiments in all fractions of either kaolinite (with or without Calgon) and coincides with that of the bulk (Figs. 7.4, 7.5). This implies that the intermolecular interactions of NMF with the inner surface OH as well as between the individual NMF molecules penetrating in the interlayer are the same and independent of the particle size involved in the reaction. Of course, this comparison is limited to the accessible part of the material, because non-reactive kaolinite is not probed by NMF.

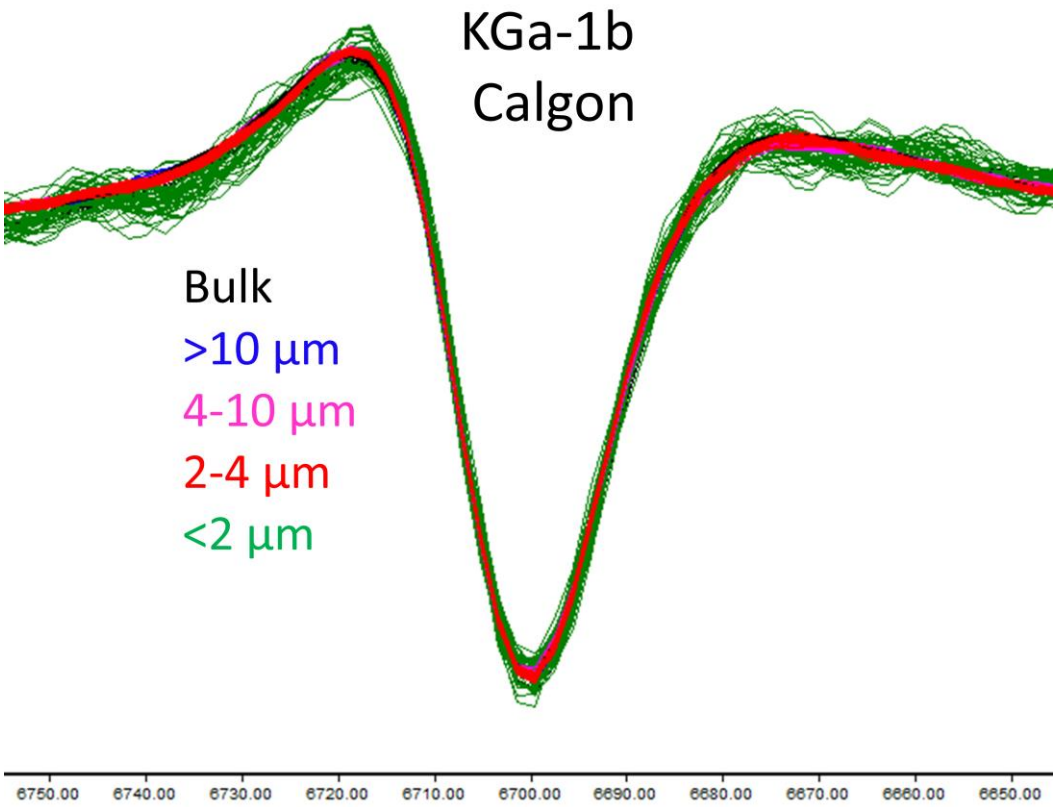

Figure 7.4. 2nd derivative with 9 points smoothing (Δν=2) of the 2ν(NH) mode, vector normalized at the displayed frequency range, for bulk and particle size fractions with Calgon of KGa-1b intercalation kinetics with NMF at 45°C.

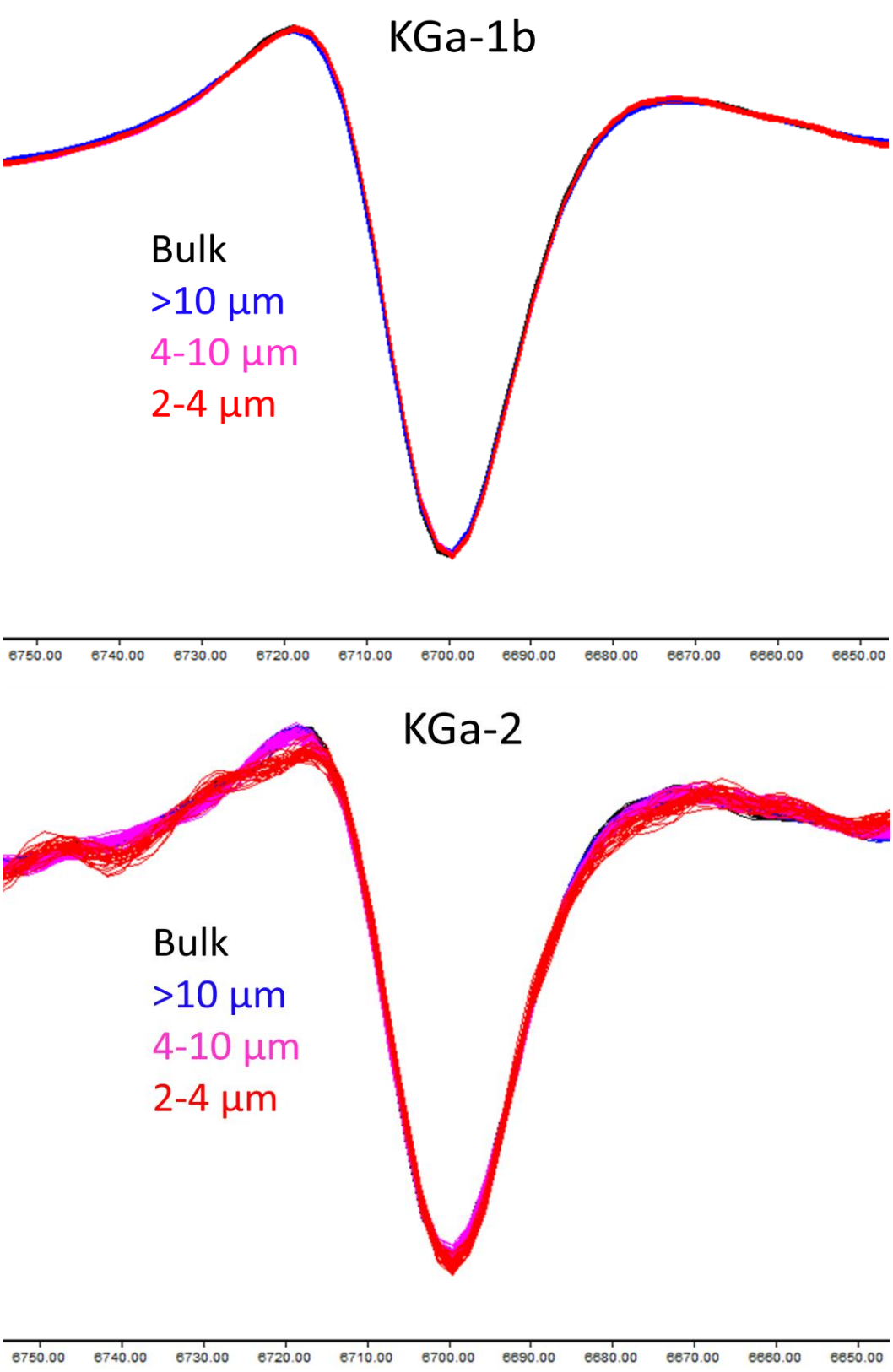

Figure 7.5. 2nd derivative with 9 points smoothing (Δν=2) of the 2ν(NH) mode, vector normalized at the displayed frequency range, for bulk and different particle size fractions without Calgon of KGa-1b (upper) and KGa-2 (lower) intercalation kinetics with NMF at 45°C. It was shown previously (Fig. 6.7) that the signatures of bulk KGa-1b and KGa2 also have identical shape.

Considering the above, the effect of particle size on intercalation is not a consequence of different arrangement of NMF molecules in the interlayer and must therefore be attributed to some other property of the particles, such as the stacking order/disorder of the particles, the crystal imperfections, the structural stress induced by the misfit of the two sheets ([Den02], and references therein), or a combination of more than one factors.

An interesting observation is that the shape of the kinetics of the <2 μm particles in KGa-1b is similar to the corresponding shape of the 2-4 μm particles of KGa-2 (Fig. 7.1, lower), despite the fact that these fractions differ in terms of stacking disorder: According to Sakharov et al. [Sak16], KGa-2 consists almost exclusively of the LOK phase. KGa-1b is also consisting of ~72% LOK, which is mostly found in the larger particles [Uwi93, Dri15] (Section 2.1). If this observation could be generalized, it would mean that the shape of the intercalation sigmoidal is determined mostly by particle size and not stacking order.

The reduction in NMF uptake with the decrease of the particle size has been already observed by Uwins et al. [Uwi93]. They separated KGa-1 and KGa-2 by using a dispersant (Calgon) before sedimentation [Mac93] and produced fractions with >2, 0.5-0.6 and 0.3-0.4 μm particles. Intercalation with NMF was performed after hydrazine pretreatment and its progress was calculated by Eq. 3.2 on intercalated samples after ~15 h of reaction at 60 °C. It was found that the uptake of NMF was less in the smaller fractions. The comparison of these findings to our results can only be qualitative, due to the fact that the fractions are not the same and the estimated values by Uwins et al. were based on a single XRD measurement of the end-point. Deng et al. [Den02] studied also the effect of particle size on the intercalation of a Georgia kaolinite with hydrazine monohydrate and potassium acetate. The sample was separated into nine fractions and their intercalation progress was investigated by *ex-situ* XRD measurements. Under these conditions, the smaller fractions displayed lower intercalation rate and bigger portions of non-intercalated material.

7.2 Artificial particle size fractions

Except of the size separation of the natural particles described above, the bulk can be also comminuted by artificial methods. One such method is the wet milling by a McCrone mill, which is known for producing narrow distributions of smaller particles with minimum induced amorphicity [Oco86]. For that purpose, 4 g of KGa-1b was milled with 5 ml of methanol for 2, 10, 20 and 30 min in a polypropylene vessel with corundum beads. The samples were collected in a slurry form, then dried and intercalated with 90%NMF-10%H_2O solution in a 1:1 wt mixture. The experimental conditions for monitoring intercalation were the same as for the natural particle size fractions.

All the kinetics, derived from the normalized intensities of the 2nd derivative of the 2ν(NH) band to those corresponding to 2ν(OH) band of inner OH groups, display the same final NMF yield (Fig. 7.6, upper). However, the shape is deformed as the milling time increases, causing reduction in the incubation time and smoother increase of the intercalation progress.

The artificially smaller fractions demonstrate a behavior which is completely opposite to the naturally smaller particles (Figs. 7.1 upper, 7.3): Longer milling times (smaller particles) shift the kinetics towards shorter times, but the same end-point is reached in all cases. It is obvious that milling caused changes in some unknown structural aspect which affects the shape of intercalation kinetics but not the NMF uptake. As part of the standard procedure, we check for possible modifications of the interlayers of kaolinite by the examination of the 2nd derivative widths of the 2ν(NH) band (Fig. 7.7, lower). The signature of intercalated NMF is independent of the milling time and coincides with the bulk, verifying that this is not the cause of the observed differentiation. Thus, the change should be laid in some unknown size or structural difference of milled kaolinite which needs further investigation.

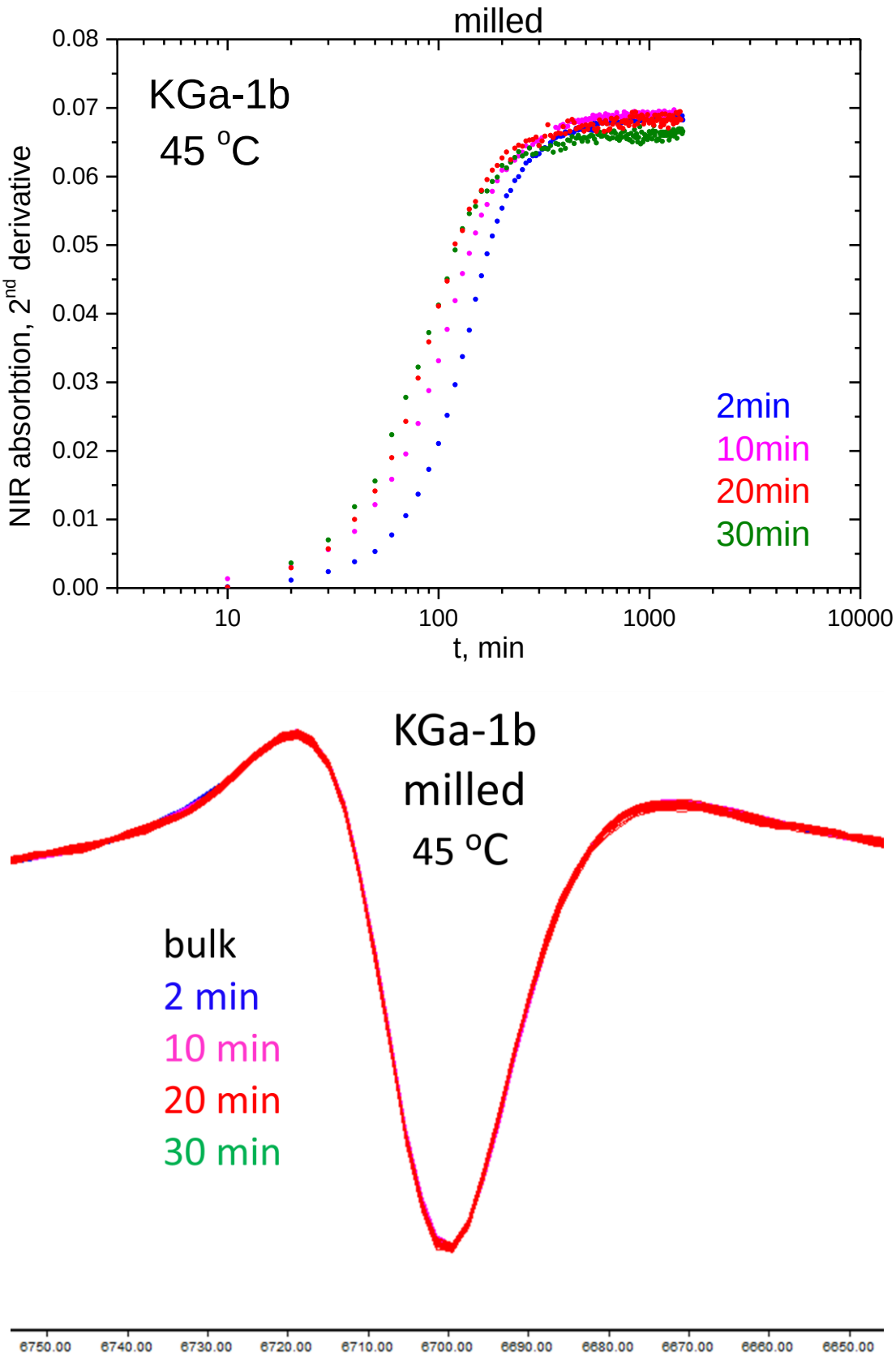

Figure 7.6. NIR-based intercalation kinetics at 45 °C for the artificial particle size fractions for 2 (blue), 10 (magenta), 20 (red) and 30 min (green) of milling time (upper) and their 2nd derivative with 9 points smoothing (Δν=2) of the 2ν(NH) mode, vector normalized at the displayed frequency range, compared to the bulk (lower).

Knowing that milling time decreases the incubation time of the kinetics and affects the shape of the sigmoidals, it is interesting to investigate whether this has an effect on activation energy, too. For that, additional experiments were performed to record the intercalation kinetics at 30 (Fig. 7.7, upper) and 70 °C (Fig. 7.8, upper) of the artificial particle size fractions, in addition to the previously presented 45 °C (Fig. 7.6, upper).

Besides the anticipated shifting of the kinetics towards shorter times at 70 °C and longer times at 30 °C, they demonstrate identical behavior with the corresponding at 45 °C. In all diagrams, the sigmoidals of the particles milled for longer periods display less sharp shape and they are shifted towards shorter times, so that the incubation time decreases. All the kinetics reach a well-defined plateau, indicating that particles of different size absorb the same amount of NMF in the interlayers. The small reduction of the NMF uptake end-point resulting from the increase in temperature is similar to that observed for the bulk sample (Section 6.4).

The width of the 2nd derivative of the 2v(NH) peak of the various particle sizes were identical to each other and to the bulk at any temperature investigated (Figs. 7.7 lower, 7.8 lower, c.f. with Section 6.3).

The kinetics of the particles generated by the same milling time superimpose perfectly when normalized to the long-term asymptotic values and plotted at reduced times (t/t_0) (Fig. 7.9). Consequently, the shape of the sigmoidals is dependent only on the milling time and it is characteristic for each artificial particle size distribution.

Despite the different shape, Arrhenius plots derived from the t_0 values display matching activation energy to the bulk sample, although it cannot be accurately calculated due to the deviation induced at high temperatures (Section 6.2). The rate-determining step of the mechanism seems to be the same throughout the examined temperature range for all the milled and non-milled particles.

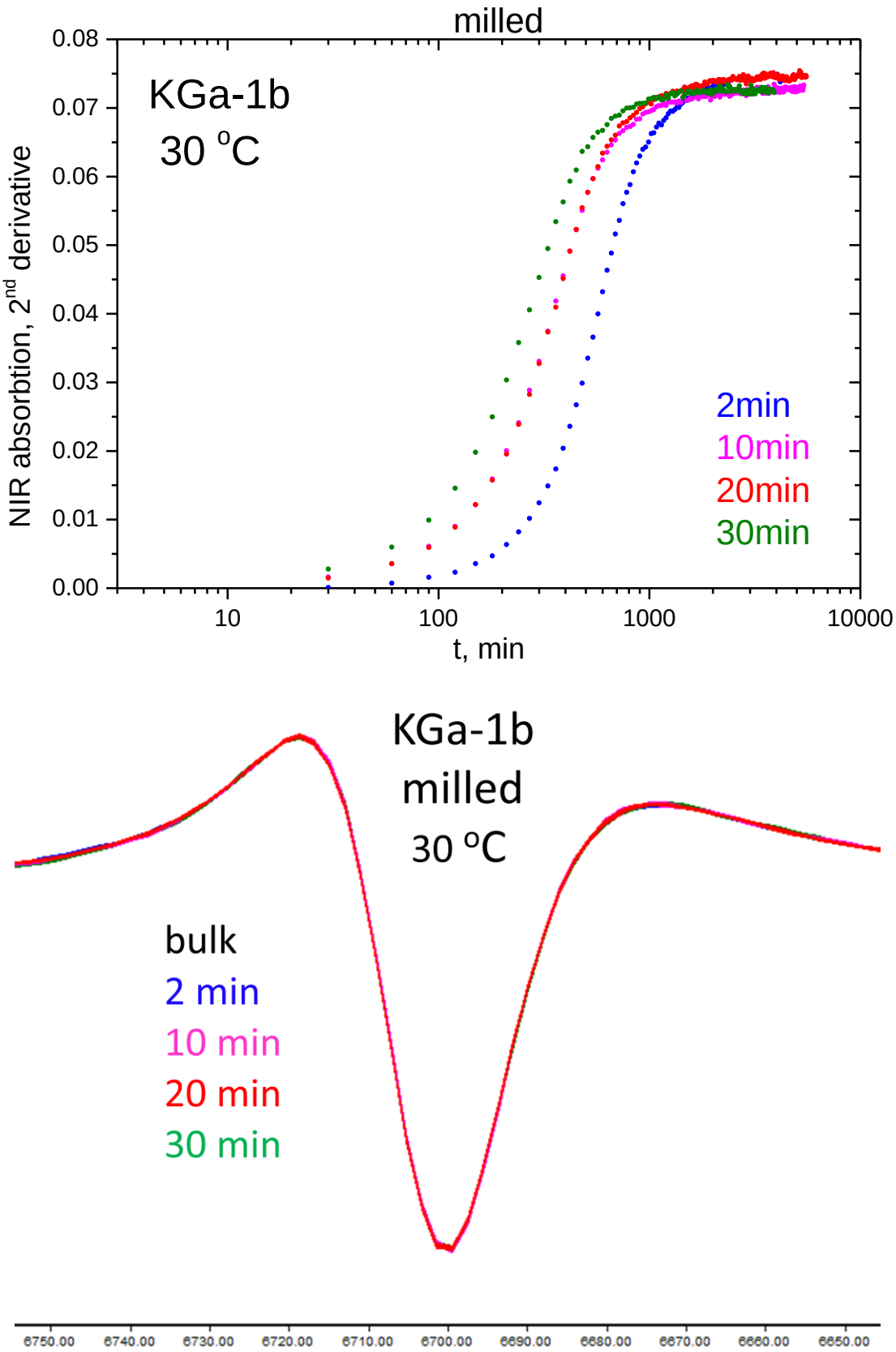

Figure 7.7. NIR-based intercalation kinetics at 30 °C for the artificial particle size fractions for 2 (blue), 10 (magenta), 20 (red) and 30 min (green) of milling time (upper) and their 2nd derivative with 9 points smoothing (Δν=2) of the 2ν(NH) mode, vector normalized at the displayed frequency range, compared to the bulk (lower).

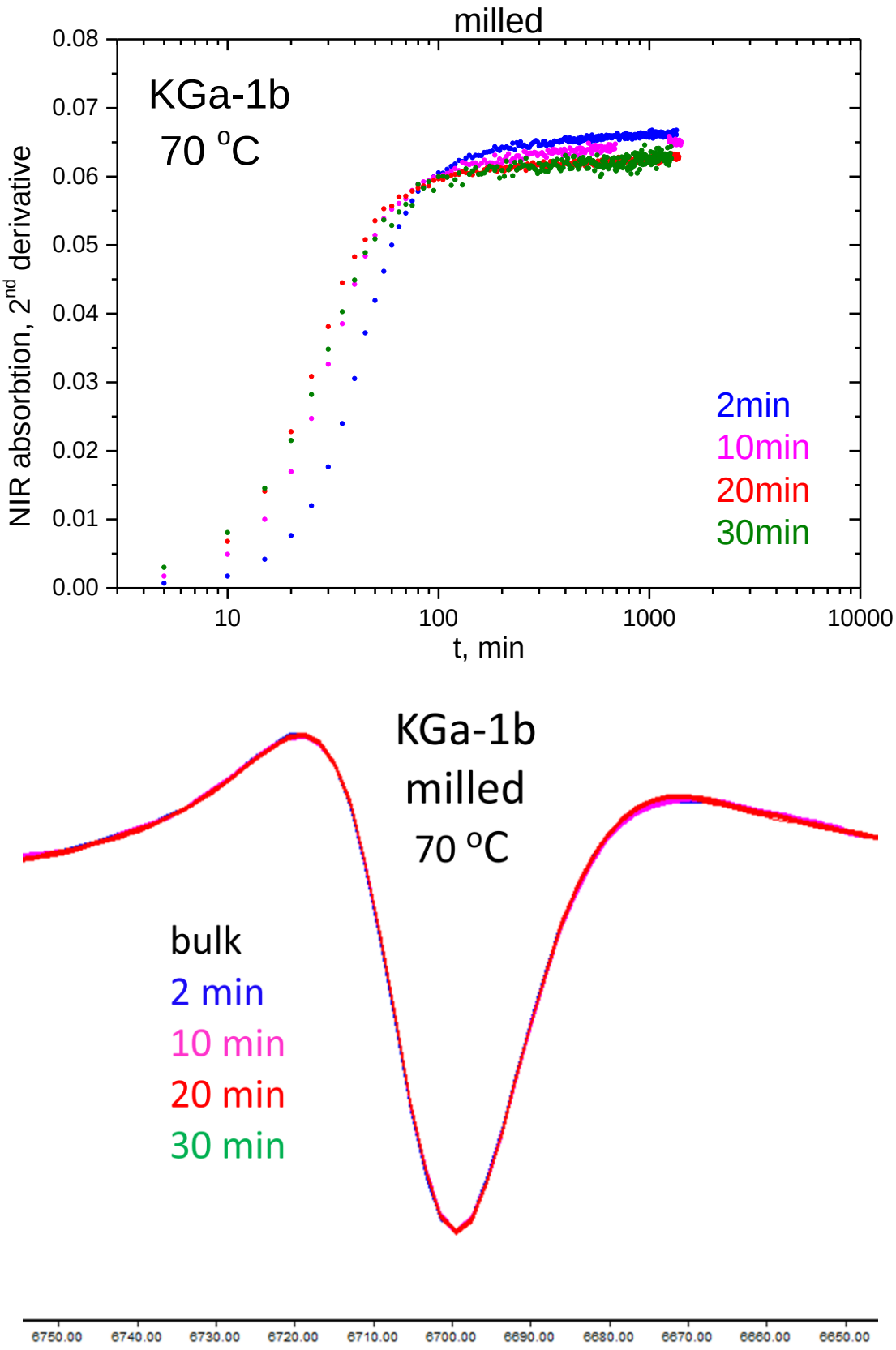

Figure 7.8. NIR-based intercalation kinetics at 70 °C for the artificial particle size fractions for 2 (blue), 10 (magenta), 20 (red) and 30 min (green) of milling time (upper) and their 2nd derivative with 9 points smoothing (Δν=2) of the 2ν(NH) mode, vector normalized at the displayed frequency range, compared to the bulk (lower).

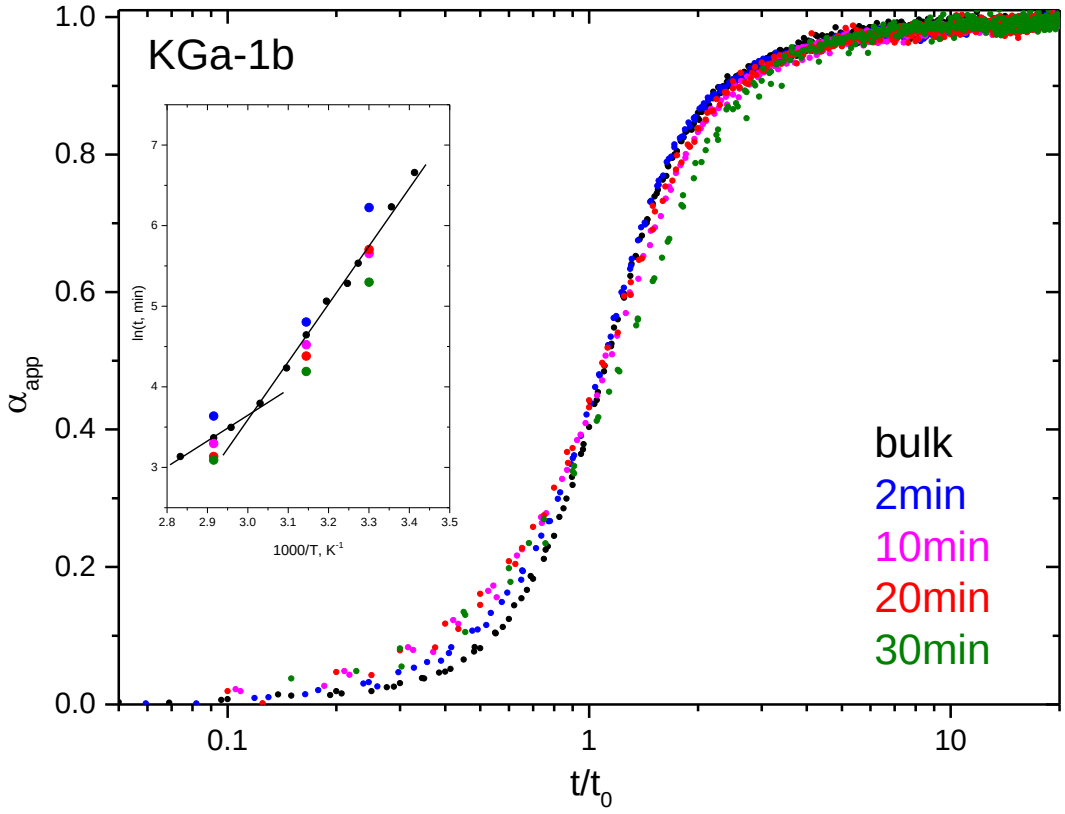

Figure 7.9. NIR-based time-temperature superposition of the kinetic data (blue) of the artificial particle size fractions of KGa-1b for 30, 45, 70 °C from Figs. 7.6, 7.7, 7.8. Bulk KGa-1b data are included for comparison (black). Reduced t/t_0 times are used. Insert: Arrhenius plots of t_0 values of the kinetic data.

Overall, natural and artificial methods employed for the separation of the particle size fractions of kaolinite were found to display different trends of intercalation kinetics. Thus, particle size alone cannot explain the variability of intercalation kinetics. Besides size, the aspect ratio of the particles may contribute to the shape of the sigmoidals. The natural particles in the bulk are reported to exhibit a log-normal distribution of *N*, the number of layers per particle [Sak16]. When the bulk is separated into fractions by sedimentation, it is reasonable to assume that each fraction has a different distribution of *N*. The presence of very thin particles could explain to some extend the presence of inert material, because the degree of intercalation is proportional to *N-1*, and not *N*. On the other hand, milling can be thought to form particles that are smaller in the *ab*-plane, but maintain their original distribution of *N*. The effect of the particle edges could be more pronounced in these small but thick particles. More research is needed to test these hypotheses.

Chapter 8

Conclusions-Perspectives

Kaolinite intercalation has been found to obey a sigmoidal time-dependence progress based on previous *ex-situ* XRD studies [Wei63, Ole68, Hac69, Ole70, Cas15, Mak19]. For the first time, near-infrared (NIR) spectroscopic technique in the diffuse reflectance mode was employed for the *in-situ* study of kaolinite intercalation kinetics with NMF under environmentally controlled conditions. Low-defect KGa-1b and high-defect KGa-2 kaolinites from Georgia, USA, provided by the Clay Minerals Society, displaying a bimodal and a unimodal particle size distribution along *ab*-plane, respectively [Dri15, Sak16], were studied.

Among other vibrational spectroscopic techniques, like ATR, the main advantage of NIR is that it can clearly distinguish the intercalating species in the presence of liquid NMF. This is because the stretching of the N-H bonds in liquid NMF is harmonic due to H-bonding, so that the 2ν(NH) overtone in the NIR range is weak and broad. On the contrary, the stretching of the dangling N-H of intercalated NMF is anharmonic and its overtone appears as strong and sharp bands in the NIR spectrum [Fol71, Sie02]. The same property was explored in the study of other systems involving dangling bonds such as the SiOH terminal defects in sepiolite [Buk13], the interlayer H_2O in montmorillonite [Tsi18] or the study of the indigo-palygorskite complex known as Maya blue [Tsi12]. In addition, NIR provides fast data acquisition under environmentally controlled conditions.

Opposite to XRD that probes the progress of coherently expanded interlayers along *c*-axis, NIR records the increasing concentration of the intercalated molecules. This means that NIR can record intercalation even before the formation of the

critical coherence-length needed to be detected by XRD. Moreover, due the chemical specificity of NIR, guest-guest and guest-host interactions during intercalation can be observed. Thus, a diffusion process as described in literature [Hac69, Mak19] should be observable in the NIR, and its presence should yield a time-dependence behavior proportional to $\sqrt{t}$. Additionally, In the case of fully expanded but partially filled interlayers, XRD would produce 100% intercalation, whereas definitely not complete intercalation would be derived by NIR spectroscopy.

The 2nd derivative of the sharp 2ν(NH) band at 6700 cm^{-1} corresponding to intercalated NMF was selected for monitoring reaction progress. Sealed samples of kaolinite/NMF (1:1 wt, paste) were investigated at various temperatures in the 20-80 °C range for 1 to 5 days with a temporal resolution between 2 and 30 min, depending on the temperature. Besides pure NMF, similar experiments were performed for NMF:H_2O solutions for different proportions of H_2O (90:10, 80:20 and 70:30, wt%). Kaolinite/NMF:H2O pastes intercalated at 30 and 70 °C were then examined by thermogravimetric analysis (TGA). The recording of intercalation with NMF was also accomplished in natural fractions of KGa-2 and in natural fractions separated by two different methods and artificial fractions of KGa-1b.

The signature of intercalated NMF, expressed via the 2nd derivative of the 2ν(NH) band at 6700 cm^{-1}, was found to be constant in terms of width and position throughout the whole intercalation procedure for each examined sample. This implied that guest-guest intermolecular interactions do not change during the reaction, which would definitely happen in the case of diffusion along *ab* plane. As changes in bonding are not detected within the temporal resolution of NIR, diffusion was considered to be fast and the increase in the concentration of NMF in the interlayer space was attributed to the progressive increase of the number of fully intercalated interlayers. This was compatible with the observation that every spectrum can be reproduced by a linear combination of two spectra, one for the pristine and one for the fully intercalated kaolinite (two-mode behavior).

All of the NIR-based intercalation kinetics of the bulk samples displayed sigmoidal shapes, similar to XRD, and lack a detectable diffusion step. The surprising agreement between the kinetics probed by two techniques suggested that they both probe the same aspect of intercalation, which should be the expansion of interlayers

along *c*-axis, although it is still unknown whether the elementary intercalating unit is a single interlayer, a stack of interlayers in a single particle or a whole particle. New XRD experiments focusing on the evolution of coherence during intercalation are expected to answer this question.

Each kaolinite investigated, yielded the same S-shape when intercalated with anhydrous NMF at any given temperature in the 25-75 °C range. Normalizing the kinetic data to their long term asymptotic value and plotting them versus reduced time (t/t_0, where t_0 is the inflection point) resulted in a perfect time-temperature superposition, with unique shape for each kaolinite: the sigmoidal of KGa-1b was sharper and with a better defined plateau than that of KGa-2.

Despite the different sigmoidal shapes of KGa-1b and KGa-2, a single activation energy was estimated (~60 kJ/mol, ~0.62 eV, ~14.3 kcal/mol) implying that the rate-determining step is the same in the two samples, within the examined temperature range.

The difference between the sigmoidals of KGa-1b and KGa-2 cannot be attributed to different interlayer environment. If this were the case, the widths and positions of the 2nd derivative of the 2ν(NH) band at 6700 cm^{-1} would differ between the two kaolinites. Instead, they coincide. Thus, particles of distributed properties (e.g. defects, crystallinity, size) with the same interlayer environment are exposed to an intercalating agent at zero time and display a sigmoidal time-dependence intercalation with different characteristics between KGa-1b and KGa-2. Since diffusion was not observed, the sigmoidals were considered to correspond to the switching of the interlayer from the pristine to the fully intercalated state, which is distributed over time because the expanding kaolinite has distributed properties. Given that the interlayers are the same, the only thing that can affect this distribution should be related to the "external" structural characteristics of the particles, their size, aspect ratio and/or structure of the edges, which is related to the stacking order.

Opposite to previous publications that reported 90% NMF uptake in KGa-1b after 2-3 days [Tun96], it was found that intercalation of KGa-1b, even after a year in the presence of liquid excess NMF, is by no means approaching completion. This is indicated by the non-elimination of the inner surface 2ν(OH) and ν+δ(OH) signatures

in the NIR spectra. Preliminary XRD studies by the Clay Minerals Laboratory of the Institute of Geological Sciences/Polish Academy of Sciences, confirm the existence of non-intercalating material, due to the non-full elimination of the 12.5° 2θ which corresponds to d_{001}-spacing of ~7.2 Å (pristine kaolinite). The degree of intercalation estimated by the residual NIR signature of non-intercalated material as well as by thermogravimetric analysis in KGa-1b was ~0.8 and ≥0.7, respectively. In KGa-2, the extent of intercalation was even lower, ~0.4 and ~0.3, using NIR and TGA, respectively, in qualitatively agreement with literature [Uwi93]. Further XRD experiments are expected to reveal the exact amount and structural characteristics of unreacted kaolinite in both types.

The time-temperature superimposable kinetic curves displaying different shape but the same activation energy, were used for the identification of one model that could fit equally well both sigmoidals. Many models proposed in literature were tried to fit the data, such as Avrami-Erofeev [Hac69, Mak19] or consecutive reactions [Cas15], and all of them include two steps for the completion of the reaction. Diffusion models were also checked since it is referred to be the step following adsorption, nucleation or wedging process [Hac69, Lag06, Mak19]. These models failed to fit satisfactorily the NIR sigmoidal data. Common solid-state reaction models were also used, e.g. Prout-Tompkins equation [Pro44, Bro97], modified Prout-Tompkins [Bro97], Pérez-Maqueda [Per06], Cai-Liu [Cai09], Ng [Ng75], Sesták Berggren [Ses71] and the generalized logistic function [Tso02]. As the number of the parameters in the examined model equation increased, the fitting improved. Excellent fitting was found with the 4-parameter generalized logistic function, but lacked physical content.

For this reason, a totally different approach was adopted based on the NIR investigation: the sigmoidals are likely to correspond to the distribution of the times needed for the switching of the interlayer from empty to full. This is not conceptually different from the distribution of the reaction times (onset of symptoms, death etc.) of a population exposed to a biological agent. Exactly like the a population of soldiers who were inoculated the same day with the same batch of faulty serum hepatitis vaccine [Lim01], all the kaolinite particles are introduced to a chemical agent (NMF) at the same time. Each member of the respective populations can be in one of two

states: healthy vs. ill, pristine vs. intercalated. Some soldiers will never get sick, some material will never be intercalated. When dealing with properties of populations (e.g. the age of first marriage in Western civilization or the body weight [Lim01, Gua19]) or with their response to an external stimulus, the so-called log-normal distribution is frequently applicable. In fact, KGa-1b and KGa-2 consist of particles with log-normal particle-size distribution along *ab*-plane, respectively [Uwi93, Dri15], or log-normally distributed number of layers per particle [Sak16]. Log-normal distribution matched perfectly with the KGa-2 kinetics and little less perfectly with KGa-1b. The latter was improved with the introduction of a second log-normal distribution, justified by its bimodal particle-size distribution [Dri15].

When exposing kaolinite particles to NMF:H_2O solutions instead of anhydrous NMF, a non-monotonic effect was obtained with increasing H_2O content in the solution. This was basically due to the competition of two phenomena: A small amount of water facilitates the attachment of molecular NMF on the edges of the particles and, consequently, the entrance of NMF molecules in the interlayer by breaking down the H-bonded network of NMF molecules. However, as the concentration of water increases, the probability of NMF to be attached to the edges and succeed in intercalating is getting lower [Ole68, Ole70]. It was found that highest intercalation rate and smallest incubation time were observed with ~10 wt% H_2O.

Interestingly, the same interlayer bonding was detected when comparing spectra of kaolinite samples intercalated with anhydrous NMF and NMF:H_2O solutions at a specified temperature and the sigmoidal maintained its shape. These indicated that water present in the liquid phase does not enter the interlayer and solely NMF molecules are inserted. The fact that H_2O does not intercalate is another proof of the two-states system: In the case of partially intercalated and slowly intercalating kaolinite, there would always be free space for the H_2O to penetrate, but this was never observed.

Temperature was found to have a hitherto unknown effect on intercalation when high H_2O content was present in the solution. High temperatures led to suppression of the reactivity of kaolinite, which resulted in less NMF uptake. Decreasing the temperature resulted in a revival of intercalation, but this was not a reversible phenomenon. In the closed system of the intercalated samples, once the

molecules were arranged inside the interlayer space, they could not be de-intercalated by increasing the temperature. This can only be explained by assuming that the temperature-dependent equilibria take place outside the interlayer, between the liquid and the outer surface of the mineral particles.

Moreover, the sigmoidal shape of the intercalated samples seemed deformed at high H_2O content in the solution and high intercalating temperature, so that these curves didn't superimpose with the sigmoidal time-temperature superposition of the anhydrous samples. As the H_2O ratio in the solution increased, the temperature at which the deformation of the sigmoidals occurs decreased. For example, in the case of intercalation by the 90:10 NMF:H2O solution only the 80 °C kinetics displayed deviations, whereas when using a 70:30 solution all kinetics >40 °C appeared deformed. Since interlayer H_2O was not detected, the change in the sigmoidal shape can only be attributed to changes in the distribution of the "incubation" times of individual interlayers or particles and these should be related to temperature-dependent competitive NMF-H_2O interactions with the outer surface of kaolinite.

The effect of particle-size on intercalation was also examined at 45 °C on fractions separated by sedimentation in the presence of a dispersant. All the particle fractions were found to have the same interlayer environment for NMF. The progressive reduction of the reaction rate and the degree of reaction with decreasing size was observed. The sigmoidal almost disappeared in the smaller particle fractions of both kaolinites, despite the fact that these are very different in terms of stacking disorder [Uwi93, Dri15, Sak16]. Based on this observation, it could be hypothesized that the shape of the sigmoidal is determined mostly by particle size and not stacking disorder [Den02].

Artificial fractions produced by milling with 5 ml of methanol for 2, 10, 20 and 30 min were intercalated and compared to the natural. This time, the smaller particles displayed smaller incubation periods and the reaction was completed sooner. In addition, there was no dependence of the final NMF uptake on milling time. The activation energy of the sigmoidals and the bonding of NMF inside the interlayers did not seem to differ from the bulk sample, so the mechanism of intercalation remains the same. Clearly, the changes in structural properties of

kaolinite induced by the milling affected the shape of the sigmoidal in a totally different way than that observed with the natural particles. Particle size is not the only factor that influences the reaction, aspect ratio and stacking order need also to be explored. More types of kaolinite need to be studied to separate the effects of stacking order and particle size on intercalation, including another low-defect kaolinite, like KGa-1b, but with low order in its smaller particle fractions.

Until now, most XRD studies of intercalated kaolinite dealt with the determination of reaction progress by recording the change in integrated areas of *001* reflections of the pristine and intercalated kaolinite. The present NIR investigation revealed new phenomena and proposed a novel description of intercalation as a distributed event that call for new complementary studies by XRD. A much more detailed investigation of the evolution of coherence length should be possible, under intercalation of different kaolinitic types. Simulations of XRD diagrams are also very promising to shed light on hidden aspects of intercalation, such as the defects or particle thickness.

It is not known whether intercalation changes the stacking order of kaolinite, de-intercalation is reported in literature to alter the structure and properties of the original kaolinite [Bar77, Pla93]. What is known, instead, based on the work of Barrios et al. [Bar77] is that de-intercalation causes stacking defects in the structure, something that was later confirmed by Plastinina et al. [Pla93]. In addition, de-intercalating can cause exfoliation and nano-scrolling phenomena related to the mineral halloysite [Sin96, Det14, Li15, Li19]. The effect of these phenomena on a subsequent intercalation is still unknown. Preliminary experiments included repeated cycles of de-intercalating and re-intercalating kaolinite with NMF. The monitoring of intercalation in these de-intercalated samples resulted in higher NMF uptake and a completely new kinetic shape displaying exponential time-dependence in the initial step of the reaction. This novel behavior indicates a possible new mechanism and further investigation could probably identify the structural origin of both the incubation period and the non-reacted material.

References

[Ada78] Adams J.M., Differential scanning calorimetric study of the kaolinite: N-methylformamide intercalate, *Clays and Clay Minerals*, **26**, 169-172 (1978)

[Ada79] Adams J.M., The crystal structure of a dickite: N-methylformamide Intercalate [$Al_2Si_2O_5(OH)_4 \cdot HCONHCH_3$], *Acta Christallographica*, **B35**, 1084-1088 (1979)

[And18] Andreou F., Κινητική μελέτη παρεμβολής NMF στον καολινίτη μέσω δονητικής φασματοσκοπίας, undergraduate thesis (in Greek), NTUA (2018), http://dx.doi.org/10.26240/heal.ntua.16296

[And19] Andreou F., Siranidi E., Gionis V., Chryssikos G.D., Derkowski A., NMF intercalated kaolinite: a comparative vibrational and XRD investigation, Book of abstracts, p. 570, Euroclay (2019)

[Art95] Artioli G., Bellotto M., Gualtieri A., Pavese A., Nature of structural disorder in natural kaolinites: a new model based on computer simulation of powder diffraction data and electrostatic energy calculation, *Clays and Clay Minerals*, **43**, 438-445 (1995)

[Bar77] Barrios J., Plançon A., Cruz M.I., Tchoubar C., Qualitative and Quantitative Study of Stacking Faults in a Hydrazine Treated Kaolinite-Relationship with the Infrared Spectra, *Clays and Clay Minerals,* **25**, 422-429 (1977)

[Ben17] Bentea L., Watzky M.A., Finke R.G., Sigmoidal Nucleation and Growth Curves Across Nature Fit by the Finke–Watzky Model of Slow Continuous Nucleation and Autocatalytic Growth: Explicit Formulas for the Lag and Growth Times Plus Other Key Insights, *The Journal of Physical Chemistry C*, **121**, 5302–5312 (2017)

[Bis93] Bish D.L., Rietveld refinement of the kaolinite structure at 1.5K, *Clays and Clay Minerals*, **41**, 738-744 (1993)

[Bri86] Brindley G.W., Kao C.-C., Harrison J.L., Lipsicas M., Raythatha R., Relation between structural disorder and other characteristics of kaolinites and dickites, *Clays and Clay Minerals*, **34**, 239–249 (1986)

[Bri06] Brigatti M.F., Galan, E., Theng, B.K.G., Structures and mineralogy of clay

minerals. In Bergaya F., Theng B.K.G., Lagaly G., Eds., *Handbook of Clay Science*, 1st ed., pp. 35–43, Elsevier, Amsterdam, The Netherlands (2006)

[Bro80] Brown M.E., Dollimore D., Galwey A.K., Eds., *Reactions in the solid state*, Comprehensive Chemical Kinetics, Vol. 22, Elsevier, Amsterdam (1980)

[Bro97] Brown M.E., The Prout-Tompkins rate equation in solid-state kinetics, *Thermochimica Acta*, **300**, 93–106 (1997)

[Buk13] Vanessa J.B., Tsampodimou M., Gionis V., Chryssikos G.D., Synchronous ATR infrared and NIR-spectroscopy investigation of sepiolite upon drying, *Vibrational Spectroscopy*, **68**, 51-60 (2013)

[Cag10] Caglar B., Afsin B., Eren E., Tabak A., Cirak C., Cubuk O., The spectral, structral and thermal characterizations of dimethyl sulphoxide, pyridine, ethanolamine and N-methylformamide intercalated kaolinites, *Zeitschrift fur Naturforschung - Section A Journal of Physical Sciences*, **65**, 1009–1019 (2010)

[Cag13] Caglar B., Çırak Ç., Tabak A., Afsin B., Eren E. Covalent grafting of pyridine-2-methanol into kaolinite layers, *Journal of Molecular Structure*, **1032**, 12–22 (2013)

[Cai09] Cai J., Liu R., Kinetic Analysis of Solid-State Reactions: A General Empirical Kinetic Model, *Industrial & Engineering Chemistry Research*, **48**, 3249–3253 (2009)

[Cas15] Castrillo P.D., Olmos D., González-Benito J., Kinetic study of the intercalation process of dimethylsulfoxide in kaolinite, *International Journal of Mineral Processing*, **144**, 70-74 (2015)

[Chi01] Chipera S.J., Bish D.L., Baseline studies of The Clay Mineral Society Source Clays: Powder X-ray diffraction analyses, *Clays and Clay Minerals*, **49**, 398-409 (2001)

[Chr17] Chryssikos G.D., Modern infrared and Raman Instrumentation and sampling methods. In Gates W.P., Kloprogge J.T., Madejova J., Bergaya F., Eds., *Infrared and Raman Spectroscopies of Clay Minerals*, pp. 34-63, Elsevier Publisher, London (2017)

[Ded14] Dedzo G.K., Detellier C., Intercalation of two phenolic acids in an ionic

liquid–kaolinite nanohybrid material and desorption studies, *Applied Clay Science*, **97-98**, 153–159 (2014)

[Den02] Deng Y., White G.N., Dixon J.B., Effect of structural stress on the intercalation rate of kaolinite, *Journal of Colloid and Interface Science*, **250**, 379–393 (2002)

[Den03] Deng Y., Dixon J.B., White G.N., Molecular configurations and orientations of hydrazine between structural layers of kaolinite, *Journal of Colloid and Interface Science*, **257** , 208–227 (2003)

[Det14] Detellier C., Schoonheydt R.A., From platy kaolinite to nanorolls, *Elements*, **10**, 201-206 (2014)

[Dri15] Drits V.A., Derkowski A., Kinetic behavior of partially dehydroxylated kaolinite, *American Mineralogist*, **100**, 883-896 (2015).

[Dri16] Drits V.A., Derkowski A., Sakharov B.A., Zviagina B.B., Experimental evidence of the formation of intermediate phases during transition of kaolinite into metakaolinite, *American Mineralogist*, **101**, 2331-2346 (2016)

[Fol71] Foldes A., Sandorfy A.C., Model calculations on the energy levels of diatomic anharmonic oscillators: Relation to hydrogen bonding, *Canadian Journal of Chemistry*, **49**, 505-510 (1971)

[Fro98] Frost R.L., Johansson U., Combination bands in the infrared spectroscopy of kaolins-A DRIFT spectroscopic study, *Clays and Clay Minerals*, **46**, 466-477 (1998)

[Fro02] Frost R.L., van der Gaast S.J., Zbik M., Kloprogge J.T., Paroz G.N., Birdwood kaolinite: a highly ordered kaolinite that is difficult to intercalate—an XRD, SEM and Raman spectroscopic study, *Applied Clay Science*, **20**, 177–187 (2002)

[Gal99] Kinetic models for solid state reactions. In Galwey A.K., Brown M.E., Eds., *Thermal Decomposition of Ionic Solids Volume 86*, pp. 75-115, Elsevier Science, Oxford (1999)

[Gar00] Gardolinski J. E., Ramos L. P., de Souza G. P., Wypych F., Intercalation of Benzamide into Kaolinite, *Journal of Colloid and Interface Science*, **221**,

284–290 (2000)

[Gua19] Gualandi S., Toscani G., Human Behavior and Lognormal Distribution A Kinetic Description, *Mathematical Models and Methods in Applied Sciences*, **29**, 717-753 (2019)

[Gug01] Guggenheim S., Koster van Groos A.F., Baseline studies of the clay minerals society source clays: Thermal analysis, *Clays and Clay Minerals*, **49,** 433–443 (2001)

[Hac69] Hach-Ali P.F., Weiss A., Estudio de la reaccion de caolinita y N-metilformamida, *Quimica LXV*, 769–790 (1969)

[Joh84] Johnston C.T., Sposito G., Bocian D.F., Birge R.R., Vibrational spectroscopic study of the interlamellar kaolinite-dimethyl sulfoxide complex, *The Journal of Physical Chemistry*, **88**, 5959-5964 (1984)

[Kal11] Kalendova A., Zykova J., Matejka V., Machovsky M., Malac J., PVC inorganic hybrids based on kaolinite/urea intercalates, *Proceedings of the Fifth International Conference on Quantum, Nano and Micro Technologies*, 109–113 (2011)

[Klo19] Kloprogge J.T., Intercalation of the kaolin minerals with simple molecules. In Kloprogge J.T., Eds., *Spectroscopic Methods in the Study of Kaolin Minerals and their Modifications*, pp. 243-319, Springer Mineralogy, Cham, Switzerland (2019)

[Kha06] Khawam A., Flanagan D. R., Solid-State Kinetic Models: Basics and Mathematical Fundamentals, *The Journal of Physical Chemistry B*, **110**, 17315–17328 (2006)

[Kog05] Kogure T., Inoue A., Determination of defect structures in kaolin minerals by high-resolution transmission electron microscopy (HRTEM), *American Mineralogist*, **90**, 85-89 (2005)

[Kog10] Kogure T., Elzea-Kogel J., Johnston C.T., Bish D.L., Stacking Disorder in a Sedimentary Kaolinite. *Clays Clay Minerals*, **58,** 62–71 (2010)

[Kot15] Koteja A., Matusik J., Di- and triethanolamine grafted kaolinites of different structural order as adsorbents of heavy metals, *Journal of Colloid and Interface Science*, **455**, 83–92 (2015)

[Kri18] Kristóf T., Sarkadi Z., Ható Z., Rutkai G., Simulation study of intercalation complexes of kaolinite with simple amides as primary intercalation reagents, *Computational Materials Science,* **143***,* 118-125 (2018)

[Lag06] Lagaly G., Ogawa M., Dékány I., Clay Mineral Organic Interactions. In: Bergaya F., Theng B.K.G., Lagaly G., Eds., *Handbook of Clay Science*, pp. 309–377, Elsevier Science, Amsterdam (2006)

[Led66] Ledoux R.L., White J.L., Infrared studies of hydrogen bonding interaction between kaolinite surfaces and intercalated potassium acetate, hydrazine, formamide and urea, *Journal of Colloid and Interface Science*, **21**, 127-152 (1966)

[Li15] Li X., Liu Q., Cheng H., Zhang S., Frost R.L., Mechanism of kaolinite sheets curling via the intercalation and delamination process, *Journal of Colloid and Interface Science*, **444**, 74–80 (2015)

[Li19] Li X., Wang D., Liu Q., Komarneni S., A comparative study of synthetic tubular kaolinite nanoscrolls and natural halloysite nanotubes, *Applied Clay Science*, **168**, 421–427 (2019)

[Lim01] Limbert E., Stahel W.A., Abbt M., Log-normal Distributions across the Sciences: Keys and Clues, *BioScience*, **51**, 341-352 (2001)

[Lin20] Linton N.M., Kobayashi T., Yang Y., Hayashi K., Akhmetzhanov A.R., Jung S.-M., Yuan B., Kinoshita R., Nishiura H., Incubation Period and Other Epidemiological Characteristics of 2019 Novel Coronavirus Infections with Right Truncation: A Statistical Analysis of Publicly Available Case Data, *Journal of Clinical Medicine*, **9***,* 538 (2020)

[Mac93] Mackinnon I.D.R., Uwins P.J.R., Yago A., Page D., Kaolinite particle sizes in the <2 μM range using laser scattering, *Clays and Clay Minerals*, **41**, 613-623 (1993)

[Mak19] Makó É., Kovács A., Kristóf T., Influencing parameters of direct homogenization intercalation of kaolinite with urea, dimethyl sulfoxide, formamide, and N-methylformamide, *Applied Clay Science*, **182**, 105287 (2019)

[Mur88] Murray H. H., Kaolin Minerals: Their Genesis and Occurrences. In: Bailey

S.W., Eds., *Hydrous Phyllosilicates*, pp. 67-89, Mineralogical Society of America, Washington DC (1988)

[Mur00] Murray H. H., Traditional and new applications for kaolin, smectite, and palygorskite: a general overview, *Applied Clay Science*, **17**, 207–221 (2000)

[Ned99] Neder R.B., Burghammer M., Grasl T., Schulz H., Bram A., Fielder S., Refinement of the Kaolinite Structure From Single-Crystal Synchrotron Data, *Clays and Clay Minerals* , **47**, 487–494 (1999)

[Ng75] Ng W-L., Thermal Decomposition in the Solid State , A*ustralian Journal of Chemistry,* **28**, 1169-1178 (1975)

[Ngn16] Ngnie G., Dedzo G. K., Detellier C, Synthesis and catalytic application of palladium nanoparticles supported on kaolinite-based nanohybrid materials, *Dalton Transactions*, **45**, 9065–9072 (2016)

[Oco86] O'Connor B. H., Chang W.-J., The amorphous character and particle size distributions of powders produced with the Micronizing Mill for quantitative x-ray powder diffractometry, *X-Ray Spectrometry,* **15**, 267–270 (1986)

[Ole68] Olejnik S., Aylmore L.A.G., Posner A.M., Quirk J.P., Infrared spectra of kaolin mineral-dimethyl sulfoxide complexes, *The Journal of Physical Chemistry*, **72**, 241-249 (1968)

[Ole70] Olejnik S., Posner A.M., Quirk J.P., The intercalation of polar organic compounds into kaolinite, *Clay Minerals*, **8**, 421-434 (1970)

[Ole71a] Olejnik S., Posner A.M., Quirk J.P., The I.R. spectra of interlamellar kaolinite-amide complexes-I. The complexes of formamide, N-methyl-formamide and dimethylformamide, Clays and *Clay Minerals*, **19**, 83-94 (1971)

[Ole71b] Olejnik, S., Posner A. M., Quirk J. P., The infrared spectra of interlamellar kaolinite-amide complexes II. Acetamide, N-methylacetamide and dimethylacetamide, *Journal of Colloid and Interface Science*, **37**, 536–547 (1971)

[Pet99] Petit S., Madejová J., Decarreau A., Martin F., Characterization of

octahedral substitutions in kaolinites using near-infrared spectroscopy, *Clays and Clay Minerals*, **47**, 103-108 (1999)

[Per06] Pérez-Maqueda L.A., Criado J.M., Sánchez-Jiménez P.E., Combined kinetic analysis of solid-state reactions: A powerful tool for the simultaneous determination of kinetic parameters and the kinetic model without previous assumptions on the reaction mechanism, *The Journal of Physical Chemistry A*, **110**, 12456-12462 (2006)

[Pla77] Plançon A., Tchoubar C., Determination of structural defects in phyllosilicates by X-ray powder diffraction - II. Nature and proportion of defects in natural kaolinites, *Clays and Clay Minerals*, **25**, 436-450 (1977)

[Pla88] Plançon A., Giese R.F., Snyder S., The Hinckley index for kaolinites, *Clay Minerals*, **23**, 249-260 (1988)

[Pla89] Plançon A., Giese R.F., Jr., Snyder R., Drits V.A., Bookin S.A., Stacking faults in the kaolin-group minerals: Defects structures of kaolinite, *Clays and Clay Minerals*, **37**, 203-210 (1989)

[Pla93] Plastinina M.A., Fedorenko J.G., Shpigun A.A., De-intercalated kaolinites: The nature of created defects and estimation of structural characteristics by the expert system of Plançon and Zacharie, *Clays and Clay Minerals*, **28**, 101–108 (1993)

[Pro44] Prout E.G., Tompkins F.C., The thermal decomposition of potassium permanganate, *Transactions of the Faraday Society*, **40**, 488 (1944)

[Pru93] Pruett R.J., Webb H.L., Sampling and Analysis of KGa-1B Well-Crystallized Kaolin Source Clay, *Clays and Clay Minerals*, **41,** 514–519 (1993)

[Sak16] Sakharov B.A., Drits V.A., McCarty D.K., Walker G.M., Modeling Powder X-Ray Diffraction Patterns of the Clay Minerals Society Kaolinite Standards: Kga-1, Kga-1b, and Kga-2, *Clays and Clay Minerals*, **64**, 314–333 (2016)

[Set78] Seto H., Cruz M.I., Fripiat J.J., Long-range organization in the ammonium propionate intercalation complexes of kaolinite, *American Mineralogist*, **63**, 572-583 (1978)

[Ses71] Šesták, J., Berggren G., Study of the kinetics of the mechanism of solid-state reactions at increasing temperatures, *Thermochimica Acta*, **3**,

1-12 (1971)

[Sie02] Siesler H.W., Applications to polymers and textiles. In: Siesler H. W., Osaki Y., Kawata S., Heise H. M., Eds., *Near-infrared spectroscopy*, pp. 213–245, Wiley-VCH, New York (2002)

[Sin96] Singh B., Mackinnon I.D.R., Experimental Transformation of Kaolinite to Halloysite, *Clays and Clay Minerals,* **44,** 825–834 (1996)

[Sor03] Soro N., Aldon L., Olivier-Fourcade J., Jumas J.C., Laval J.P., Blanchart P., Role of Iron in Mullite Formation from Kaolins by Mössbauer Spectroscopy and Rietveld Refinement, *Journal of the American Ceramic Society*, **86**, 129–134 (2003)

[Sta03] Starink M., The determination of activation energy from linear heating rate experiments: a comparison of the accuracy of isoconversion methods, *Thermochimica Acta*, **404**, 163–176 (2003)

[Str17] Struijk M., Rocha F., Detellier C., Novel thio-kaolinite nanohybrid materials and their application as heavy metal adsorbents in wastewater, *Applied Clay Science*, **150**, 192–201 (2017)

[Sug86] Sugahara Y., Kitano S., Satokawa S., Kuroda K., Kato C., Synthesis of Kaolinite-Lactam Intercalation Compounds, *Bulletin of the Chemical Society of Japan*, **59**, 2607-2610 (1986)

[Tan48] Tanner C.B., Jackson M.L., Nomographs of sedimentation times for soil particles under gravity or centrifugal acceleration, *Soil Science Society of American Proceedings*, **11**, 60-65 (1948)

[Tch18] Tchoumene R., Dedzo G.K., Ngameni E., Preparation of methyl viologen-kaolinite intercalation compound: controlled release and electrochemical applications, *ACS Applied Materials & Interfaces*, **10**, 34534−34542 (2018)

[Tsi12] Tsiantos C., Tsampodimou M., Kacandes G.H., Sánchez del Río M., Gionis V., Chryssikos G.D., Vibrational investigation of indigo–palygorskite association(s) in synthetic Maya blue, *Journal of Materials Science*, **47**, 3415–3428 (2012)

[Tsi18] Tsiantos, C., Gionis, V., & Chryssikos, G. D., Smectite in bentonite: Near infrared systematics and estimation of layer charge, *Applied Clay Science*,

160, 81-87 (2018)

[Tso02] Tsoularis A., Wallace J., Analysis of logistic growth models, *Mathematical Biosciences,* **179**, 21–55 (2002)

[Tun96] Tunney J. J., Detellier C., Chemically modified kaolinite. Grafting of methoxy groups on the interlamellar alumino surface of kaolinite, *Journal of Materials Chemistry*, **6**, 1679-1685 (1996)

[Ufe15] Ufer K., Kleeberg R., Monecke T., Quantification of stacking disordered Si–Al layer silicates by the Rietveld method: application to exploration for high-sulphidation epithermal gold deposits, *Powder Diffraction*, **30**, S111-S118 (2015)

[Uwi93] Uwins P.J.R., Mackinnon I.D.R., Thompson J.G., Yago A.J.E., Kaolinite:NMF intercalates, *Clays and Clay Minerals*, **41**, 707–717 (1993)

[Wad61] Wada K., Lattice expansion of kaolin minerals by treatment with potassium acetate, *The American Mineralogist*, **46**, 78-91 (1961)

[Wat97] Watzky M. A., Finke R.G., Transition Metal Nanocluster Formation Kinetic and Mechanistic Studies, A New Mechanism When Hydrogen is The Reductant: Slow, Continuous Nucleation and Fast Autocatalytic Surface Growth, *Journal of the American Chemical Society*, **119**, 10382-10400 (1997)

[Wei63] Weiss A., A secret of Chinese porcelain manufacture, *Angewandte Chemie International Edition*, **2**, 697-748 (1963)

[Wei66] Weiss A., Thielepape W., Orth H., Neue kaolinite-einlagerungouerbindungen, *Proceedings of the International Clay Conference*, Jerusalem, **1**, 277-293 (1966)

[Wie69] Wiewiora A., Brindley G. W., Potassium acetate intercalation in kaolinites and its removal: effect of material characteristic, *Proceedings of the International Clay Conference*, Tokyo, **1**, 723-733 (1969)

[Zha16] Zhang S., Liu Q., Gao F., Li X., Liu C., Li X., Liu C., Li H., Boyd S. A., Johnston C. T., Teppen B. J., Mechanism Associated with Kaolinite Intercalation with Urea: Combination of Infrared Spectroscopy and Molecular Dynamics Simulation Studies, *The Journal of Physical Chemistry C*, **121**,

402–409 (2016)

[Zha18] Zhang S., Liu Q., Gao F., Teppen B. J., Molecular Dynamics Simulation of Basal Spacing, Energetics, and Structure Evolution of a Kaolinite–Formamide Intercalation Complex and Their Interfacial Interaction, *The Journal of Physical Chemistry C*, **122**, 3341–3349 (2018)

[Zvy96] Zvyagin B.B., Drits V.A., Interrelated features of structure and stacking of kaolin mineral layers, *Clays and Clay Minerals*, **44**, 297-303 (1996)